A dissertation entitled

Experimental and numerical investigations of shell and tube latent heat storage system under simultaneous charging and discharging process

A Dissertation

Submitted in partial fulfilment of the requirements for

the award of the degree of

DOCTOR OF PHILOSOPHY

in

MECHANICAL ENGINEERING

By

KHOBRAGADE SANDIP DIGAMBAR

(Roll No: 718021)

Supervisor

Dr. D. JAYA KRISHNA

(Professor)

Department of Mechanical Engineering

National Institute of Technology,

Warangal (TS), India.

September 2022

Thesis approval for Ph.D

This thesis entitled "**Experimental and numerical investigations of shell and tube latent heat storage system under simultaneous charging and discharging process"** is approved for the degree of Doctor of Philosophy.

Examiners

_____

_____

_____

Supervisor

(Dr. D. Jaya Krishna)
Professor
Department of Mechanical Engineering,
National Institute of Technology, Warangal

Chairman

(Dr. V. Suresh Babu)
Professor and Head
Department of Mechanical Engineering,
National Institute of Technology, Warangal

NATIONAL INSTITUTE OF TECHNOLOGY- WARANGAL

CERTIFICATE

This is to certify that the thesis entitled "**Experimental and numerical investigations of shell and tube latent heat storage system under simultaneous charging and discharging process"** being submitted by **Khobragade Sandip Digambar (Roll No: 718021)** for the award of the degree of **Doctor of Philosophy (Ph.D.) in Mechanical Engineering** to the National Institute of Technology, Warangal, India, is a record of the bonafide research work carried out by him under my supervision. The thesis has fulfilled the requirements according to the regulations of this Institute and in my opinion has reached the standards for submission. The results embodied in the thesis have not been submitted to any other University or Institute for the award of any degree.

Date:

Prof. D. Jaya Krishna
Thesis Supervisor
Department of Mechanical Engineering,
National Institute of Technology, Warangal

Prof. V. Suresh Babu
Chairman, DSC & Head
Department of Mechanical Engineering,
National Institute of Technology,
Warangal

DECLARATION

This is to certify that the work presented in the thesis entitled "**Experimental and numerical investigations of shell and tube latent heat storage system under simultaneous charging and discharging process"** is a bonafide work done by me under the supervision of Dr. D. Jaya Krishna (Professor, MED) and was not submitted elsewhere for award of any degree.

I declare that this written submission represents my ideas in my own words and where others' ideas or words have been included, I have adequately cited and referenced the original sources. I also declare that I have adhered to all principles of academic honesty and integrity and have not misrepresented or fabricated or falsified any idea/data/fact/source in my submission. I understand that any violation of the above will be a cause for disciplinary action by the Institute and can also evoke penal action from the sources which have thus not been properly cited or from whom proper permission has not been taken when needed.

Date: (Khobragade Sandip Digambar)

Place: Warangal Roll No. 718034

ACKNOWLEDGEMENT

I would like to express my sincere gratitude and it gives me an immense pleasure to acknowledge the people who were the part of this research work in plenty ways. It would not have been possible without close association with many people. I take this opportunity to extend my sincere gratitude and appreciation to all those who made this research work possible. First and foremost, I want to thank my thesis supervisor Dr. D. Jaya Krishna. He cultivated the seed of the research in me and inspired to apply this knowledge not only in laboratories but also in the personal life. His invaluable contributions of time and ideas during Ph.D. stay provide me wealthy in experiences, which is productive and stimulating in all aspects. His positive attitude at any diverse situations taught me how to tackle the hurdles at any stage with joy and enthusiasm. He provided me an excellent platform to nourish and grow my professional as well as personal life.

I wish to sincerely thank university authorities, Prof. N.V. Ramana Rao, Director, National Institute of Technology, Warangal and other higher officials who gave me an opportunity to carry out research work.

I also sincerely thank Dr. G Naga Srinivasulu (Thermal Section head) and Prof. V. Suresh Babu, Head, Mechanical Engineering Department, National Institute of Technology Warangal for his continuous support towards carrying out research work.

I wish to express my sincere and whole hearted thanks and gratitude to my doctoral scrutiny committee (DSC) members Dr. V. Rajesh Khana Raju, Professor, Mechanical Engineering Department, Dr. V.P. Chandramohan, Professor, Mechanical Engineering Department, Dr. Arockia Kumar, Associate Professor, Metallurgy Department, National Institute of Technology, Warangal for their kind help, encouragement and valuable suggestions for successful completion of research work.

I would like to extend my thanks to all the faculty members in the Department of Mechanical Engineering for their valuable suggestions and encouragement. I am also thankful to all the supporting and technical staff of the Department of Mechanical Engineering who has directly or indirectly helped during the course of my work.

I am thankful to all my senior and fellow research scholars especially, Dr. Lokesh Kalapala, Dr. G. Uma Maheswararao , Dr. Ganesh R Gawale, Dr. Abhay Lingyat, Dr. Uday Bagale, Dr. Gajanan Surywanshi, Dr. Harshal Patil, Mr. A. Gopi Krishna, Mr. T. Markandeyulu,

Mr. Upendra Murya, Mr. Vikas Hakke, Mr. Raj Kumar, Mr. Rampalli Sashidhar, Mr. G. Amarnath, Mr. Ajoy Nandy, Mr. Nandan Hegede, Mr. Abhishek Kumar, Mr. Chinmay Kumar Das, Mr. Ajit Mohanty, Mr. Debanjan Pathak, Mrs. Soumyashree Dixit Pathak, and many others for always standing by my side and sharing a great relationship as compassionate friends. I will always cherish the warmth shown by them.

I should thank all my friends back in Aurangabad Mr. Suraj Chamle, Mr. Swapnil Pupulwad, Mr. Ramdas Narwade, Mr. Vishal Waduje, Mr. Hitesh Kukade, Mr. Pramod Kastewad, Mr. Vipul Dhawale, Mr. Sachin Gore supporting me from there, and all my hostel mates for making my stay at NIT Warangal become more memorable.

Last but not the least; In this auspicious moment, I owe my deepest regards family members and well-wishers for their eternal support and understanding of my goals and aspirations. My heartfelt regards go to my parents Digambar Khobragade and Shrada Khobragade. Finally, I would like to thank my sister Supriya Khobragade for her moral support.

(Khobragade Sandip Diagambar)

Abstract

The defilement of the environment due to pollutants and day by day increase in demand for energy are key issues that need serious consideration for a better society. To overcome these issues attention needs to be focused on sustainable and cleaner methods of energy usage. Solar energy is one of the potential energy sources for a sustainable society. However, due to the fluctuations, the continuous availability of solar energy is uncertain. Thermal energy storage (TES) is a key approach for energy utilization that can solve the problem of disharmony between energy supply and demand. Among the different TES methods, the latent heat storage system (LHSS) based on the phase change materials (PCMs) has the potential to solve the mismatch between the energy supply and demand due to its higher storage density capacity at a small range of temperature difference. Out of various configurations, shell and tube type LHSS is preferred due to minimum heat loss to the surrounding. The thermal performance of LHSS has a significant impact on the operating parameters, geometric design and properties of PCM. However, the low thermal conductivity of the PCMs hinders the thermal performance of LHSS. To enhance the thermal transport for the PCM based applications multiple promising techniques viz. fins, insertions of nanoparticles, metal foam and encapsulation are available. Among these, fins are considered to be a promising method for practical applications in terms of cost and stability

The present research work is aimed at analyzing the influence of various parameters on the thermal behavior of PCM under simultaneous charging and discharging process (SCD). In the literature, charging (melting) and discharging (solidification) were performed independently. But for efficient tapping of solar thermal energy a heat storage system should undergo the charging and discharging process simultaneously. In the simultaneous charging and discharging (SCD) process, the hot and cold heat transfer fluids (HTFs) are made to circulate simultaneously. The influence of HTF parameters is analyzed in shell and tube LHSS. Also, the effect of latent heat storage system (LHSS) orientation on the thermal performance of PCM is evaluated. Adding fins enhances the heat transfer and makes the LHSS energy and exergetically efficient. Finally, perforation is employed on solid fin for the effective utilization of natural convection.

Initially, the influence of heat transfer fluid parameters such as temperature gradient between hot and cold HTF, mass flow rate, and directions (parallel and counter flow) on

melting characteristics of PCM is analyzed numerically. Two cases are considered to analyze the influence of the temperature gradient of the hot and cold HTFs. In case 1 the hot fluid inlet temperature is varied and the cold fluid inlet temperature is maintained constant(ΔT_h), and for case 2 the cold HTF inlet temperature is varied and the hot HTF inlet temperature is maintained constant (ΔT_c). It is found that the melting process can be considerably improved for case 1 by increasing the temperature gradient. However, in case 2 by increasing the temperature gradient the influence on the melting process is not significant for horizontal but exhibited a stronger influence for vertical configuration. With the reduction of ΔT_h from 53 °C to 33 °C the energy storage is noted to decrease by 50.83 % and 43.99 % in vertical and horizontal configurations. Additionally, the mass flow rates and direction of hot and cold HTFs are observed to have less effect on thermal transport.

Experimental and numerical investigations are carried out to realize the effect of LHSS orientation on its thermal performance. Results illustrated that better thermal performance is provided by the horizontal (0°) configuration. The effect of natural convection on the PCM under the SCD melting process has differed with the inclination. A maximum average temperature of 58°C, maximum exergy efficiency of 7.54% and maximum energy storage of 231 kJ is observed for the horizontal position. The maximum energy stored at the horizontal (0°) configuration is 41.72 % higher than the vertical position. Also, the steady-state condition is observed earlier in the horizontal position. The low thermal conductivity of the PCM and thermal resistance over the cold HTF tube due to the formation of a solid PCM layer results in less recovery of thermal energy by the cold HTF.

To address this issue, the simultaneous charging and discharging (SCD) process for LHSS with fins is considered. Employing fins improved the thermal performance of the LHSS. In a vertical position, the melting behavior in the upper half of the LHSS is more for all the considered configurations. It is also observed that the LHSS with fins gave 18.31 % higher melt fraction than without fins for vertical configuration. The horizontal configuration with fins gave a higher uniform temperature and higher average Nusselt number. Hence, the presence of fins leads to better thermal transport from the cold HTF to the upper section in comparison to unfinned LHSS with the decrease of inclination. Also, the maximum energy storage (224 kJ) and exergy efficiency (12.9 %) are obtained for horizontal configuration. The energy storage and exergy efficiency obtained for the horizontal position are 14.87 % and 33.75 % higher than the vertical configuration with fins. However, it is noted that the

flow of melted PCM is restricted by the fins which leads to the suppression of natural convection and lowers the melting process.

One of the possible options to overcome this problem can be perforated fins. Here the melted PCM can move through the perforation and can help to enhance natural convection. Also, the influence of the orientation of LHSS with perforated fins on natural convection is investigated. It is observed that perforated fins gave a better thermal performance in vertical and 60° configurations. However, the effect of perforation is insignificant at the end stage of the melting process hence melting is unaffected by the type of fins. Compared to important aspects such as exergy efficiency and heat recovery out of without and with solid and perforated fins, LHSS with solid fins shows improved thermal performance.

Keywords: Latent heat storage, PCM, simultaneous charging and discharging, melting; perforated fin; circular fins, orientation.

CONTENTS

List of Figures

List of Tables

Nomenclature

b	Body force (N)
C	Mushy zone parameter (kg/m^{3}s)
C_p	Specific heat (kJ/ kg K)
E	Energy stored **(**kJ)
Ex	Exergy (kJ)
h	Sensible specific heat (J/kg)
H	Total specific enthalpy (J/kg)
k	Thermal conductivity (W/mK)
L	Latent heat (kJ/kg)
m	Mass of PCM (kg)
$\dot{m}$	Flow rate of HTF (kg/s)
p	Pressure (N/m^2)
Q	Heat transfer (W)
r	Radius (m)
S_h	Source term
t	Time (s)
T	Temperature (K)
v	Velocity (m/s)
W	Weighting factor

Greek symbol

ρ	Density (kg/m^3)
μ	Dynamic viscosity (kg/m-s)
γ	Liquid fraction
β	Thermal expansion coefficient (1/K)
λ	Latent heat of fusion (J/kg)
ΔH	Specific enthalpy (J/kg)
ΔT	Temperature gradient (°C)

η	Exergy efficiency

Subscripts

a	Ambient
avg	Average
c	Cold
h	Hot
ini	Initial
i	Instantaneous
in	Inlet
l	Liquidus
out	Outlet
s	Solidus
t	Total
r	Radial
θ	Circumferential
z	Axial

Abbreviations

HTF	Heat transfer fluid
HP	Heat pipe
MF	Metal foam
NePCM	Nano enhanced PCM
LHSS	Latent heat storage system
PCM	Phase change material
SCD	Simultaneous charging and discharging
TTHX	Triplex tube heat exchange
TES	Thermal energy storage

Chapter 1

Introduction

The defilement of the environment due to pollutants and wastage of energy are key issues that need serious consideration for a better society. Also, recently more attention is given towards the development and improvement of more reliable methods to replace or decrease the use of fossil fuels due to pollution and limited energy resource. Rapid industrial growth and enormous technological improvement continue to escalate energy demand. As per the International Energy Agency (IEA) report, energy consumption throughout the world has been increasing by 2.5% every year which is equivalent to 600 TWh [1]. To overcome these issues attention needs to be focused on sustainable and cleaner methods of energy usage. Renewable energy is one of the potential energy sources for a sustainable society.

Hence, renewable sources of energy such as wind, geothermal and solar are the most alternative sources of energy. Without a doubt, all of the sources are advantageous, but solar energy emerges as the most valued of all due to its numerous desirable benefits. Solar energy can be easily extracted because of which a huge variety of solar-powered consumer products are available in the market. On a broader scale, producing electricity from solar radiation requires a lot of space and has a high starting cost. On the other hand, it can be easily harnessed for household uses such as water heating, space heating, and cooking, etc. Moreover, solar energy is transient in nature. This problem can be reduced by using the thermal storage system.

1.1Thermal energy storage

Thermal energy can be stored via. sensible heat storage (SHS), latent heat storage (LHS) and thermochemical energy storage. The comparison of these storage techniques is shown in Table 1.1. Energy is stored in SHS by increasing the temperature of the storage material without any phase change; thus, the quantity of energy stored depends up on the material's heat capacity, the changes in temperature, and the amount of storage material. Thermochemical energy storage utilizes the heat generated from the reversible reaction. However, these reactions take place at high temperatures and for low temperature applications, this method is not suitable. Also, the installation cost for thermochemical energy storage is high. On the other hand, LHS implies the phase change of the storage material between one form to another, such as solid-liquid, solid-solid, or liquid-gas, and vice versa, when heated to the transformation temperature. Solid-solid transition involves

low energy storage density per unit volume of material whereas a liquid-gas transition requires a large volume for the same energy storage. As a result, the solid-liquid transformation is employed in LHS applications; this is more effective than the other transitions, thus the most often used. In comparison to LHS, SHS needs more space for a specified amount of thermal energy and lower installation cost as compared to thermochemical storage. Therefore, LHS is highly potential and attractive because of its compactness and capacity to store energy at an almost constant temperature. The material utilized in LHSS is known as phase change material (PCM).

Table 1.1 Comparison of different storage techniques

Ref.	Storage techniques	Sensible energy storage	Latent energy storage	Thermochemical energy storage
[2]	Type of energy	Thermal	Thermal	Thermochemical
[1]	Energy storage density (kWh/m^3)	25	100	500
[1]	Energy storage density (kWh/ton)	10-50	50-150	150-250
[3]	Storage capacity (MW)	0.1-300	0.1-300	0.1-300
[4]	Durability (years)	10-30	10-30	10-30
[4]	Durability (cycles)	2000-14600	2000-14600	2000-14600
[5]	Energy cost (USD/kWh)	0.1-13	10-56	12-100
[1]	Efficiency (%)	50-90	75-90	75-100

1.2 Phase change material

A phase-change material is a substance, commonly referred to as PCM. PCMs are products that store and release thermal energy during the processes of charging and discharging. There are different types of PCMs such as organic, inorganic, and eutectics as shown in Fig 1.1. Details on the classifications of the PCMs are available in the literature with different melting/freezing points, thermal conductivity, and latent heat [6–10].

Because of its diverse advantages, PCM attracted various applications. Table 1.2 shows the summary of various applications where PCMs are employed. In view of enormous

applications, active research is being carried out on the development of different kinds of PCMs, and a few available PCMs for low temperature applications are listed in Table 1.3.

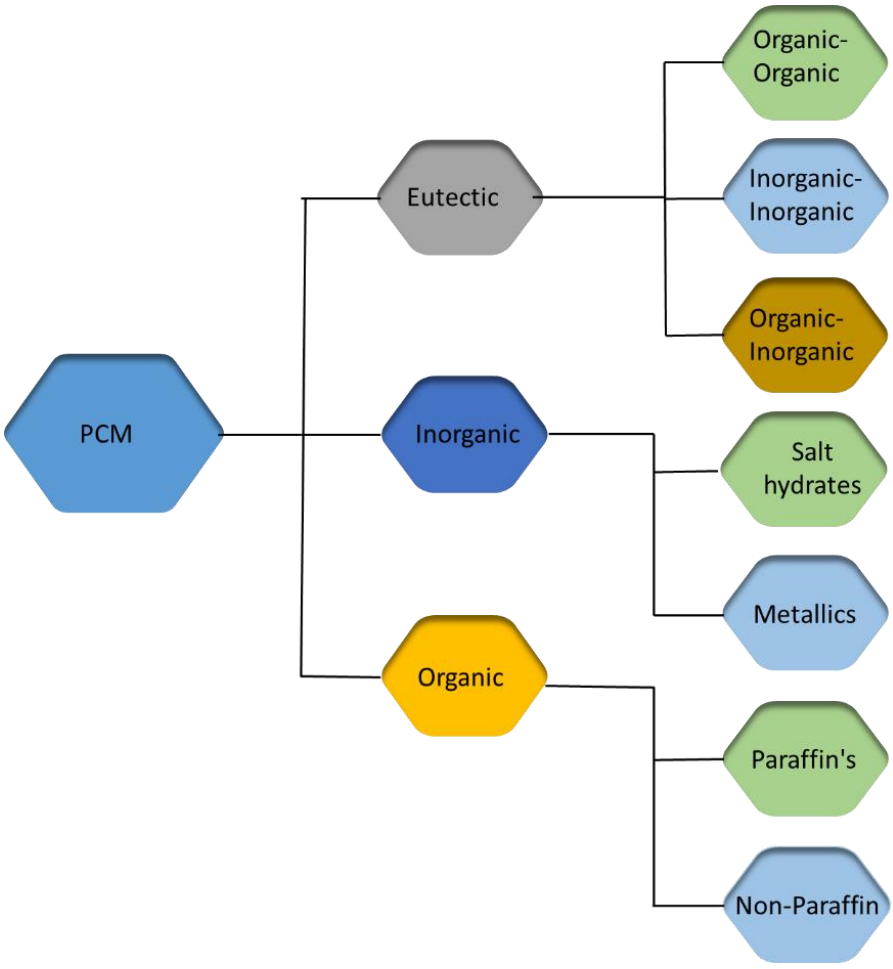

Fig. 1.1 Classification of PCMs

Table 1.2 Summary of recent review papers on PCMs based application

Ref.	Application	Contents
[11]	Solar water heater	Performance enhancement of solar water heater embedded with PCMs
[12]	Solar water heater	Improvement of heat transfer and utilization of PCMs in solar water heater
[13]	Solar water heater	Investigation of PCMs for solar and space heating applications
[14]	Thermal management	Batteries thermal management using PCMs
[15]	Thermal management	Li-ion batteries for vehicles integrated with PCMs

[16]	Thermal management	Introduced potential PCMs for thermal management system
[17]	Automobile industries	Use of PCMs in the automotive industries
[18]	Distillation system	Use of PCMs in the solar still for distillation
[19]	Heating and cooling of building	Review of PCMs for heating and cooling of building application
[20]	Heating and cooling of building	Role of PCMs in heating and cooling of building with hybrid application
[21]	Solar dryer	Role of PCMs in solar dryer application to improve the efficiency of agricultural products.
[22]	Refrigeration	Investigation and recent development of PCMs in refrigeration system
[23]	Solar chimney	Review on the solar chimney associated with PCMs
[24]	Medical application	Use of PCMs in medical application for thermal management
[25]	Textile	Implementation of PCMs in textile industries

Table 1.3 List of PCMs [26][27][28][29][30]

		Melting Point (°C)	**Latent heat (kJ/kg)**
Organic PCM	N-pentadecane	10	205
	Propyl palminate	19	186
	Paraffin C18	28	244
	Capric acid	36	152
	Medicinal paraffin	40-44	146
	Lauric acid	49	178
	Myristic acid	58	199
	Stearic acid	69.4	199
	Acetamide	81	241
Inorganic PCM	H_2SO_4	10.4	100
	P_4O_6	23.7	64

	$TiBr_4$	38.2	23
	$H4P_2O_6$	55	213
	$SbCl_3$	73.4	25
Eutectic PCM	$C_5H_5C_6H_5$+ $(C_6H_5)_2O$	12	97.9
	$C_{14}H_{28}O_2$+$C_{10}H_{20}O_2$	24	147.7
	Myristic acid + glycerol	31.96	154.3
	NH_2CONH_2+NH_4NO_3	46	95
	Palmitic acid + glycerol	58.5	185.9
	Stearic acid + glycerol	63.45	149.4
	$AlCl_3$+NaCl+KCl	70	209
	$LiNO_3$ + NH_4NO_3+NaNO3	80.5	113

1.3 Scope of research work

Thermal energy storage is essential for the efficient tapping of solar energy for various applications. In this direction, latent heat storage system (LHSS) has many advantages over other storage media. Therefore, to maximize the performance of latent heat storage system extensive research should be carried out. Along with thermophysical properties, there are many geometrical and operating parameters that influence the performance of the LHSS. Also, due to the low thermal conductivity of PCM augmentation of heat transfer methods should be explored. Hence, research can be done to improve the thermal behavior of LHSS by various influential parameters associated with heat transfer enhancement techniques. The present work is focused on analyzing the operating and geometrical parameters and also to improve the thermal performance of the LHSS by employing fins.

1.4 Organization of thesis

In this thesis, numerical and experimental analyses of the effect of various parameters on the performance of shell and tube LHSS under simultaneous charging and discharging are examined. The entire thesis is presented in 7 chapters.

Chapter 1 provides a brief introduction to thermal storage system and phase change materials

Chapter 2 presents the literature review on the charging / discharging process, simultaneous charging and discharging and heat transfer enhancement techniques employed in the LHSS.

Chapter 3 deals with the experimental and numerical procedure adapted in the current study

Chapter 4 provides the effect of heat transfer fluid parameters such as flow rate and inlet temperature on thermal performance.

Chapter 5 deals with the influence of the LHSS orientation on its thermal transport

Chapter 6 provides the numerical and experimental analysis of solid fins for heat transfer augmentation.

Chapter 7 details of experimental assessment of perforated fins on the flow behavior of PCM.

Chapter 8 provides the major findings of the current research work and the scope for future studies.

1.5 Closure

In this chapter, the feasibility of solar energy and need for the thermal energy storage is highlighted. The advantages of latent heat storage compared with other storage methods are briefly discussed. Also, the type of PCMs for low temperature applications and various industrial applications based on PCMs are reviewed. As a concluding remark, thermodynamic studies of latent heat storage need to be carried out and the influence of various parameters on the thermal performance of PCM should be conducted.

Chapter 2

Literature review

2.1 Introduction

Latent heat storage is essential to utilize solar radiation for various applications. In this direction, latent heat storage is proven to be superior and more effective than other storage methods. Latent heat storage systems (LHSS) exhibited better energy density and charging/discharging rate. The thermal performance of LHSS has a significant impact on the operating and geometric parameters which need to be analyzed. Also, for effective tapping of energy, the LHSS should be used continuously hence simultaneous charging and discharging process (SCD) is important. To enhance the thermal transport for the phase change material based applications multiple promising techniques are necessary. In this chapter, a brief literature review pertaining to individual and simultaneous charging and discharging is provided. Studies related to the influence of various parameters and thermal enhancement techniques are discussed.

2.2 Configurations of latent heat storage system

The performance of a latent heat storage system (LHSS) is mostly determined by the phase change materials (PCMs) and container shape. PCM is often chosen depending on the desired applications, temperature range and thermophysical properties. Another key factor to be considered is the selection of the geometry container. A comprehensive review of the literature on LHSS indicated that the most commonly used shapes are cylindrical and square cavity. Cylindrical containers are broadly divided into two main categories viz. triplex tube heat exchanger (TTHX) and shell and tube heat exchanger (STHX). In TTHX, three concentric tubes are used and PCM is placed in the middle tube. Whereas, in STHX, the heat transfer fluid circulated through pipe and PCM placed in the shell side. Agyenim et al. [30] highlighted that more than 70 % of work pertaining to LHSS is corresponding to the STHX. It was mentioned that the shell and tube type thermal storage system is preferred due to minimum heat loss to the surrounding. Also, STHX is considered to be a promising method for practical applications in terms of stability and easy of fabrication. Hence, STHX is chosen for current research work and most of the literature in the following section is pertaining to the STHX.

2.3 Effect of operational parameters on thermal performances of latent heat storage system

The parametric study of the LHSS plays important role in the thermal transport between the heat transfer fluid and PCM. Hence, it also effects the thermal performance of LHSS. Various researchers studied the influence of parameters viz. flow rate, inlet temperature and orientation of LHSS on the charging/discharging process.

2.3.1 Flow rate

The mass flow rate of heat transfer fluid (HTF) is an important parameter to study due to its direct effect on the heat transfer between the HTF and PCM. In this regard, Cao and Faghri [31] was the first study to conduct a parametric study on LHSS and compared the different mass flow rates. It was noted that the charging time decreased with the increase in mass flow rate. Agarwal and Sarviya [32] studied the flow rate on the discharging process and observed that discharging time reduces as the flow rate increases. Saddegh et al. [33] and Kibira et al [34] numerically investigated the influence of mass flow rate on the charging process. They highlighted that charging time reduces with the increase in mass flow rate. Esen et al. [35] conducted the numerical study on four different PCMs and the influence of mass flow rate on their charging time. It was observed that for all PCMs similar behavior was noted i.e decrease in melting time with the increase in mass flow rate. All the above studies suggested that as the flow rate increases the charging time decreases due to an increase in heat transfer rate. Wang et al. [36] studied the influence of mass flow rate on energy storage and found that with the increase in the mass flow rate from 0.0015 to 0.015 kg/s the energy storage was enhanced by 10 %. Contrary to this, Wang et al. [37] experimentally investigated the impact of mass flow rate on energy stored and reported that mass flow rate between 90 kg/h to 140 kg/h shows no difference in energy stored. In line with these works Akgun et al. [38] and Sari et al. [39] reported the insignificant effect of mass flow rate on thermal transport. Seddegh et al. [40] also reported that mass flow rate has negligible impact on the heat transfer coefficient. Therefore, there is ambiguity between the effects of mass flow on the thermal performance in literature. Therefore, it is necessary to study the influence of flow rate before performing the experimental work.

2.3.2 Inlet temperature

Fath [41] studied the impact of the HTF temperature on energy storage and heat transfer rate. It was noted that with the increase in HTF temperature the melting rate and energy stored increased. This increase was due to the increase in temperature gradient between HTF and PCM. Lacroix [42] carried out the experimental and numerical study and observed that the higher inlet temperature of HTF resulted in higher charging rate. Same result was also noted by Kabria et al. [43]. In their study, LHSS was considered in a horizontal position and the HTF inlet temperature varied from 77°C to 88°C during charging. The melted PCM was noted to decrease with the increase in heat transfer fluid inlet temperature. In line with this, Avci and Yazici et al. [44] observed that charging time decreased by 25 % if HTF temperature increased from 75°C to 85°C. Esen et al.[35] investigated the influence of the HTF temperature on paraffin wax. The result indicated that with the inlet temperature of 50°C the melting time for the PCM was 10 hr, whereas for 65°C the melt time decreased to 4 hr. Seddegh et al. [45] highlighted that the decrease of inlet temperature resulted in a higher charging time. The horizontal configuration was observed to attain superior thermal behavior of PCM during the charging process as compared to the vertical configuration. Kalapala and Krishna [46] evaluated the influence of mass flow rate, heat transfer fluid (HTF) inlet temperature and design parameters on thermal transport for a shell and tube heat exchanger. Aldine and Qarnia [47] analyzed the thermal performance of LHSS with different PCMs and investigated the impact of HTF inlet temperature on the melting behavior of PCM. The authors noted that HTF inlet temperature has a higher impact on the thermal behavior of PCM. Hosseini et al. [48] observed that with the increase in inlet temperature from 70 °C to 80 °C the charging time was noted to decrease by 37 %. Trp et al. [49] reported the effect of the inlet temperature of HTF on total energy storage and storage density. They observed that both the total energy storage and storage density increase with the increase in inlet temperature. From the above studies, it is observed that the temperature gradient between the inlet temperature of HTF and PCM is the driving force for thermal transport between HTF and PCM. Hence, the inlet temperature of HTF has a significant effect on thermal transport.

2.3.3 Orientation

In addition to the flow rate and inlet temperature of HTFs, the orientation of LHSS is an important parameter that influences thermal transport. The heat transport by buoyancy-

induced flow was observed to do a dominant part on the melting and solidification process. As convection heat transport is significantly influenced by the orientation of LHSS, it is vital to study the effect of orientation on the thermal performance of an LHSS. Seddegh et al.[33] numerically highlighted the effect of orientation on melting and solidification for vertical and horizontal LHSS. They reported that the rate of thermal transport was higher in the horizontal position in comparison to the vertical position. Koush et al. [50] experimentally analyzed the influence of inclination on the performance of LHSS by varying HTF inlet temperature. They considered 0°, 30°, 60° and 90° angles and found similar results as that of Seddegh et al. [33]. Siyabi et al. [51] reported melting behavior and propagation of melt profile of PCM along with the axial and radial directions. It was observed that the temperature gradient along the axial direction decreased as the orientation change from 0° to 90°. The solid-liquid interface movement was faster in the axial direction as compared to the radial direction for 0° and reverse for 90°. Recently, Kalapala and Krishna [52] performed energy and exergy analysis for the latent heat storage unit and observed maximum exergy efficiency at vertical configuration.

However, very less work is presented related to the effect of inclinations on the melting and thermal behavior characteristics of an LHSS when fins are attached to the HTF tube. Bouzennada et al. [53] carried out a numerical study to check the thermal behavior of PCM with 90°, 45° and 0° inclinations. They observed that with fins the melting time reduced by 1.28 %, 12.82 % and 20.52 % for 90°, 45° and 0° respectively. Mahdi et al. [54] reported that the influence of inclination is negligible with the introduction of fins. On other hand, Karami and Kamkari [55] numerically investigated the thermal behavior of finned LHSS at different orientations and observed that change in inclination angle from vertical to horizontal resulted in a decrease of melting time. However, Kalapala and Devanuri [56] explored the influence of orientation on the melting and solidification process of circular finned LHSS and came to a different conclusion. It was concluded that vertical arrangement has a larger thermal efficiency although the energy release rate is unaltered by the orientation. In contrast, Seddegh et al. [57] found that horizontal units perform effectively as compared to vertical configurations due to the strength of natural convection is less in the vertical position. From the above studies, it is noted that some work show horizontal and other shows vertical configuration as a better position. Therefore to get the optimum position it is necessary to further explore the orientation effect on thermal performance.

2.4 Heat enhancement techniques

Many researchers study the thermal performance of PCM under the charging/discharging process. They reported that due to the low thermal conductivity of the PCM melting rate was less. Therefore most of the recent studies focused on heat transfer enhancement techniques. Many researchers introduce different heat transfer intensifying methods for improving the thermal conductivity of PCMs. These techniques are mainly categorized into two types, firstly improve thermal transport between heat transfer fluid (HTF) and PCM by implementing the methods such as fins and heat pipe. Secondly enhanced the heat transfer within PCM by inserting the high thermal conductivity materials such as a nanoparticle, encapsulation of PCMs, etc. In this section, the works pertaining to all the heat transfer enhancement techniques are discussed. However, the review of literature is focused mainly on the employment of fins as in the present work the heat transfer enhancement technique using fins is considered.

2.4.1 Employing of fins

Fins are a well-known and effective approach for improving heat transfer rates. To boost the thermal efficiency in PCM-based heat exchangers, different types of fins such as longitudinal, radial, or circular fins as well as pin fins have been used. Longitudinal and annular fins are commonly utilized in shell and tube models, and the following discussion will focus on studies pertaining to design specifications for these fin types.

Circular fin

Circular/annular fins in shell and tube heat exchanger are used around the circumference of the heat transfer fluid (HTF) tube to improve the heat transfer between the HTF and PCM shown in Fig. 2.1. Yang et al. [58] investigated numerically the melting behavior of paraffin wax placed in shell and tube LHSS. They compared the melting time of PCM with fin and without finned surface and it is observed that melting time was significantly reduced by using circular fin. Inline to this analysis, Pu et al. [59] also compared the melting time of finned and without fin LHSS and revealed the same result as Yang et al. [58]. Cheng et al. [60] employed the circular fins in LHSS where paraffin melting behavior was observed. They stated that when the fin tube is replaced with the un-finned tube, the HTF flow rate has little influence on the heat transfer rate. Cheng et al. [60] employed circular fin configurations in a latent heat storage system where paraffin melting behavior was observed. They stated that when the fin tube is replaced with the un-finned tube, the heat transfer fluid

(HTF) flow rate has little influence on the heat transfer rate. Seeniraj et al. [61] suggested the fin-shell specifications and recommended the fin diameter should be equal to the shell diameter. This can provide better structure stability and also endorse cascade PCM arrangement.

The fin parameters such as fin thickness, fin radius, the distance between fins and the number of fins have a great effect on the performance of the LHSS. As fin radius and number increase subsequently area of heat transfer increases. Therefore, the rate of heat transfer also enhance. Moreover, this results to reduce the PCM volume which can impact the decrease in energy storage capacity of LHSS. Hence, such parameters should be optimized by taking into account the rate of heat transfer and energy storage. Zhao and Tan [62] carried out a numerical analysis of LHSS in terms of dimensionless radius (fin radius/outer radius) and observed that if the dimensionless fin radius is greater than 0.66 the impact of fin radius was insignificant. Ogoh and Groulx [63] highlighted the effect of fin number and reported that 15 fins are the optimized fin number. With a further increase in fin number, the maximum storage capacity of PCM was decreased. Inline to this, Jmal and Baccar [64] also reported the excessive number of fins effect the flow of PCM due to the smaller space available between fins. Thirunavukkarasu et al. [65] insisted on the optimization of the number of fins with respect to heat exchanger length. They stated that there is no substantial reduction in the melting time following a growing number of fins after a certain amount. However, Yang et al. [58] optimized the design parameters of fins for optimal reduction of the PCM melting time around the vertical finned tube (number of fins, fin height and fin thickness). The following optimized parameters have been observed: the fin thickness/ length ratio = 0.0248, number of fin = 31 and the fin pitch/ length ratio = 0.0313.

Shahsavar et al. [66] carried out numerical analysis to study the effect of fin parameters (thickness, location and diameter) during the melting and solidification of PCM. They observed that uniform distribution of fin improves the performance of LHSS during the melting process. On other hand, the non-uniform distribution of the fin gives a better performance during solidification. Furthermore, the melting time decreases by decreasing the thickness of the fin and the diameter of the fin up to a certain diameter. This is due to an increase in fin radius limiting the convection effects. Hence, operating parameters such as mass flow rate inlet HTF temperature should be amended to nullify this effect. The combined effects of fin geometric and operating parameters were also studied. Hosseini et al. [67] examined the overall effect of fin height and inlet HTF temperature on PCM

solidification and melting time. They found that the overall melting time decreases as the height of fins increase and melting time decrease even more with inlet temperature. They also stated that fin height affects the time to solidify PCM more than melting time. Elmaazouzi et al. [68] studied the effect of finned exchanger on the heat transfer rate. The height of the fins was increased the average heat transfer rate was increased by 50 % at a fin height of 14 mm. Santos et al. [69] compared the numerical data with experimental and developed the correction for the solid-liquid interface, velocity of PCM and discharging time. They proposed that their correlation can predict the solid-liquid interface, velocity of PCM and discharging time with deviations of 4 %, 7 % and 1.03 % respectively. Kalapala and Devanuri [70] experimentally observed the discharging process considering the orientation effect and indicated that orientation did not have any influence on the solidification process. This is due to the solidification process mainly depend upon the conduction which is independent of orientation.

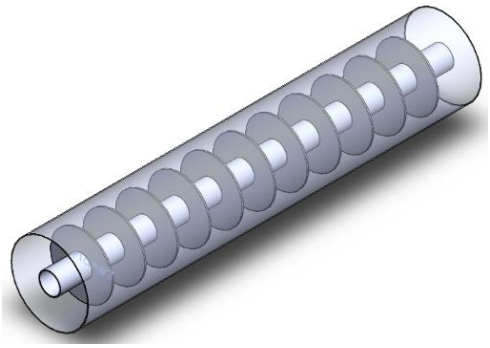

Fig.2.1 Circular or annular fin

Longitudinal fin

Many researchers successfully installed longitudinal fins as shown in Fig. 2.2 on the tube surface of LHSS. Khan and Khan [71] experimentally studied the charging behavior of paraffin with longitudinal fins. They compared the thermal response of shell and tube heat exchangers with various operating conditions. They observed that the influence of inlet temperature is more significant when compared to the mass flow rate of HTF during charging with longitudinal fins. Raul et al. [72] compared the melt fraction versus time with and without fins, a significant improvement in melt fraction by using longitudinal fins was noted. By observing the heat transfer rate over time, they also concluded that with the increase in the number of fins the rate of heat transfer increased. Rathod and Banarjee [73] have experimentally studied the impact of fins on paraffin wax charging and solidification

behavior with longitudinal fins and their findings showed that, as compared to charging, the effect of fins on solidification was more significant. The melt time was reduced by 24.52 % while the solidification time was 43.6 %. This work suggests that the use of longitudinal fins significantly increases the rate of heat transfer in the solidification and melting process regardless of the LHSS orientation.

Various authors optimized the parameters of longitudinal fins to achieve maximum heat transfer rate. Zhang et al. [74] studied the solidification behavior of finned tube for ice-storage application. They considered various fin parameters to reduce solidification time. The optimized parameters were observed to be: Fins number = 10, Fin Height = 40 mm and Fin width = 3 mm. They observed that fin number and width play insignificant role whereas fin height shows a significant role on the ice storage performance. Nobrega et al. [75] carried out an experimental investigation on the solidification characteristics of PCM around a vertical finned tube. They concluded that enhancement of solidification rate increases as fin width and fin number increase. They suggested number of fins equal to 5 and fin width of 50 mm has shown optimized solidification time. Shademan and Nezhad [76] optimized the number of fins in a LHSS and observed that a heat exchanger with more than 16 fins increases the melting time. Due to the restriction of flow for melted PCM which leads to the suppression of natural convection. They also studied the effect of boundary condition viz. couple and constant wall temperature and recommended that coupled boundary condition shows better thermal performance. Li et al. [77] carried out the numerical simulation to optimize the fin thickness and fin length of longitudinal fin and found out the optimized values such as fin thickness should be 2 mm and fin length should be 44 mm respectively.

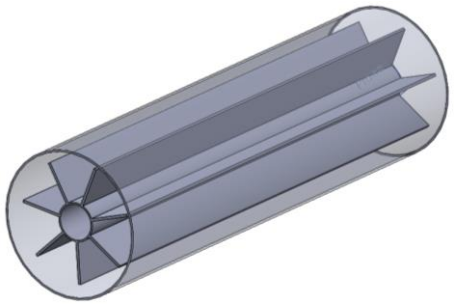

Fig. 2.2 Longitudinal fin

2.4.2 Heat pipe

Phase Change materials based LHSS play a very important role in many applications such as air conditioning, heating, and waste heat recovery. However, the low thermal

conductivity of PCM reduces and hinders thermal performance. LHSS embedded heat pipe (HP) is commonly utilized in applications due to its ability to transfer heat over a distance [78][79] and is shown in Fig. 2.3

Sharifi et al. [80] investigated the influence of heat pipe (HP) on the melting process of PCM. The performance of a vertical positioned heat pipe with PCM was simulated. Results showed that the melting rate of PCM was significantly improved due to HP. They also compared the HP, solid and hollow tube effect on the melting process. Out of all, HP provided the maximum melting rate. Shabgard et al. [81] analyzed the heat transfer process in the LHSS incorporated with HP. In their study, two cases were investigated with HP orientation. Case-1, PCM is placed inside the shell side and HTF flow through tube and Case-2, PCM is placed inside the tube and HTF flow over the PCM. In case-1 orientation of HP shows negligible changes in energy storage whereas, in case-2 orientation of HP shows significant influence on energy storage. They also observed that effectiveness of LHSS was decreased by increasing HP wall thickness. Nityanandam and Pitchumani [82] numerically investigated the HP-assisted LHSS and evaluated the thermal performance by varying parameters viz. length and radius of HTF tube and flow rate. They observed that the melting rate of the PCM decreases with mass flow rate and length, while similar trend is obtained for increasing radius. They also carried out studies similar to Shabgard et al. [81]. Results indicated that case-1 showed more effectiveness and lowered charging time as compared to case-2. Motahar et al. [83] experimentally investigated the influence of HP on the melting and solidification of PCM in shell and tube heat exchanger. A constant thermal reservoir was incubated to provide a constant temperature for heating and cooling of PCM. They observed that HP improved the heat transfer rate during the melting and solidification process. Melting time decreased by 53 % with 15 ^{o}C increases in temperature whereas, 49 % decrease in solidification time was observed with a decrease of 10 ^{o}C of the reservoir temperature.

Ebrahimi et al. [84] numerically investigated on the performance of LHSS with HP in shell and tube heat exchanger. The effect of parameters such as number of tube and angle of HP (0^{o} to 90^{o}) were studied. Results depicted that melting time reduce by 12 % with increasing tubes from one to three. HP with 30^{o} inclination reduces the melting time by 90 % when compared to no heat pipe condition. Chopra et al. [85] experimentally investigated HP embedded LHSS with and without PCM for the water heating system. Stearic acid was used as a phase change material. They observed that the thermal efficiency of LHSS with PCM-

HP was enhanced by 37.56 % as compared to the without PCM. Song et al. [86] optimized the HP parameter integrated with LHSS. The optimized parameters considered were length of the condenser, length of evaporator and length of PCM. They also gave the relation between the HP parameter and exergy efficiency using genetic algorithm. Results showed that optimized parameter were: length of evaporator = 0.36 m, length of condenser = 0.43 and length of PCM = 0.43 m with a maximum exergy efficiency of 97 %.

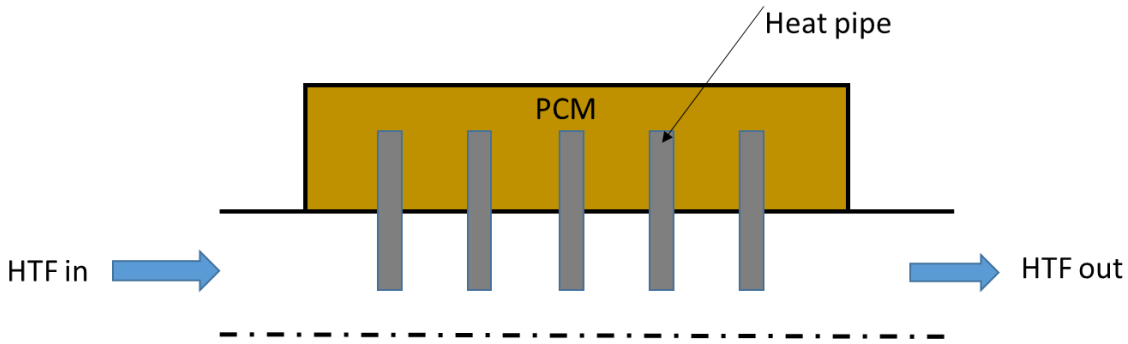

Fig. 2.3 Heat pipe associated with PCM

2.4.3 Dispersion of nanoparticles

The addition of nanoparticles to a liquid improves its thermal characteristics. Likewise, inserting nanoparticles to PCMs can be viewed as a viable solution for improving its thermal conductivity and enhanced thermal transport in latent heat storage. These kinds of PCMs are termed as nanoparticle enhanced phase change materials (NePCM) shown in Fig. 2.4. Khan et al. [87] analyzed the charging/discharging process with NePCM and observed that the percentage enhancement in the charging rate of SiO_2 based nano-PCM samples with 1% and 5% volume concentrations are 29.45% and 41.04%, respectively. Likewise, the discharging rates are improved by 21.09% and 30.08%, respectively. They also performed the economic assessment of NePCM and suggested that SiO_2, Al_2O_3, MgO and TiO_2 are preferable nano-additives due to their relatively lower cost and excellent thermal enhancement. Kant et al. [88] examined the concentration of graphene nanoparticles with different concentrations in LHSS and highlighted that the effective thermal conductivity of all three latent heat storage media can be significantly increased by using smaller volumetric concentrations of graphene particles although the convection heat transfer gets hampered by the same additives. Du et al. [89] numerically studied the effect of flow rate and temperature of HTF on NePCM and found out that increasing HTF inlet flow rate (from 0.25 to 1 m^3/h) would shorten the melting time by 9.29% (from 8080 to 7329 s). For the LHSS unit using

NePCM, increasing HTF inlet temperature (from 60 to 75 °C) can reduce the melting time by 34.68% (from 8080 to 5278 s). Deneshazarian et al [90] developed a new numerical approach to optimize the nanoparticle concentration in PCM. They suggested that the increase of wt % of NPs does not necessarily lead to an improvement in thermal storage capacity or heat transfer rate. In fact, at 0.5wt%, the nano-PCM presents the highest overall system efficiency. Akhmetov et al. [91] analyzed the thermal characteristics of NePCM to improve the energy storage design. They noted that nanoparticles, which enhanced the heat transfer properties of the PCM improved the charge and discharge performance of the sequentially connected LHSS devices, without significant reduction of the overall thermal energy storage capacity of the system. Regardless of the above study, many researchers focused on the thermal stability of the NePCM and their properties with respect to the concentration [92–101]

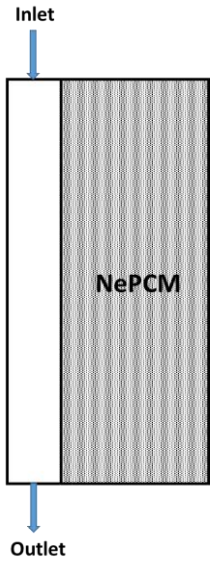

Fig. 2.4 Nanoparticle enhanced phase change materials (NePCM)

2.4.4 Metal foam

As previously stated, the PCMs' main disadvantage is their poor thermal conductivity. One way for improving PCMs thermal conductivity is to incorporate a high conductive porous metal foam such as copper or aluminum as shown in Fig. 2.5. Due to the porous structure of metal foams, it has a large surface area per specific volume and high thermal conductivity which makes it suitable for high heat transfer applications.

Yang et al. [102] numerically studied the circumferential and radial graded nickel foam and highlighted that circumferential graded metal foam (MF) introduce the non-uniform melting

of PCM and also improved the meting time by 38.60 %. Chibani et al. [103] numerically analyzed the heat transfer and energy storage of PCM with respect to MFs of different porosity. They suggested that the porosity of the MF play an important role, particularly when the selected MF is of lower thermal conductivity, i.e. like titanium as compared to copper and aluminum. Sardari et al. [104] examined the influence of porosity, pore density of MF on the melting performance of PCM. They also compared the LHSS unit with and without MF and observed that reducing the charging time by 85 %. Lei et al. [105] embedded the MF with the paraffin which resulted in a significant improvement of the heat transfer performance of LHSS. Compared with pure paraffin, the full melting time was reduced by 73.7%. Similarly, Wang et al. [106] presented the same observation. Chen et al. [107] numerically investigated the thermal transport between the HTF and PCM where MF is implemented on both sides (i.e on HTF and PCM side). They observed that the increase in HTF temperature reduces the charging time by 93.6 % and accelerated the heat transfer rate by 9 times as compared to without MF. Tian et al. [108] developed numerical models with a tilted design and validated them using experimental data melting interface progression and temperature data. The maximum difference in total melting time between the four orientations was 6.27 % (the case with 0.98 porosity and 10 PPI pore density). This indicated that tilted LHSS had only a little effect on the total melting time of PCM implanted in metal foams with varying pore characteristics. Duan and Li [109] studied the lab-based experiment associated with Artificial neural network (ANN) to examine the effect porosity and pore density of metal foam in the LHSS. ANN results were compared with the experiments and highlighted that ANN classifier can achieve the best performance of 92.5% accuracy, 87% precision, 100% recall. Various researchers also showed the effect of porosity, pore density, gradient MF on thermal performance [110–117].

Venkateshwar et al. [118] numerically developed the imperial correlation to evaluate the effect of porosity on solidification time. They also observed that inserting a Cu metal foam with 0.99 porosity gave 40 % less solidification time whereas SS metal foam shows 2 %. Alhusseny et al. [119] analyzed the bundled tube LHSS with different tube numbers viz. 15, 20, 25 and 30 with pore density 25 PPI. It was noted that more number of tubes increased the discharging process due to the acceleration of thermal transport between the water and PCM-metal foam composite. Sardari et al. [120] compared the discharging time of pure PCM and MF-PCM composite. It was observed that solidification time and heat retrieved from PCM are enhanced by 45 % and 75 % respectively. They also studied the effect of

inlet temperature of cold fluids with 0°C, 10°C and 22°C with MF and observed that at lower temperatures of cold HTF amount of heat from PCM retrieved is more.

Fig. 2.5 Shell and tube heat exchanger with metal foam [121]

2.4.5 Encapsulation

This is another method to enhance the heat transfer rate of PCM by coupling with suitable material (coating /shell). Encapsulation PCM is classified into two main criteria i.e macro-encapsulation and micro-encapsulation based on shape or size. An encapsulation shell larger than 1 mm is referred to as micro-encapsulation whereas an encapsulation shell size smaller than 1 cm is macro-encapsulation. Each method has its own advantage. Macro-encapsulation flexible in shape and size leads to a simple manufacturing process according to practical application. Using macro- encapsulation mechanical stability of PCM system was improved. In addition, micro-encapsulation increases the heat transfer rate due to the higher surface to volume ratio, homogenous PCM melting and solidification processes.

Xu et al. [122] experimentally investigated latent heat storage system integrated with macro-encapsulated PCM during the charging and discharging process. They studied the effect of parameters such as mass flow rate, inlet temperature of HTFs and orientation on the melting and solidification process. They observed that the increase in the HTF inlet temperature from 55 °C to 60 °C reduces the melting time by 42 %. During solidification, by reducing the inlet temperature from 35 °C to 30 °C solidification time was decreased by 52 %. Similarly, increasing the mass flow rate of HTF from 1.5 to 4.3 l/h, solidification and melting times reduced by 14 and 13 % respectively. Furthermore, comparing vertical and horizontal configurations, vertical orientation shows a higher natural convection effect and reduces the melting time by 20 %. Aziz et al. [123] experimentally and numerically studied the performance of encapsulated PCM in shell and tube heat exchanger. Three configurations of encapsulated PCMs (with and without pin, with and without copper

plating) were investigated. They observed that the encapsulated PCM with pin reduced the melting time by 27 %, whereas with copper coating decreases by 37 % as compared to plain encapsulated PCM. He et al. [124] investigated the latent heat storage system with and without encapsulated PCM. The result depicted that encapsulated PCM gave improved performance and extracted more energy from the PCM. Fang et al. [125] analyzed the temperature distribution at various radial positions and the progress of solid-liquid interface for the thermal energy storage system. They investigated the effect of encapsulated particle fraction and PCM core fraction. They concluded that more encapsulation particle fraction leads to more accumulated energy by the PCM. However, small difference in temperature profile and accumulated energy with different core fractions was observed. Amin et al. [126] studied the suitability of Ɛ-NTU method for thermal energy storage system with encapsulated PCM. An empirical correlation was evaluated to find out the effectiveness at a given mass flow rate. They observed that the increase in the mass flow rate decreased the effectiveness of LHSS. Lee et al. [127] studied the effect of capsule conduction and capsule outside convection on the latent heat storage system. They considered three models based on boundary conditions on the external surface of capsule i.e isothermal surface, constant temperature and natural convection. They concluded that constant temperature and convection boundary condition outside the capsule resulted to lower discharging rate than isothermal condition alone. They also suggested that capsule material with low thermal conductivity should be preferable.

2.4.6 Comparison of various heat enhancement techniques

Comparing bibliographic analysis for charging/melting and discharging/solidification process with different heat transfer enhancement methods are given in Fig. 2.6. In this analysis data is extracted from the web of science. In early 2015, study on encapsulated PCM is another research area that has grown rapidly due to the leakage of PCMs during melting and reaction of shell materials with PCMs. Still, studies on encapsulated PCMs related to the thermal and chemical stability of PCMs and shell materials should be carried out. From 2016-2018 the PCMs literature is more focused on the thermal performance of PCMs during the charging and discharging process. At this time more literature related to the metal foam and heat pipe enhancement techniques were published. From 2018-2020 there was large focus on the development of heat transfer enhancement techniques to improve the thermal performance especially by using fins and nano particles, composite PCMs. Most of the research is associated with the fin parameters and hybrid nanoparticles.

Embedding the metal foam increases the weight and cost of LHSS, moreover the thermophysical properties of PCM when embedded in metal foam may get deteriorated. Similarly, nano enhanced PCMs thermal stability needs a proper investigation. On the other hand, employing fins is very efficient and easy to fabricate. Hence for the current research work, fins are chosen for augmentation in heat transfer rate.

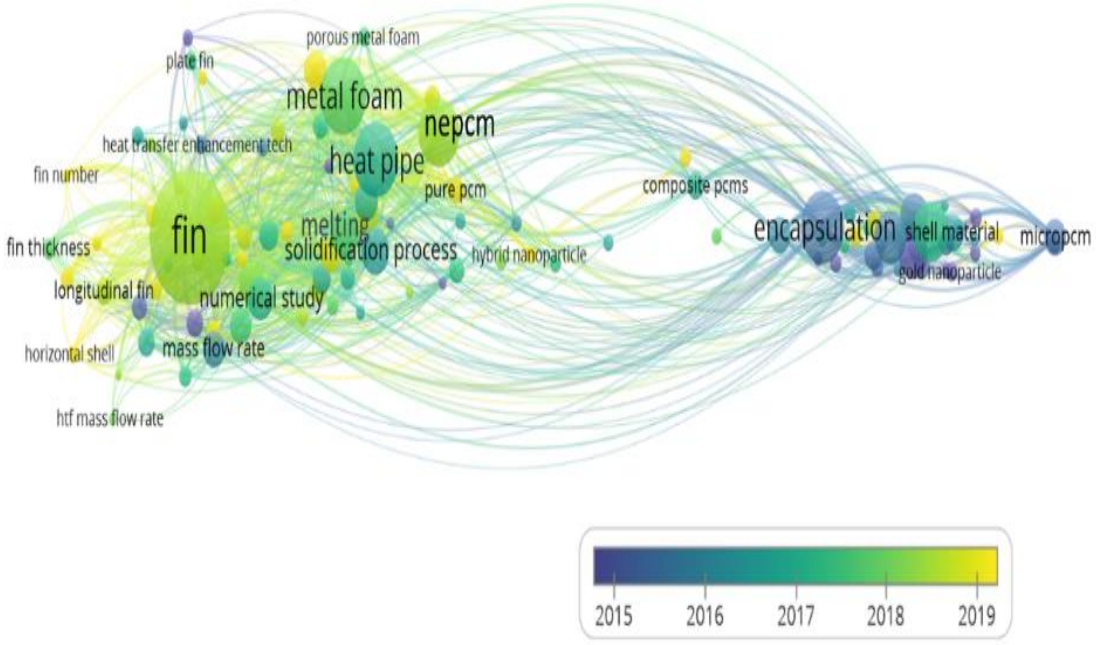

Fig. 2.6 Bibliographic analysis of research article with heat transfer enhancement techniques from 2015-2020

2.5 Simultaneous charging and discharging

Most of LHSS research often focuses on the charging or discharging process separately, with the premise that the systems can be charged or discharged without interruption. In real life applications, the discontinuous energy supply and fluctuating energy demand may occur at the same time. To prevent repeated On/Off between the charging and discharging process and to maintain stable operation, LHSS should be charged/discharged simultaneously. Fig. 2.7 shows the simultaneous charging and discharging process (SCD) where the hot and cold HTF are circulated through the tube simultaneously.

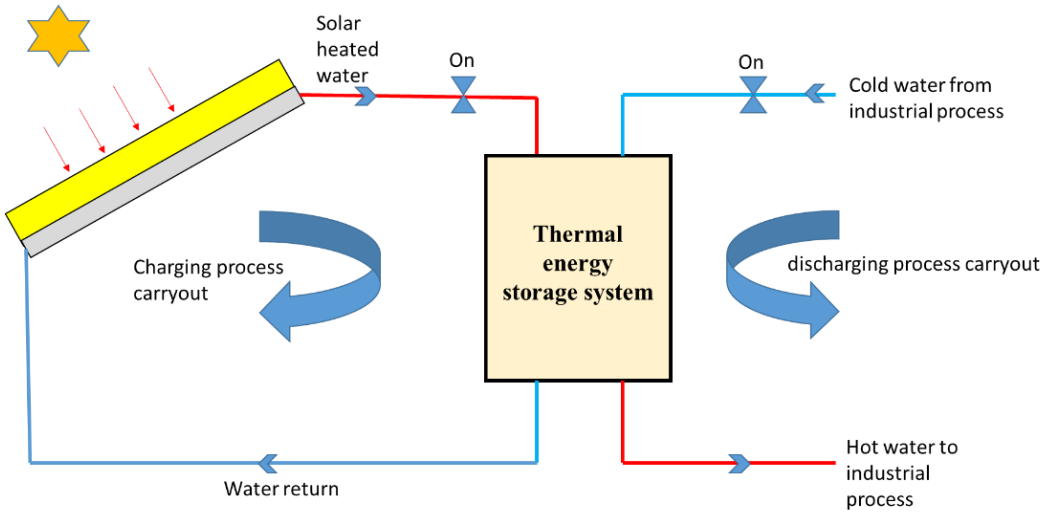

Fig. 2.7 Schematic view of simultaneous charging and discharging process

In the SCD process, Liu et al. [128] carried out the experiment based on the thermal resistance analysis in 2005 on heat pipe. They observed that during the SCD process, more heat is absorbed by the cold HTF due to the less thermal resistance between the cold and hot HTF pipes compared to the thermal resistance of the PCM side. This is usually a desirable case, in most practical situations; the heat is expected to be transferred from the hot fluid mainly to the cold fluid. Wang et al. [129] carried out experiments and analyzed the energy storage of air heater integrated with heat pipe and solar collector. It was obtained that the low airflow led to high outlet temperature and low useful power. The high flow rate resulted in a high convective heat transfer coefficient. However, the heat exchange time between HTF and heat pipe decreased. Liang et al. [130] studied the influence of cold HTF inlet temperature, flow rate and initial condition of PCM (solid and liquid) associated with metal foam under the SCD process. When cold water temperature reduces from 30°C to 25°C the melting time increases by 25 %. Therefore, the lower temperature of cold water reduces the charging time by absorbing more heat from the PCM. They also highlighted the influence of flow rate, initial condition and metal foam of PCM does not effect the final temperature of PCM. However, metal foam greatly influences the time required to attain the steady state condition. Sharifi et al. [131] considered the effect of aspect ratio (height to diameter) of the heat exchanger and observed that a larger enclosure i.e 40 mm height and 20 mm diameter shows better thermal performance. Based on the geometry of LHSS during the SCD process, the following literature is presented.

2.5.1 Shell and tube heat exchanger

Murray and Groulx [132] experimentally investigated the vertical LHSS which is charged and discharged simultaneously and examined the thermal behavior based on the initial condition of PCM and intermitted flow rate. Also, thermal transport during simultaneous operations was investigated. Result depicted that the rate of heat transfer differ according to the initial condition of PCM. It was noted that higher energy exchange occurred between the cold and hot HTFs through initially melted PCM. However, the energy transport between cold and hot HTFs through solid PCM was constrained by the thermal resistance offered by the solid PCM. Fang et al. [133] analyzed the thermal performance of latent thermal energy storage system when charged and discharged simultaneously. The temperature and stored energy in the LHSS as well as the charging/discharging power were studied under various charging/discharging flow rates and initial states of the PCM. It was noted that the variation of power due to the change in thermal transport between the HTFs and PCM. Initially, the energy storage by the PCM was more and then the stable condition was achieved. Thus, the energy storage process was gradually shifted to the direct thermal transport between the cold and hot HTFs. Omojaro and Breitkopf [134][135] experimentally studied the SCD process where PCM was placed inside the annulus and the cooling air was externally circulated over the annulus. The time-dependent temperature profile was utilized to assess the influence of heat flux on the liquid fraction and the time required to change the conduction to convection mode of heat transfer (transition-time). The result demonstrated that heat flux does not show significant influence on the conduction heat transfer when compared to effect on the natural convection. However, it has a considerable impact on transition-time and melting rate with larger heat fluxes yielding a melt fraction of 38–63 % higher for the SCD process. Mazhar et al. [136] numerically optimized the plate fin parameters such as pitch and size and also compared the LHSS with and without fins. They observed that 40 × 90 mm and 10 mm pitch gave higher thermal performance. It was noted that finned LHSS shows the 72.44 % higher thermal efficiency as compared to non-finned LHSS. ELSihy et al. [137] analyzed the SCD condition with different flow rates and observed that larger charging flow rates and shorter non charging periods gave the better thermal performance of PCM. It was observed that increasing the flow rate ratio leads to an increase in thermocline thickness. Mahadavi et al. [138] employed the four tubes inside the LHSS which consists of two tubes for hot HTF and two tubes for cold HTF. The objective of their study was to evaluate the melting process of PCM associated with fin and

nanoparticles. Comparing the effect of fin and nanoparticle, adding nanoparticles was to compensate the weak thermal conductivity of paraffin. The study did not demonstrate any justifiable improvement under SCD.

2.5.2 Triplex tube heat exchanger

Mahdi et al.[139] analyzed the thermal behavior of the triplex tube heat exchanger (TTHX) by employing the novel fins and nanoparticles. They optimized the angle of upper side of the fins and angle between the V-shaped fins at the bottom of TTHX. The optimized values of angle of upper side and V-shaped fins were 51.20° and 34.74° respectively. They also compared the optimized fins with the nanoparticle. It was noted that fins configuration gave better thermal response as compared to the nanoparticle. Joyabri et al. [140] investigated the different cases as shown in Fig. 2.8 based on the boundary condition and initial condition shown in Table. 2.1. They compared the results by two models: firstly, pure conduction was taken and second natural convection. They observed that Case-1 gave better heat transfer enhancement as compared to the case-3 with natural convection models. For Case-2 and case-4 which is initially melted PCM condition pure conduction can be applied. Further Joyabri et al. [141] studied the case-1 to improve the thermal performance of PCM by employing fins. They optimized the fins based on the position and number of fins. They recommended that one external fins (90°) and three internal fins at bottom portion of TTHX (225°, 270° and 315°) gave the better thermal performance.

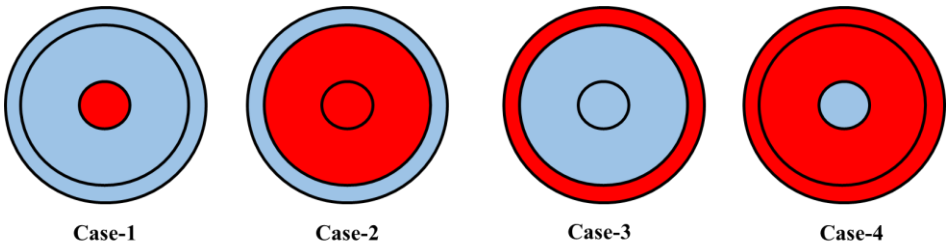

Fig. 2.8 TTHX with different boundary condition and initial temperature of PCM [140]

Table. 2.1 Different boundary condition and initial temperature of PCM

Case	Boundary condition	Initial condition of PCM
1	Internal heating and external cooling	Solid
2	Internal heating and external cooling	Liquid

3	Internal cooling and external heating	Solid
4	Internal cooling and external heating	Liquid

2.5.3 Square cavity

Wang et al. [142] developed the analytical equation considering conduction as a dominant mode of heat transfer in the PCM. However, they also suggested that this method leads to unacceptable error when natural convection was considered into account. Arlcl et al. [143] studied the effect of nanoparticles on the performance of melting and energy storage of PCM filled in an enclosure. They considered the alumina nanoparticle with volume fractions of 0, 1, 2 and 3 %. For, 1 % volume fraction of nanoparticles the stored energy was 67.2 kJ whereas 65.3 kJ was observed for 3 % volume fraction. The decrease of energy storage is due to more nanoparticles, which increases the viscosity thereby resists the fluid motion, and an increase of viscosity reduces the benefit of natural convection. They also noted that nano-enhanced PCM gave 3.6 % higher stored energy as compared to pure PCM for 1% volume fraction. Nie et al. [144] analyzed various different positions of cold and hot walls. It was noted that heating from the bottom shows a higher melt fraction and energy storage capacity. The position of cold portion does not show significant effect on the charging process. They highlighted that strength of natural convection depends on the position of cold and hot portions. The positions of the cold portion at the bottom suppressed the natural convection more as compared to the hot portion at bottom. Hong et al. [145] numerically studied the thermal behavior of PCM and the effect of mushy zone constant. It was noted that the rate of energy storage was maximum for mushy zone constant $10^{4,}$ after that rate of energy storage decreases with increases in mushy zone constant from 10^5 to 10^8. Hong et al. [146] also studied the effect of orientation of square cavity at 0°, 30°, 45°, 60° and 90° angles. It was observed that inclination angle affects the energy stored at the given melting time. The maximum energy stored is found for inclination angle 0° and the minimum energy stored for inclination angle 90°. From Fig. 2.9 bibliographic analysis is considered to compare the charging/discharging and SCD process. From the figure it is noted that the SCD process are at early stage of development as compared to the charging/ discharging process and has not garnered much attention over a years. Most of the research articles were focused on the separate charging/discharging process.

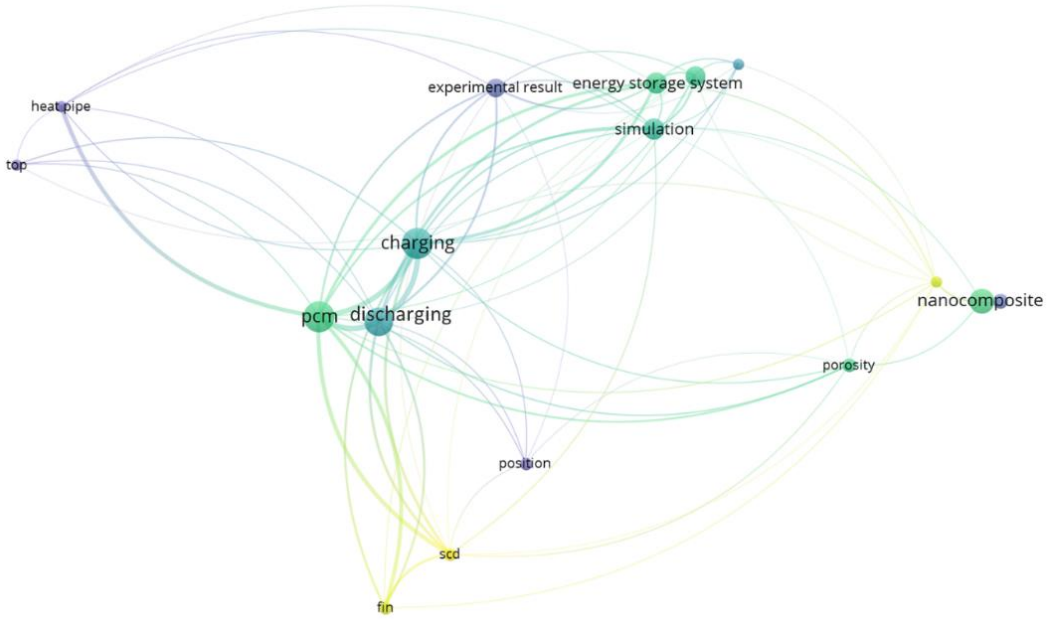

Fig. 2.9 Bibliographic analysis of research articles on SCD process from 2015-2021

2.6 Observation from literature review

- There are several parameters that influence the thermal transport of the shell and tube heat exchanger. The influence of mass flow rate, inlet temperature and orientation was studied by several authors. However, there is ambiguity for the reported thermal performance of vertical and horizontal configurations.
- A comprehensive search and analysis of the available literature highlighted that most research that was conducted on LHSS focused on the separate charging or discharging process.
- Although many studies were conducted on thermal intensification, further work is needed to fully explore the insight of thermal transport. Most of the LHSS strategies were designed based on heat transfer enhancement with indivisible charging and discharging process.
- The use of SCD techniques were very superior, which enables to apply the PCM based latent heat storage system in practical applications. However, the SCD process is at early stage of development and most of the literature focused on the thermal performance of PCMs. Very limited study was presented on the SCD process with heat transfer augmentation. Hence, in the current research work, SCD process is carried out by employing fins.

2.7 Research gap

- Numerical and experimental investigation to analyze the melting behavior for a LHSS with simultaneous charging and discharging is scarce.
- Effects of HTF parameters such as flow rate and inlet temperature on SCD were not addressed in the literature
- Effect of inclination on the thermal performance of LHSS needs further investigation as the existing studies contradict each other's results.
- Studies pertaining to the influence of the orientation of finned LHSS on its performance are very few and no study is available examining the effect of inclination when annular perforated fins are employed.
- Providing perforations for annular fins can enhance the thermal performance of the LHSS but no study is available on effect of perforation for SCD.
- Studies on energy and exergy analyses of a shell and tube latent heat storage system positioned at different orientations are scarce.

2.8 Objective

Based on the above-mentioned research gaps, the following objectives are formulated for a shell and tube LHSS under simultaneous charging and discharging (SCD) process.

1. To study the effect of inlet temperature and mass flow rate of heat transfer fluids on the phase change behavior and thermal transport.
2. To study the effect of orientation on the performance of the LHSS.
3. To employ the solid fins for heat transfer intensification and evaluate the effect of orientation on the performance of LHSS.
4. Compare the performance of perforated finned LHSS with and without solid finned LHSS at different orientations.

2.9 Closure

A comprehensive literature review on the effect of various factors on the thermal performance of a shell and tube latent heat storage system is provided. Various thermal transport enhancement approaches are being investigated. Fins were noted to the least expensive, most dependable, and require no fabrication complexity. By thoroughly identifying the research gaps, objectives for the current research work were framed. To achieve the proposed objectives both experimental and numerical experiments are needed, the details of which are discussed in the next chapter.

Chapter 3

Experimental and numerical methodology

In the previous chapter, numerous works pertaining to shell and tube latent heat storage unit were discussed and depending on the research gaps objectives were framed. To accomplish these objectives an experimental test facility was designed and fabricated. Along with the experimental work, numerical simulations are also carried out for scrupulous analysis of the phase change behavior of the PCM. The details of the experimental setup and the numerical methodology adopted for the simulations are discussed in the current chapter. The methodology adopted for evaluating various performance parameters from the experimentally measured temperature values is also provided in this chapter.

3.1 Experimental setup

The experimental facility utilized for the current analysis is given in Fig. 3.1. The LHSS consists of the shell having 254 mm (length) and 100 mm (outer diameter), which is manufactured by polycarbonate for the visualization of the solid-liquid interface. Two stainless steel tubes are used for charging and discharging of PCM due to its good corrosive resistance property with PCM [147]. Each tube has 12.7 mm inner diameter and a thickness of 1.4 mm. For simultaneous charging and discharging processes, hot HTF is circulated through one tube whereas cold HTF is circulated through another tube at the same time from the hot and cold baths. Water is used as HTF and the space between the shell and the tubes is filled with lauric acid. Hot and cold baths are installed with a digital PID controller to maintain the baths at a constant temperature. HTF flow rate in both tubes is monitored by a digital flow meter. In order to change the orientation of the LHSS, an angle adjuster is provided. Thirteen K-type thermocouples are coupled with a data acquisition system to evaluate the temperature of PCM at various locations of LHSS. Thermocouples are positioned in such a way both axial and radial direction temperature measurement is possible.

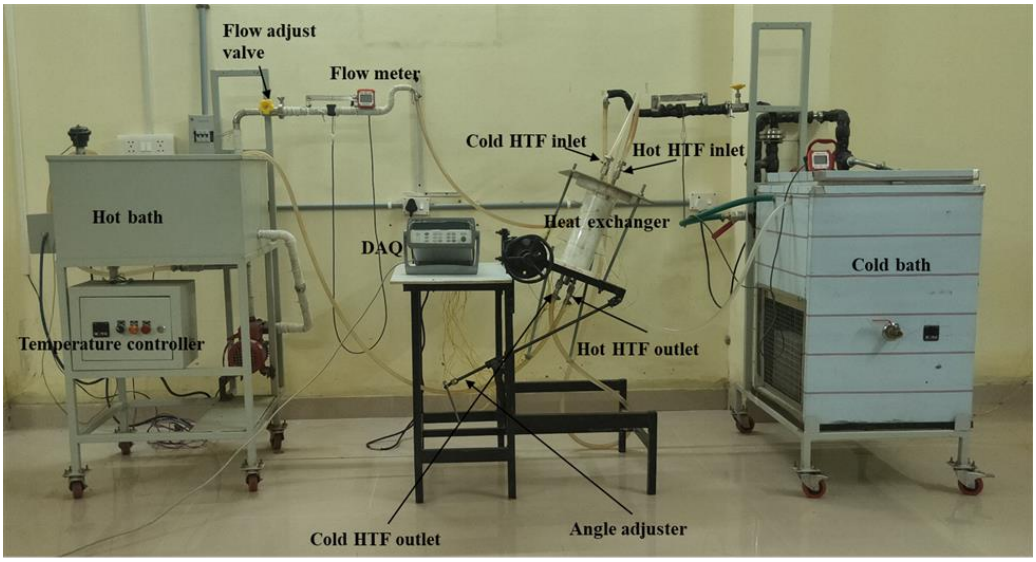

Fig.3.1: Experimental setup

3.2 Data reduction

The PCM average temperature is calculated from the experimental data by using the weighing method developed by Kalapala and Krishna [52]. The control volumes are created around each thermocouple as shown in Fig. 3.2. As the control volume of each thermocouple (T_i) is not the same a weighting factor (w_i) (control volume of the thermocouple (V_i)/total volume (V_t)) is calculated for each thermocouple. Based on the weighing factor the average temperature is calculated as

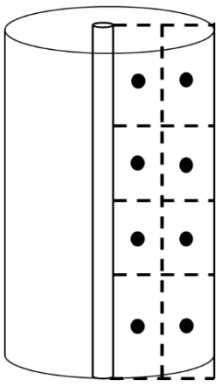

Fig. 3.2 Control volume for each thermocouple

$$T_{avg} = \sum w_i . T_i \quad (3.1)$$

The melt fraction is computed based on the temperature within each control volume. The melt fraction is given by

$$\gamma_i = \begin{cases} 0 & T < T_{solidus} \\ \frac{T_i - T_{solidus}}{T_{liquidus} - T_{solidus}} & T_{solidus} \leq T \leq T_{liquidus} \\ 1 & T > T_{liquidus} \end{cases} \quad (3.2)$$

$$\gamma = \sum W_i \gamma_i \quad (3.3)$$

Where, T_i is the instantaneous temperature of the thermocouple at each control volume and γ is the melt fraction of PCM.

The energy input and output by the hot and cold HTFs are estimated by Eqs. (3.4) and (3.5)

$$Q_{input} = \dot{m}_h C_{p,HTF} (T_{in,h} - T_{out,h}) \quad (3.4)$$

$$Q_{output} = \dot{m}_c C_{p,HTF} (T_{out,c} - T_{in,c}) \quad (3.5)$$

The energy stored by the PCM is given as eq. (3.6)

$$E_{stored} = \begin{cases} mC_{ps}(T_i - T_{ini}) & T_i < T_s \\ mC_{ps}(T_s - T_{ini}) + m\gamma L & T_s \leq T_i \leq T_l \\ mC_{ps}(T_s - T_{ini}) + mL + mC_{pl}(T_i - T_l) & T_i > T_l \end{cases} \quad (3.6)$$

The exergy of the LHSS can be estimated based on the following Eqs. (3.7)-(3.10)

$$\Delta Ex_{in(hot,HTF)} = \dot{m}_h C_{p,HTF} \left[(T_{in,h} - T_{out,h}) - T_a \, ln \left(\frac{T_{in,h}}{T_{out,h}} \right) \right] \quad (3.7)$$

$$\Delta Ex_{out(cold,HTF)} = \dot{m}_c C_{p,HTF} \left[(T_{out,c} - T_{in,c}) - T_a \, ln \left(\frac{T_{out,c}}{T_{in,c}} \right) \right] \quad (3.8)$$

$$\Delta Ex_{stored} = \dot{m}_h C_{p,HTF} (T_{in,h} - T_{out,h}) \left(1 - \frac{T_a}{T_{avg}} \right) \quad (3.9)$$

$$\Delta Ex_{released} = \dot{m}_c C_{p,HTF} (T_{out,c} - T_{in,c}) \left(1 - \frac{T_a}{T_{avg}} \right) \quad (3.10)$$

Here T_a and T_{PCM} is the ambient temperature and average temperature of PCM respectively.

Similarly, exergy efficiency under SCD can be defined by Eqn. (3.11).

$$Exergy\ efficieny \quad (\eta) = \frac{\Delta Ex_{stored} - \Delta Ex_{released} - \Delta Ex_{out(cold\ HTF)}}{\Delta Ex_{in(hot\ HTF)}} \quad (3.11)$$

3.3 Numerical procedure

The enthalpy-porosity approach is used in this analysis to simulate the LHSS. The liquid-solid interface is explicitly specified in terms of the mushy zone. The ANSYS workbench is used to create geometry and mesh. Structured meshing is performed for both vertical and horizontal LHSS. The following assumptions are considered for numerical modeling

- The solid and liquid phases of the PCM are considered to be homogenous and isotropic
- The Boussinesq approximation is regarded as valid for the density change of liquid PCM.
- Viscous dissipation effect is negligible
- The HTF flow is considered to be laminar

The 3-D model is used to analyze the performance of LHSS. The fundamental equations for conservation of mass, momentum, and energy can be written as

Continuity equation:

$$\frac{1}{r}\frac{\partial}{\partial r}(v_r r) + \frac{1}{r}\frac{\partial}{\partial \theta}(v_\theta) + \frac{\partial}{\partial z}(v_z) = 0 \tag{3.12}$$

Momentum equation:

$$\rho\left[\frac{\partial v_r}{\partial t} + \frac{1}{r}\frac{\partial(r v_r v_r)}{\partial r} + \frac{1}{r}\frac{\partial(v_r v_\theta)}{\partial \theta} + \frac{\partial(v_r v_z)}{\partial z}\right] = -\frac{\partial p}{\partial r} + \mu\left(\frac{\partial}{\partial r}\left[\frac{1}{r}\frac{\partial}{\partial r}(r v_r)\right] + \frac{1}{r^2}\frac{\partial^2 v_r}{\partial \theta^2} - \frac{2}{r^2}\frac{\partial v_\theta}{\partial \theta} + \frac{\partial^2 v_r}{\partial z^2}\right) + \rho g_r \beta\left(T - T_{ref}\right) - A v_r \tag{3.13}$$

$$\rho\left[\frac{\partial v_\theta}{\partial t} + \frac{1}{r}\frac{\partial(r v_r v_\theta)}{\partial r} + \frac{1}{r}\frac{\partial(v_\theta v_\theta)}{\partial \theta} + \frac{\partial(v_\theta v_z)}{\partial z}\right] = -\frac{\partial p}{\partial \theta} + \mu\left(\frac{\partial}{\partial r}\left[\frac{1}{r}\frac{\partial}{\partial r}(r v_\theta)\right] + \frac{1}{r^2}\frac{\partial^2 v_r}{\partial \theta^2} + \frac{2}{r^2}\frac{\partial v_\theta}{\partial \theta} + \frac{\partial^2 v_\theta}{\partial z^2}\right) + \rho g_\theta \beta\left(T - T_{ref}\right) - A v_\theta \tag{3.14}$$

$$\rho\left[\frac{\partial v_z}{\partial t} + \frac{\partial(v_r v_z)}{\partial r} + \frac{\partial(v_z v_\theta)}{\partial \theta} + \frac{\partial(v_z v_z)}{\partial z}\right] = -\frac{\partial p}{\partial z} + \mu\left(\frac{\partial}{\partial r}\left[\frac{1}{r}\frac{\partial}{\partial r}(r v_z)\right] + \frac{1}{r^2}\frac{\partial^2 v_z}{\partial \theta^2} + \frac{\partial^2 v_z}{\partial z^2}\right) + \rho g_z \beta\left(T - T_{ref}\right) - A v_z \tag{3.15}$$

In the above equations (Eqs.3.13, 3.14, and 3.15) "A" could be applied to the momentum equation to assume the effect of phase change on convection and velocity field in the solid phase to be zero. This momentum term is defined as

$$\mathrm{A} = \frac{C(1-\gamma)^2}{\gamma^3 + \varepsilon} \tag{3.16}$$

Where $''\gamma''$ is the melt fraction of the PCM. To avoid the infinite in denominator $''\varepsilon''$ is a computational constant which is introduced with a value of 0.001 [45]. "C" is a mushy zone constant in Eq. 16 that disciplines the transmission of the convection field into the mushy zone. For most methods, the mushy zone constant is recommended between 10^4 and 10^7 [46]. In the current simulation 10^5 is considered as the mushy zone constant [47].

Energy equation:

$$\rho\left[\frac{\partial h}{\partial t}+\frac{1}{r}\frac{\partial(rv_r h)}{\partial r}+\frac{1}{r}\frac{\partial(v_\theta h)}{\partial \theta}+\frac{\partial(v_z h)}{\partial z}\right]=\frac{k}{c_p}\left(\frac{1}{r}\frac{\partial}{\partial r}\left[r\frac{\partial h}{\partial r}\right]+\frac{1}{r^2}\frac{\partial^2 h}{\partial \theta^2}+\frac{\partial^2 h}{\partial z^2}\right)+S_h \tag{3.17}$$

Where the source term is:

$$S_h=\frac{\partial(\rho\Delta H)}{\partial t}+\frac{1}{r}\frac{\partial(\rho r v_r\Delta H)}{\partial r}+\frac{1}{r}\frac{\partial(\rho v_\theta\Delta H)}{\partial \theta}+\frac{\partial(\rho v_z\Delta H)}{\partial z} \tag{3.18}$$

In this equation h and ΔH account for sensible and latent heat respectively. Whereas,

$$\Delta H=\gamma\lambda \tag{3.19}$$

Where"γ" is the melt fraction and "λ" is the latent heat of fusion

$$\gamma=\begin{cases}0 & T<T_s\\ \frac{T-T_s}{T_l-T_s} & T_s\le T\le T_l\\ 1 & T>T_l\end{cases} \tag{3.20}$$

A commercial CFD tool ANSYS-Fluent is used to simulate the thermal transport in an LHSS. For pressure and velocity coupling, the SIMPLE method is adopted. The second-order upwind approach is utilized for convective formulation. The PRESTO approach is employed for pressure spatial discretization preferring better prediction by avoiding interpolation mistakes. To ensure the exactness of the results, convergence criteria of 10^{-6} is set for momentum equations and 10^{-8} for energy equation. The simulations are carried out on a Workstation with 64GB RAM and 16 core CPU.

Chapter 4

Effect of heat transfer fluid parameters on the thermal performance of latent heat storage system

4.1 Introduction

The study pertaining to the influence of operating parameters on the melting characteristics of a PCM is necessary for the understanding of heat transport. While before experimenting a latent heat thermal storage system it is essential to analyze the effect of heat transfer fluid (HTF) parameters to arrive at the optimum. It was noted that mass flow rate and inlet temperature of HTF are the most influencing parameters. After a thorough review of literature pertaining to the studies on the effect of flow rate and different inlet temperatures on the performance of a shell and tube LHSS, a contradiction among the results is noted. One of the reasons can be the difference in design parameters. Hence, current chapter includes the effect of flow rate and inlet temperature on the latent heat storage system.

4.2. Physical Model

The simulation model of a shell and tube type latent heat storage system (LHSS) under SCD processes is shown in Fig. 4.1. Phase change material (PCM) is placed in the space between the shell and two HTF tubes. The PCM considered for the study is lauric acid [151]. Lauric acid is chosen in this simulation due to its high latent heat and small volume change during the phase transition process. The thermophysical properties of lauric acid are given in Table 4.1. The HTF tubes are used to circulate cold and hot fluids. Stainless steel tubes are used due to their good corrosive resistance property with lauric acid [147,152]. The LHSS is considered in two positions (vertical and horizontal) for numerical investigation. The geometric parameters considered for the study are: length of LHSS is 254 mm, the inner radius of a shell is 100 mm, the inner radius of both HTF pipes is 12.7 mm and the thickness of HTF pipe is 1.4 mm. Both HTFs are fed from the top due to the thermocline temperature profile obtained during melting and reduction in melting time [153]. Water is used as an HTF. The initial temperature of PCM is taken as ambient i.e. 27°C.

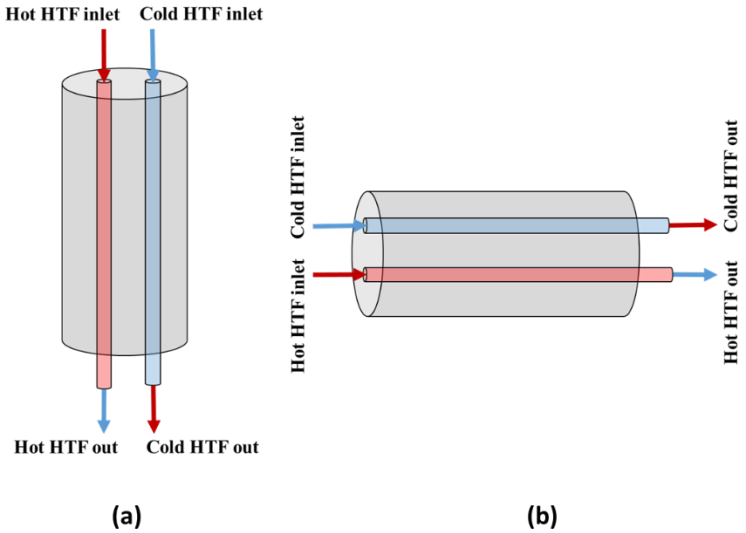

Fig. 4.1: Shell and tube heat exchanger during SCD (a) Vertical (b) Horizontal configurations

Table 4.1: Thermophysical properties of lauric acid [154]

Properties	**Value**
Melting point (°C) Solidus(s)/liquidus (l)	43.46 (s) and 49.92 (l)
Latent heat of fusion (kJ/kg)	156.82
Specific heat (kJ/kg.K)	1.39 (s)/ 1.57 (l)
Density (kg/m^3)	1051.20 (s)/885.04 (l)
Thermal conductivity (W/m.K)	0.227 (s)/0.388 (l)
Viscosity (Pa.s)	0.00435

4.3. Grid Independence and Validation

Fig. 4.2 indicates the grid and time independence studies by considering PCM temperature at the midpoint of the vertical LHSS with SCD. The mesh sizes considered are 343779, 414978, and 449510. It is observed that the variation of temperature is less than 1 % when the grid size increases from 414978 and 449510. Hence, to reduce computational effort 414978 grid elements are chosen throughout the study. By using 414978 elements size, four different time-steps 0.5 s, 0.4 s, 0.3 s, and 0.2 s are considered as shown in Fig. 4.2 (b). It is noted that the variation for temperature between 0.2 s and 0.3 s is less than 0.5 % due to which 0.3 s time step has been considered for the rest of the simulations.

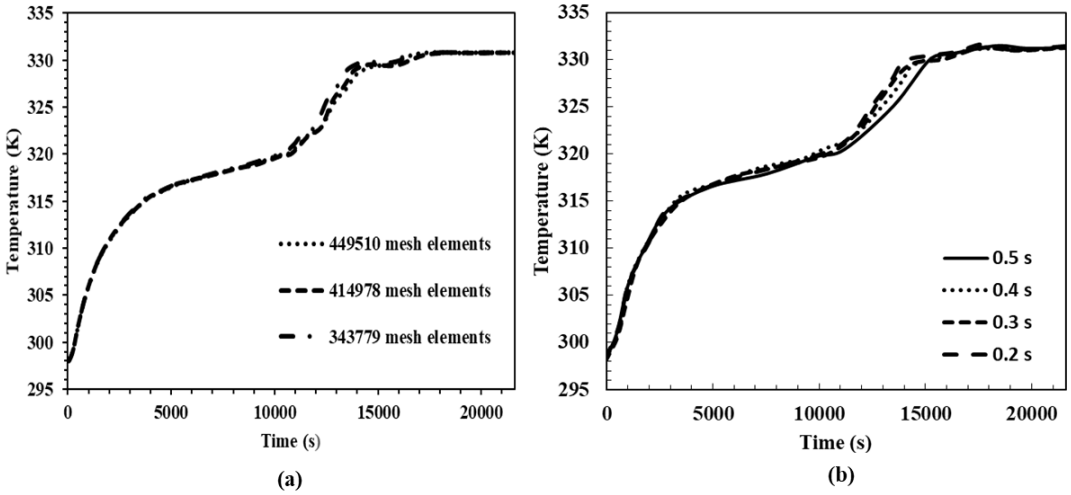

Fig.4.2: (a) Grid size and (b) Time-step independence studies

To check the validity of the present numerical methodology comparison is made with the experiments. The parameters for validation i.e. hot and cold inlet temperatures (80°C and 27°C) and mass flow (1.4 L/min) for cold and hot HTFs are the same for both experimental and numerical studies. Fig. 4.3 shows the comparison of numerical and experimental results for average temperature and the maximum variation is observed to be less than ±5 %. Based on the comparison it can be noted that the adopted numerical approach is satisfactory and can be extended for further investigation.

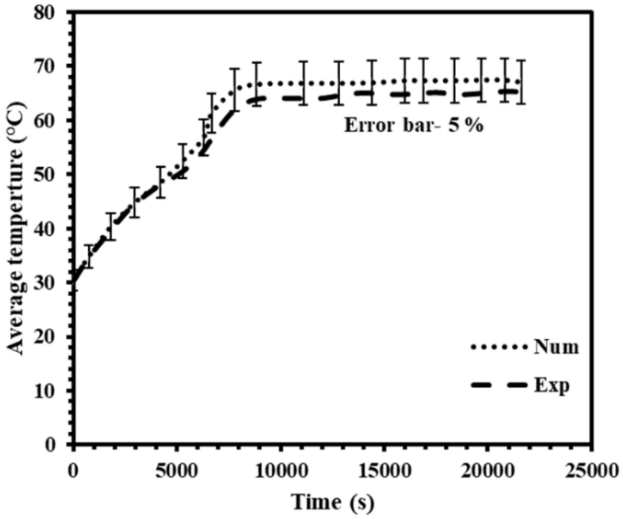

Fig. 4.3: Comparison of numerical and experimental results

4.4 Results and Discussions

The thermal behavior of PCM under simultaneous charging and discharging (SCD) in vertical and horizontal positions are explored. The effect of mass flow rate (0.25, 0.5, 0.75,

and 1 L/min) and temperature gradient $\left(\Delta T = T_{h_i} - T_{c_i}\right)$ between hot and cold HTFs inlet temperatures on the evolution of PCM temperature, melting profile, energy stored and thermal transport are examined. Two cases are considered to analyze the influence of the temperature gradient of the hot and cold HTFs. In case 1 the hot fluid inlet temperature is varied and the cold fluid inlet temperature is maintained constant (ΔT_h), and for case 2 the cold HTF inlet temperature is varied and the hot HTF inlet temperature is maintained constant (ΔT_c).

4.4.1 Direction of heat transfer fluids

Fig.4.4 shows the melt fraction evaluation over time with direction of HTFs. To evaluate the effect of direction four cases are considered. Case-1 and 2 represent the parallel flow whereas case-3 and 4 indicate the counter flow with mass flow rate of 1lit/min. For case 1 both cold and hot HTFs are circulated from the bottom and for case 2 from the top of the LHSS. Whereas, for case-3 hot HTF are circulated form the top and cold fluid is circulated from the bottom and vice versa for case-4. From Fig. 4.4 it can be noted that case-2 gave marginally higher melt fraction as compared to other cases. However, Fig. 4.4 shows that the melting process does not significantly affect by changing the direction of HTFs. The insignificant variation can be inferred to the thermal resistance offered by the PCM due to its low thermal conductivity. From Fig.7 the melt fraction for cases 1 and 2 are observed to be 0.72 and 0.729 whereas for cases 3 and 4 it is 0.71 and 0.723.

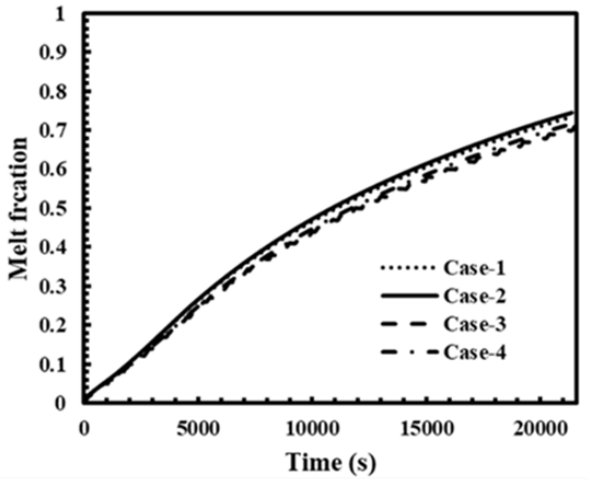

Fig. 4.4 Melt fraction evaluation over time based on direction of HTFs

4.4.2 Effect of mass flow rate

The influence of the cold and hot HTFs mass flow rates on the melting process over time in the vertical configuration is shown in Fig. 4.5. The inlet temperature of hot and cold HTFs are considered to be 80°C and 27°C for all simulations. Fig. 4.5(a) represents the melt fraction vs time with a variation of hot fluid mass flow rate by keeping cold fluid mass flow rate of 1 L/min. Similarly, Fig. 4.5(b) shows the variation of the cold fluid mass flow rate with the constant hot fluid mass flow rate of 1 L/min. As the mass flow rates of the hot and cold HTFs are increased from 0.25 L/min to 1 L/min, the melting time is observed to marginally decrease. By the increase of the hot and cold fluid mass flow rates at the end of 21600 s melt fractions increases from 0.71 to 0.73 and 0.596 to 0.623 which is 2% and 4% increase. Therefore, it can be said that the effect of the mass flow rate does not show considerable influence on the melt fraction in a vertical configuration. Similar to Fig. 4.5, Figs. 4.6 (a) and (b) reveal the influence of mass flow rate in the horizontal configuration. At a time span of 10000 s with the increase in hot and cold flow rates from 0.25 L/min to 1 L/min a variation of 0.79 to 0.85 with hot fluid and 0.702 to 0.74 with cold fluid for melt fraction is observed which is an increase by 7.05% and 5.04%. Moreover, by comparing the vertical and horizontal configurations the influence of mass flow rate is relatively more with the horizontal configuration. This is due to the un-symmetric melting condition of PCM and variation of convective strength with the position of LHSS. As the variation of mass flow rate on thermal transport is not significant the mass flow rates for hot and cold HTFs are fixed to 1 L/min for further investigation.

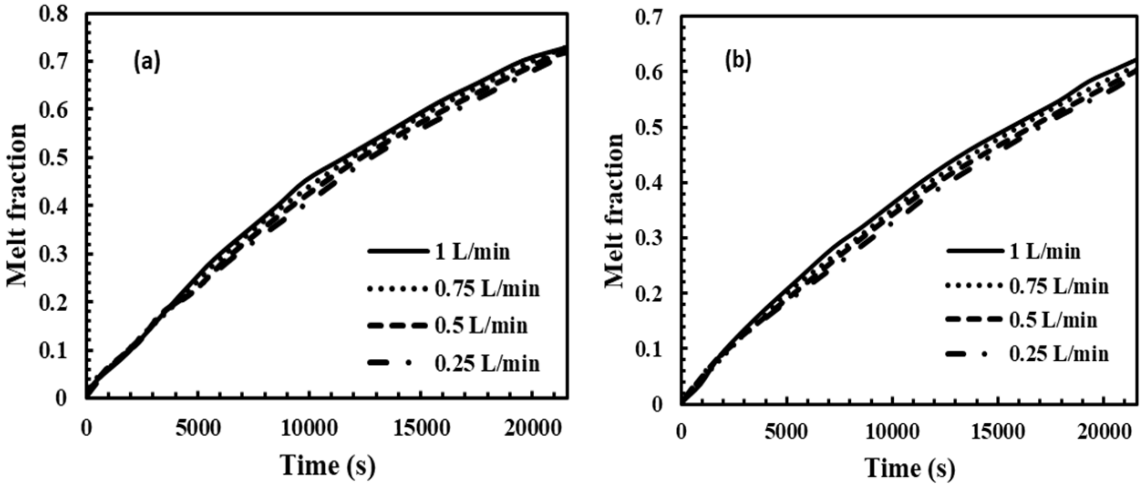

Fig.4.5: Melt fraction variation for vertical configuration with mass flow rate of (a) hot HTF (b) cold HTF

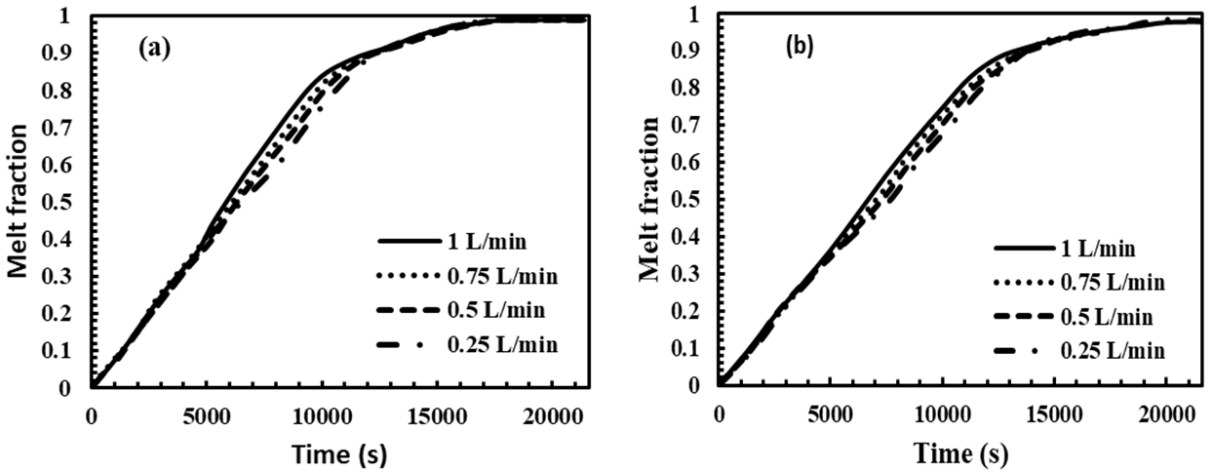

Fig.4.6: Melt fraction variation for horizontal configuration with mass flow rate (a) hot HTF (b) cold HTF

4.4.3 Case 1: Effect of temperature gradient by varying hot HTF inlet temperature

Fig. 4.7 shows the temperature contours during SCD in the vertical and horizontal configurations with different temperature gradients between the hot and cold HTFs inlet temperature (ΔT_h) by varying hot HTF inlet temperatures $\left(T_{h_{in}}\right)$ i.e. 80 °C, 70 °C, and 60 °C. The $T_{C_{in}}$ is kept constant at 27 °C. The influence of ΔT_h on the thermal behavior of PCM is investigated at three temperature gradients: 53 °C, 43 °C, and 33 °C. The mass flow rates for hot and cold HTFs are fixed to 1 L/min. For the vertical configuration, the maximum temperature within the PCM is found to be on the upper half and differs with ΔT_h as shown in Fig. 4.7 (a). It is observed that the temperature of PCM decreases as moved towards the downward portion of the LHSS. The maximum temperature is found at $\Delta T_h = 53$ °C due to higher temperature difference resulting in higher heat transport. Lower temperature can be noted towards the right side due to the influence of cold HTF. Also, thermal stratification is observed within PCM in a vertical configuration. Pertaining to the horizontal configuration as the melted PCM escalates to move up due to buoyancy the cold HTF tube is positioned in the upper portion. The heat from hot HTF dissipated to the adjacent PCM. The melted PCM move up due to buoyancy and transfer heat to the cold HTF. Due to better thermal transport lower thermal stratification is observed for horizontal configuration.

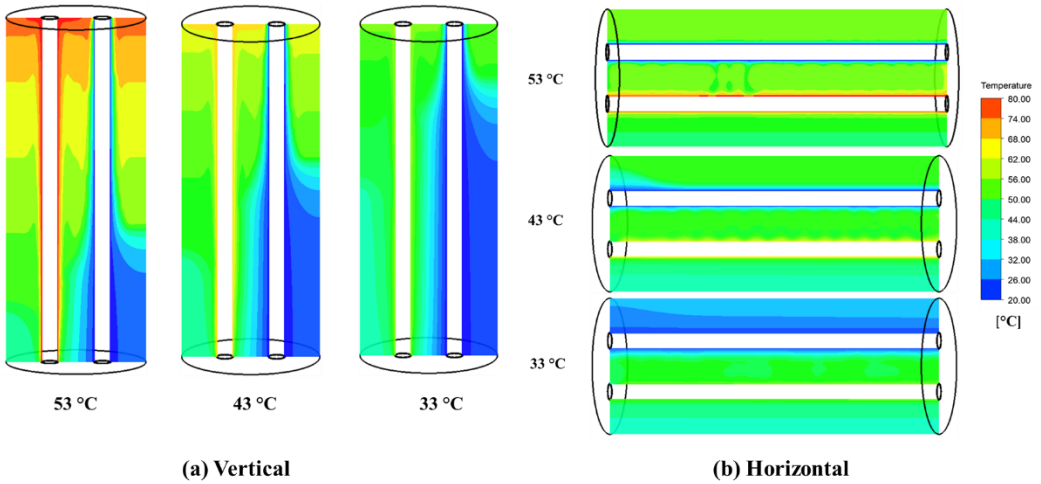

Fig.4.7: Temperature contours with ΔT_h at the end of 21600 s (a) vertical and (b) horizontal

Fig. 4.8 (a) shows the PCM melt fraction contours during SCD in the vertical configuration. It is observed that PCM near the hot HTF pipe absorbs heat from HTF and starts to melt. Melted PCM rises due to buoyancy and eventually fills the upper half of the LHSS. As time progresses, the melted PCM starts to move towards the cold HTF pipe. Therefore, the un-symmetric behavior of melt fraction can be observed in the SCD process. From Fig. 4.8 (a), the solid-liquid PCM interface can be identified at the lower half of LHSS for $\Delta T_h = 53$ °C towards the cold side. Similarly, the solid-liquid interface is observed towards the cold HTF pipe for 43 °C and 33 °C at almost half and upper portion of LHSS. For $\Delta T_h = 33$ °C PCM got melted near to the hot HTF pipe and most of the part of LHSS remains in un-melted condition.

Fig. 4.8 (b) shows the melt fraction contours of PCM under SCD in a horizontal configuration. The cold HTF pipe is placed in the upper portions of the LHSS when oriented in the horizontal position. The PCM near the hot HTF pipe first receives the energy. Once the PCM reaches the melting point the liquid PCM forms a recirculation motion around the hot tube. Due to the buoyancy effect, the melted PCM moves up and fills the upper portion of the LHSS towards the cold HTF tube. The melting rate of PCM in the horizontal configuration is high due to the increase in thermal transport assisted by convection. It is noted that PCM almost melted for $\Delta T_h = 53$ °C, while the bottom part of the LHSS remains in an un-melted state for $\Delta T_h = 43$ °C and 33 °C. It is also observed that for $\Delta T_h = 33$ °C the PCM remains in solid condition above the cold HTF pipe. The difference in melt profile with the variation of ΔT_h can be inferred to the magnitude of the temperature difference

between the PCM and ΔT_h. The higher temperature difference leads to the increase in driving force for thermal transport.

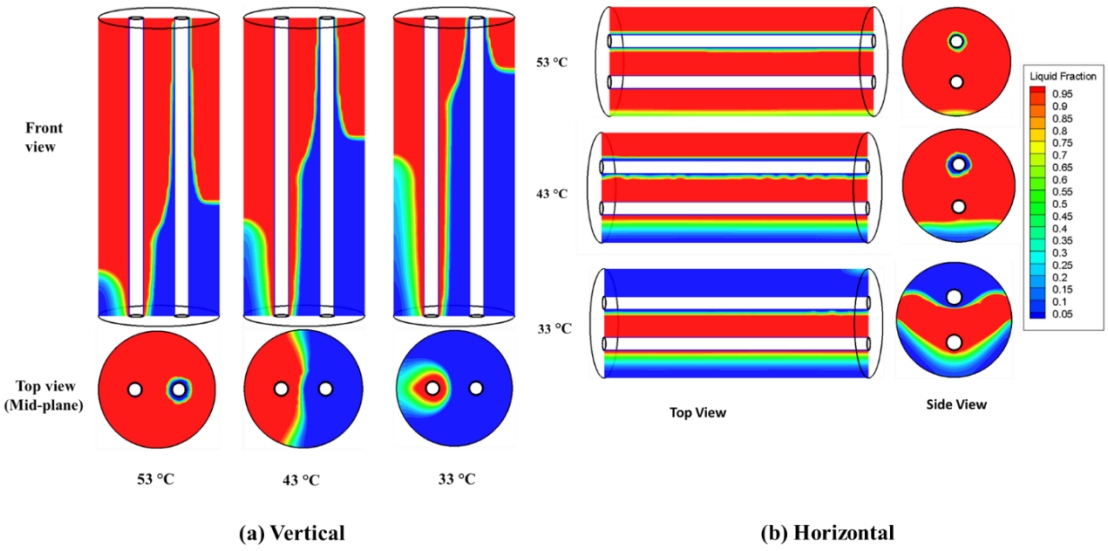

Fig. 4.8: Liquid fraction contours with ΔT_h at the end of 21600 s (a) vertical and (b) horizontal

Fig. 4.9 indicates the melt fraction over time with ΔT_h for vertical and horizontal positions. It is observed that at the end of 21600 s, the ΔT_h has a great influence on the charging process. The PCM melting time is shortened by the higher temperature gradient. However, PCM in the vertical configuration under SCD could not melt completely. For $\Delta T_h = 53$ °C, 43 °C, and 33 °C the melt fractions of PCM are noted to be 0.73, 0.51, and 0.27. With the decrease of ΔT_h from 53 °C to 43 °C; there is a reduction of melt fraction by 31.13 %. Further decrease of ΔT_h up to 33°C, the percentage of reduction is 47 %. Moreover, in horizontal LHSS, the effect of ΔT_h shows significant effect. The horizontal LHSS melted almost completely for $\Delta T_h = 53$ °C. At $\Delta T_h = 53$ °C, 43 °C, and 33 °C the melt fractions are observed to be 0.99, 0.7, and 0.51 respectively. The decrease of ΔT_h from 53 °C to 43 °C the melt fraction is noted to reduce by 29.29 % and 43 °C to 33 °C it is noted to be 27 %. The improvement in thermal performance in a horizontal position can be inferred to higher convective strength caused due to the placing of the hot HTF tube below the cold HTF tube. The melted PCM near the hot HTF moves up due to buoyancy and dissipates heat to the cold HTF which is placed in the upper position. The positioning of the hot HTF tube below the cold HTF tube intensifies the natural convection and thus leading to effective thermal transport to the cold HTF.

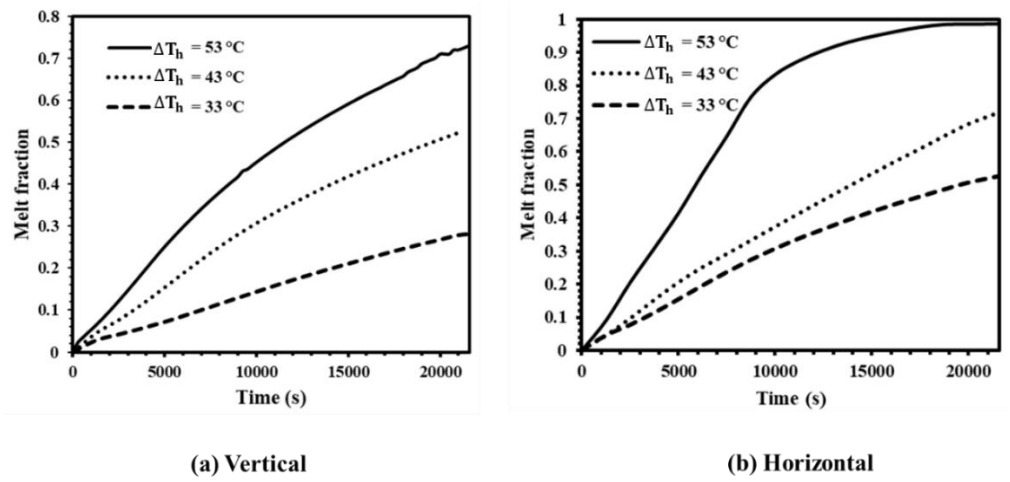

Fig. 4.9: Melt fraction variation over time with ΔT_h (a) Vertical (b) Horizontal

From the above discussion, it can be noted that with the increase of ΔT_h the performance of LHSS is significantly enhanced because of the increase in temperature difference between the hot HTF and PCM. By comparing the vertical and horizontal LHSS under SCD, horizontal shows better thermal performance with 26 % higher melt fraction than vertical LHSS for $\Delta T_h = 53$ °C. It can also be observed that the position of the cold HTF tube showed a stronger impact on the charging process. Also, the horizontal configuration showed lower thermal stratification.

4.4.4 Case 2: Effect of temperature gradient by varying cold HTF inlet temperature

The temperature contours with the variation of temperature gradient (ΔT_c) by varying cold HTF inlet temperature in vertical and horizontal LHSS positions are shown in Fig. 4.10. The influence of ΔT_c on the thermal behavior of PCM is investigated at three temperature gradients: 50 °C, 60 °C, and 70 °C. The hot HTF input temperature is kept constant at 80 °C. The mass flow rates for hot and cold HTFs are fixed to 1 L/min. From Fig. 4.10 (a) based on the temperature contours, thermal stratification can be observed for vertical configuration. Also, the temperature contours appear to be the same which highlights the insignificant influence of ΔT_c on the thermal transport. Fig. 4.11 indicates the PCM melt fraction contours in vertical and horizontal LHSS with the various ΔT_c. The melting phenomenon shows similar behavior as observed with the variation of ΔT_h (section 4.4.2). In the vertical mid-plane, un-melted PCM appears towards the cold side and left bottom portion of the hot HTF tube. Based on the horizontal section taken at half of the length, the

PCM appears to be completely melted for ΔT_c = 70 °C and 60 °C when compared to that of 50 °C. This observed behavior can be inferred to the higher temperature gradient resulting in higher thermal transport. For horizontal position, the variation of melt fraction contour is observed to be insignificant. Therefore, it can be mentioned that the variation of ΔT_c shows a negligible effect on the melting process in the horizontal position.

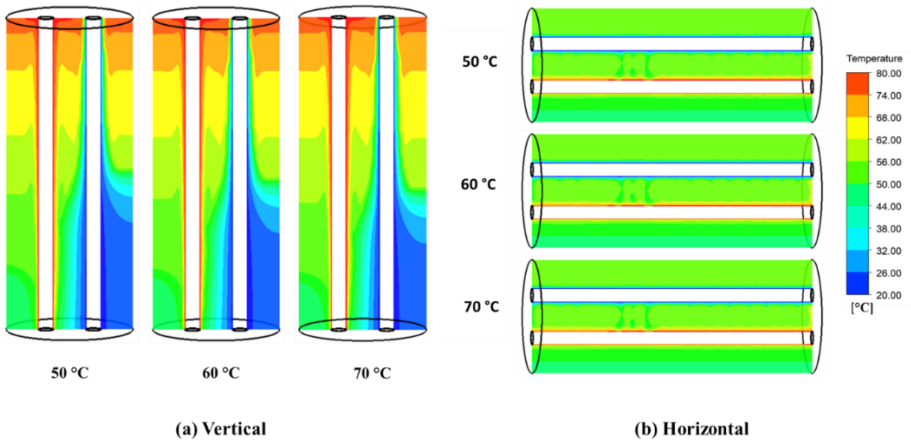

Fig. 4.10: Temperature contours with ΔT_c at the end of 21600 s (a) vertical and (b) horizontal

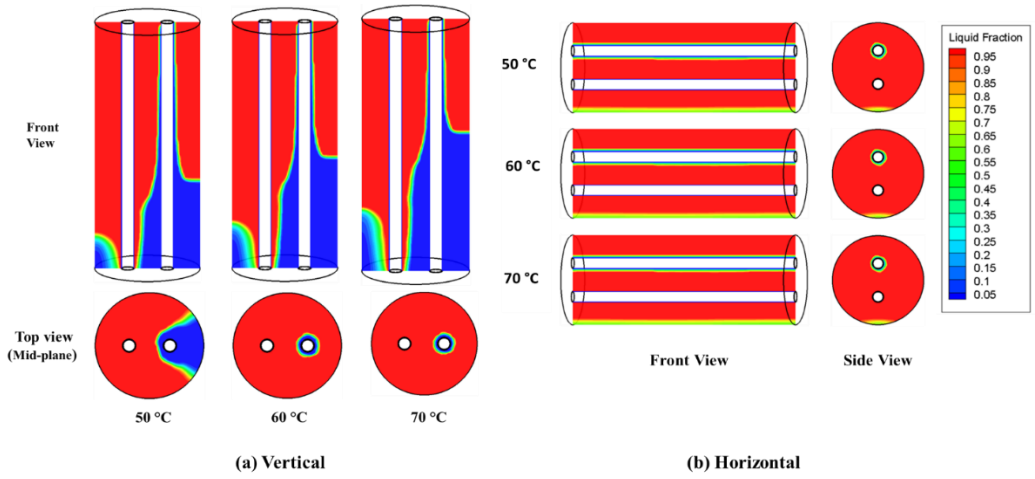

Fig. 4.11: Melt fraction contours with ΔT_c at the end of 21600 s (a) vertical and (b) horizontal

To further analyze the thermal behavior of the LHSS the variation of melt fraction with ΔT_c is plotted. Fig. 4.12 shows the comparison of the melt fraction during the SCD process in the vertical and horizontal LHSS with a variation of ΔT_c. For the vertical position, with a higher temperature gradient i.e. ΔT_c = 70 °C significant effects on the melt fraction can be noted. However, with the decrease of ΔT_c the rate of melt fraction increased. It may be noted

that in case 2, $T_{h_{in}}$ is constant (80°C) and $T_{c_{in}}$ is varied (10°C, 20°C and 30°C). With the increase of $T_{c_{in}}$ the thermal transport to the PCM increases and cold HTF decreases due to which the decrease of ΔT_c lead to the increase in melt fraction. At the end of 21600 s, for $\Delta T_c = 50$ °C, 60 °C, and 70 °C the melt fractions of the PCM are 0.72, 0.69, and 0.60. With decrease of ΔT_c from 70 to 60 °C; the increase of melt fraction is 13 %. Further decreases in ΔT_c up to 50 °C, the percentage of increase is only 4 %. Therefore, it can be stated that at a higher ΔT_c more energy transport from PCM to the cold fluid due to the more temperature gradient between cold HTF and liquid PCM. In the horizontal position, the effect ΔT_c is less in comparison to the vertical position. At 10000 s the melt fractions with ΔT_c (70 °C, 60 °C, and 50 °C) are observed to be 0.75, 0.8, and 0.85 i.e. with the decrease in ΔT_c from 70 °C to 50 °C the percentage raise in melt fraction is 3.23 %. Therefore, the change in ΔT_c does not show a significant influence on melt fraction.

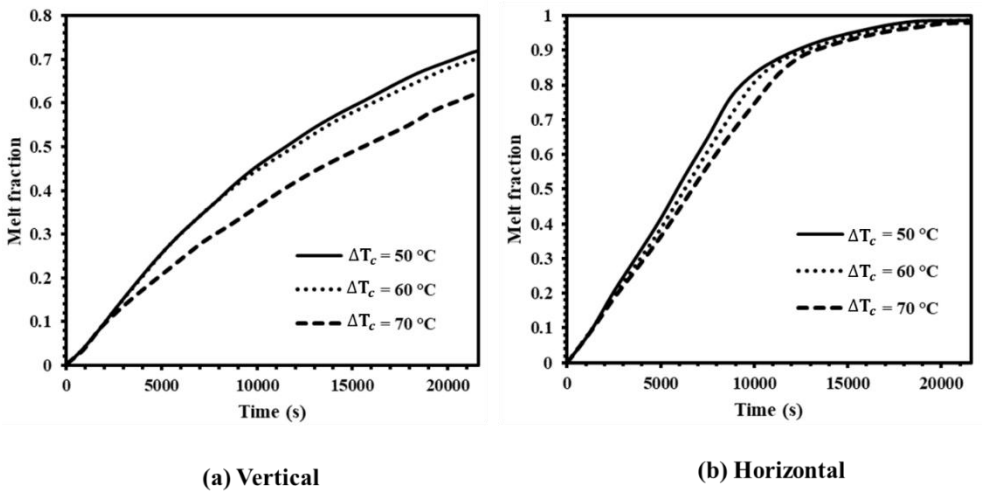

Fig. 4.12: Melt fraction variation over time with ΔT_c (a) Vertical (b) Horizontal

From the above discussion, it can be mentioned that higher ΔT_c shows a significant effect on the charging process. However, for the horizontal configuration irrespective of ΔT_c the melt fraction can be noticed to be equal at the end of 21600 s.

4.4.5 Energy storage

Fig. 4.13 reveals the total energy stored at the end of 21600 s in the vertical and horizontal configurations with the variation of temperature gradients (ΔT_h and ΔT_c). The influence of ΔT_h on total energy stored is shown in Fig. 4.13 (a). For $\Delta T_h = 53$ °C, 43 °C, and 33 °C the energy storage for the vertical configuration is 163, 122.8, and 76.4 kJ. Whereas, the total

energy stored is 235, 173.64, and 138 kJ for the horizontal configuration. This infers that the decrease in ΔT_h from 53 °C to 33 °C; leads to the decrease in the energy stored by 53.13 % and 41.27 % in the vertical and horizontal configurations. Similarly, the total energy storage with the variation of ΔT_c is shown in Fig. 4.13 (b). For $\Delta T_c = 50$ °C, 60 °C, and 70 °C the energy stored by PCM is 165, 158, and 146 kJ for a vertical configuration and 238, 227, and 216 kJ for horizontal configuration. From Fig. 4.13 (b) it can be observed that the change in ΔT_c does not show a significant variation in the energy storage in both horizontal and vertical configurations. From sections 4.4.3 and 4.4.4 it can be noted that the melt fractions for horizontal systems are high in comparison to the vertical systems. Hence, the energy storage for horizontal configuration is higher as compared to the vertical.

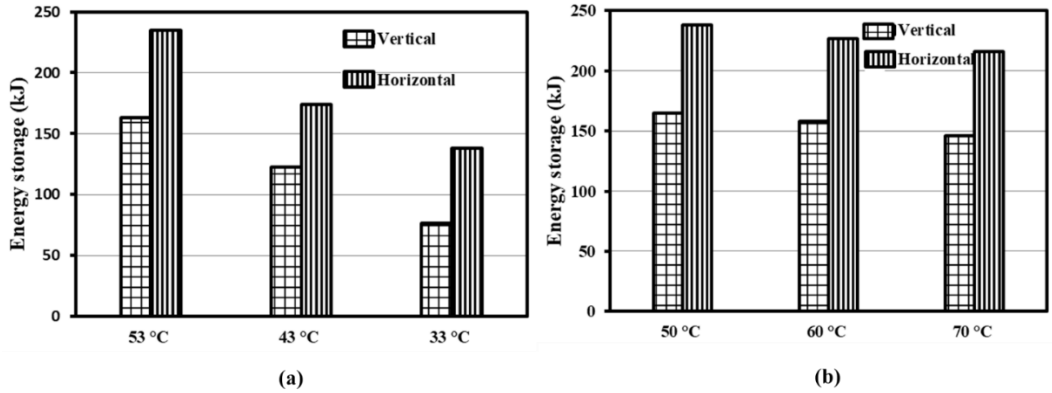

Fig.4.13: Total energy stored for vertical and horizontal configuration with change in (a) ΔT_h and (b) ΔT_c

4.4.6 Heat transfer

The effect of temperatures gradient (ΔT_h and ΔT_c) on the heat transfer (Q) from hot HTF to PCM (Charging) during the SCD process is shown in Fig. 4.14. It can be deduced from these curves that heat transfer is larger at the beginning then drops quickly and increases again, then further flatten down slowly. The descent of heat transfer from a high value to a specific point at the initial stage shows that the conduction mode of heat transfer is dominated. After that, the convection phenomenon begins due to the melting of PCM. With increasing time, the heat transport by convection diminishes slowly and attains to a stable condition. Form Fig. 4.14, it can be noted that the effect of ΔT_h has more influence on heat transfer as compared to that of ΔT_c. It is also observed that the heat transfer is higher in a horizontal configuration with the variation of ΔT_h. In the vertical configuration, heat transfer achieved stable conditions earlier (11000 s) as compared to horizontal (15000 s). Also, it

can be stated that the influence of cold HTF is stronger in the vertical position as compared to the horizontal.

Fig. 4.15 shows a comparison of heat transfer (Q) from PCM to cold HTF (discharging) for different ΔT_h and ΔT_c for the vertical and horizontal configurations. The heat transfer increases from zero as the initial temperature gradient between cold HTF and PCM is zero. Further, with the increase in temperature gradient between PCM and cold HTF the heat transfer also increases. The magnitude of heat transfer from PCM to cold HTF at the end of 21600 s is given in Table 4.2. Table 4.2 provides quantitative details about the variation of heat transfer during charging and discharging with different ΔT_h and ΔT_c. The thermal transport from PCM to cold HTF increases with ΔT_h and ΔT_c. This is due to the higher temperature difference between liquid PCM and cold HTF temperature. From Fig. 4.15 (b) it can be noted that at the horizontal position the heat transfer attains stable condition for ΔT_h =53°C. From the result, it can be said that up to the stable condition the thermal transport is from hot HTF to PCM and cold HTF. After attaining stable condition, energy absorbed by the PCM is very less and direct thermal transport occurs between hot and cold HTFs.

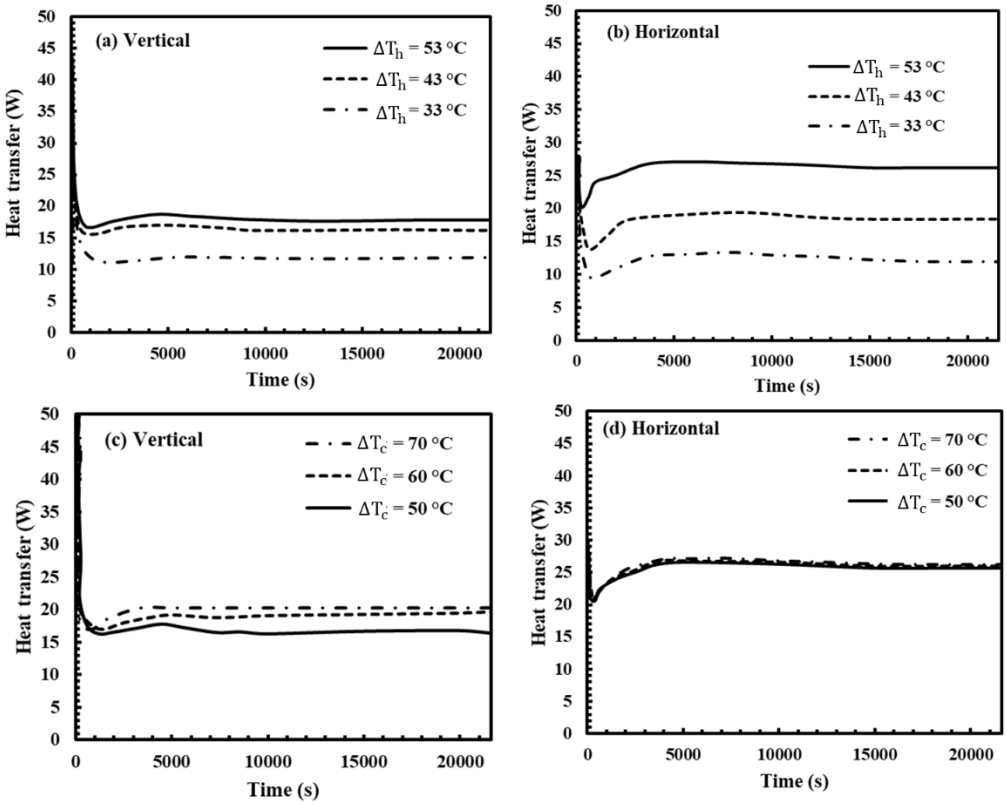

Fig.4.14: Heat transfer from hot HTF to PCM (Charging) under different ΔT_h and ΔT_c in vertical and horizontal configurations

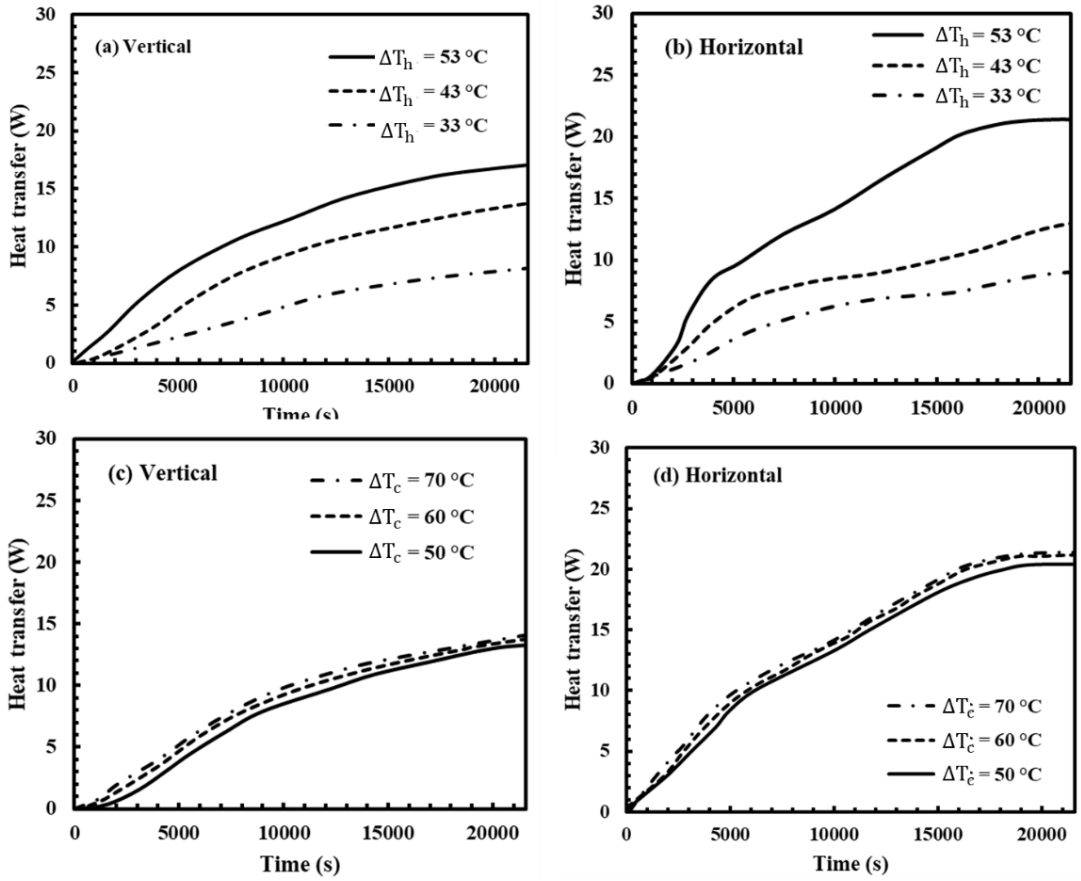

Fig. 4.15: Heat transfer from PCM to cold HTF (Discharging) under different ΔT_h and ΔT_c in vertical and horizontal configurations

Table 4.2: Heat transfer with the variation of temperatures gradient at the end of 21600 s

		Heat Transfer (W)			
		Charging		Discharging	
		Vertical	Horizontal	Vertical	Horizontal
ΔT_h	53 °C	17.7	26.20	17.70	21.46
	43 °C	16.2	18.43	14.60	13.40
	33 °C	12.10	12.00	8.86	9.56
ΔT_c	70 °C	20.30	26.20	14.76	21.43
	60 °C	19.70	26.00	14.57	20.90
	50 °C	16.40	25.70	13.90	20.39

4.5 Closure

In this study, the thermal behavior of PCM (lauric acid) in shell and tube heat exchanger with simultaneous charging and discharging (SCD) conditions is investigated. The influence of temperature gradients between hot and cold fluids (ΔT_h and ΔT_c) and mass flow rates on thermal transport have been analyzed. For this purpose, three inlet temperatures of cold and hot HTFs and four mass flow rates are considered. Based on the results the following conclusions can be drawn .

- The impact of both the hot and cold fluid mass flow rates has an insignificant influence on the melt fraction. However, when horizontal and vertical configurations are compared the influence of mass flow rate was more for the horizontal configuration.
- Reducing the ΔT_h decreases the melting rate. With the decrease of ΔT_h from 53 to 33 °C, the overall percentage reduction of melt fraction is 60 % and 48.48 % for the vertical and horizontal configurations.
- Significant effect of ΔT_c at 70 °C is found for the vertical configuration. After the further decrease in ΔT_c up to 50 °C the melt fraction percentage increased by only 4 %. In the horizontal configuration, the effect of cold HTF inlet temperature is insignificant.
- Reduction in energy storage by 53.13 % and 41.27 % is observed by changing ΔT_h from 53 to 33 °C in vertical and horizontal configurations. However, adjusting the ΔT_c does not differ the ability of energy storage.
- Heat transfer from hot HTF to PCM is found to be higher for $\Delta T_h = 53\ °C$ and $\Delta T_c = 70\ °C$ for both horizontal and vertical configurations. Moreover, the change in heat transfer is observed to be more with the increases of ΔT_h. Heat transfer from PCM to cold HTF increases as ΔT_c increases for both horizontal and vertical configurations.

Chapter 5

Experimental and numerical analysis to study the effect of inclination on the thermal behavior of latent heat storage system

5.1 Introduction

In the previous chapter, the influence of flow rate and inlet temperature of heat transfer fluids (HTFs) on the melting characteristics of PCM was discussed. Along with these two parameters, the orientation of LHSS has a prominent role in the melting of PCM because of its influence on the natural convection phenomenon. After a thorough review of literature pertaining to the studies on the effect of inclination on the performance of a shell and tube LHSS, a contradiction among the results is noted. Hence, the present study is aimed at analyzing the effect of orientation of LHSS on the SCD characteristics of PCM in terms of energy and exergy analysis.

5.2 Experimental procedure and temperature measurement

Experimental test facility, the description of which was given in chapter 3 (Fig. 3.1) is used to carry out the investigations on SCD characteristics of PCM impregnated in a shell and tube LHSS at various orientations. Leakage check and calibration are done for the initial test. The whole experiment is kept at thermal equilibrium with the surrounding before the start of the experiment. To initiate SCD, the hot water bath is heated to its optimal constant temperature and the hot HTF is circulated at a constant flow rate through the tube inside the LHSS. Simultaneously, the cold HTF also flows through the tube with the same flow rate. In the SCD process, the position of hot and cold HTF tubes is important. For all considered orientations (0° (horizontal), 30° and 60°) the cold HTF tube is placed above the hot HTF tube. The operating parameters used in this experiment based on the previous chapter 4 and given in Table 5.1. Before the commencement of the experiment, the temperature of the PCM in LHSS is maintained at 27°C. Experiments are conducted until the steady state temperature is reached. Moreover, the influence of LHSS orientation on temperature distribution, melting behavior, energy stored, exergy efficiency and energy input/recovery are discussed. Fig. 5.1. Shows the position of thermocouple in LHSS. To measure inlet and outlet temperature of the cold and hot HTFs four thermocouples are used. The remaining

nine thermocouples are placed in three sections. Each section has three thermocouples, the first thermocouple at the hot tube side, the second at the middle portion, and the third at the cold tube side.

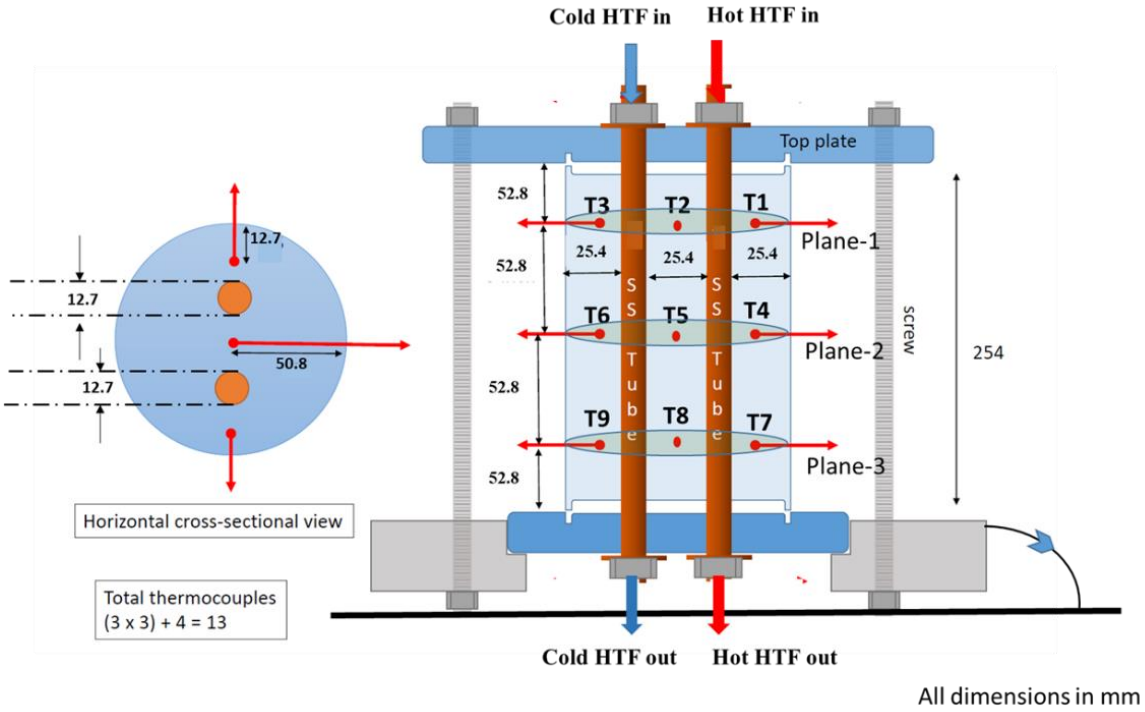

Fig. 5.1: Position of thermocouples and heat transfer tubes

Table 5.1: Operating parameters

Hot HTF temperature	80 °C
Cold HTF temperature	27 °C
Hot and cold HTF mass flow rate	1.4 L/min
Inclination angle	90°,60°,30° and 0°

5.3. Grid Independence and Validation

The numerical procedure adopted for simulation was given in chapter 3 (Sec. 3.3). Fig. 5.2 (a) shows the meshing elements of LHSS. Grid and time-step independence studies are performed and are given in Fig. 5.2 (b). The mesh sizes considered are 225638, 343779, 414978 and 509510. It can be observed that the variation of melt fraction is less than 1% when the grid size increases from 414978 and 509510. Hence, to reduce computational effort 414978 grid elements are chosen throughout the study. By using 414978 elements

size, four different time-steps 0.5 s, 0.4 s, 0.3 s and 0.2 s are considered as shown in Fig. 5.2 (c). It is observed that the variation for melt fraction between 0.2 s and 0.3 s is less than 0.5% due to which 0.3 s time step has been considered for the rest of the simulations.

To check the validity of the present numerical methodology comparison is made with experiments. The experimental facility is shown in Fig. 3.1 (chapter 3). Water is used as the HTF and lauric acid is employed between the shell and tubes. The obtained thermophysical properties are shown in Table 5.2. Prior to the SCD process, the high-temperature water bath is heated up to a constant temperature of 80°C and circulated through the hot tube via pump. At a same time, the cold water at 27 °C is also made to flow through the cold tube simultaneously with the same flow rate (1.4 L/min). The hot and cold baths are fitted with PID controllers to maintain constant inlet temperatures and the flow rates are measured by the digital flow meters. Based on Section 4.4.1 (Chapter 3) it is noted that the parallel and counter flow did not impact the melt fraction due to lower thermal conductivity of PCM. The parameters for validation i.e. hot and cold inlet temperature (80 °C and 27 °C) and volume flow rate (1.4 L/min) for cold and hot HTFs are the same for both experimental and numerical studies. Fig. 5.4 depicts the comparison of numerical and experimental data for the midpoint temperature (T_5). The maximum variation is observed to be less than ±9 %. Based on the comparison it can be noted that the adopted numerical approach is satisfactory and can be extended for further investigation.

Table 5.2: Lauric acid thermophysical properties

Property	**Measuring instrument**	**Value**	**Uncertainty**
Melting point (°C)	DSC	43.46 (s)/49.94 (l)	±1%
Latent heat (kJ/kg)		156.82	
Specific heat (kJ/kg.K)		1.39 (s)/1.57 (l)	
Density (kg/m^3)	Pycnometer	1051.20 (s) / 885.04 (l)	± 0.9 %
Thermal conductivity (W/m.K)	Hot Disk thermal constants analyzer	0.227 (s) / 0.388 (l)	±5%
Viscosity (Pa.s)	Rheometer	0.00435	± 0.42 %

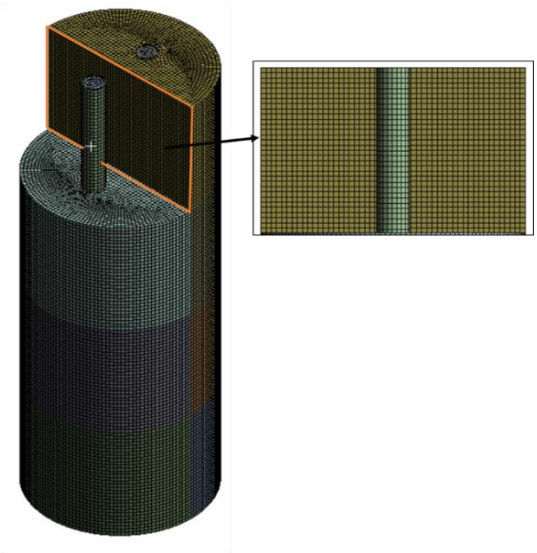

Fig.5.2 Meshing elements

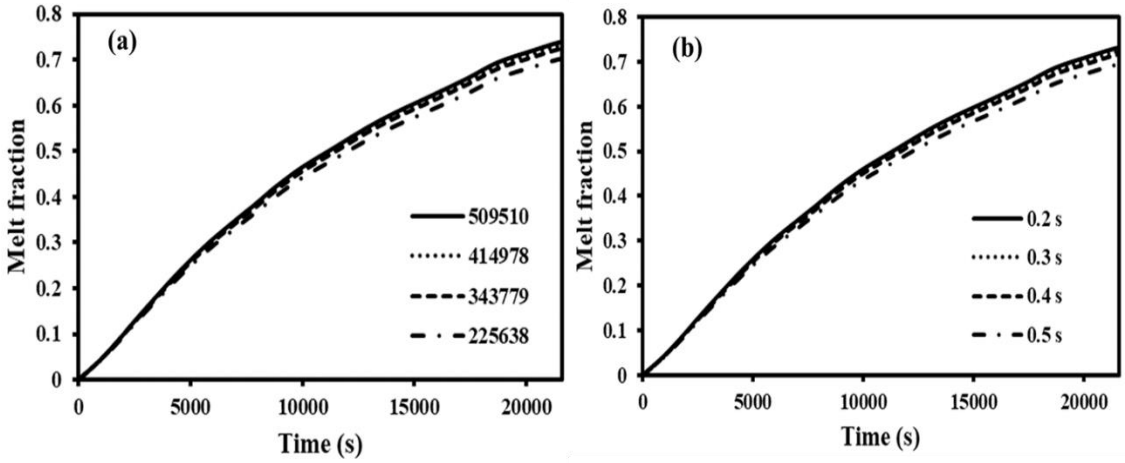

Fig. 5.3: (a) Grid (left) and (b) time step (right) independence

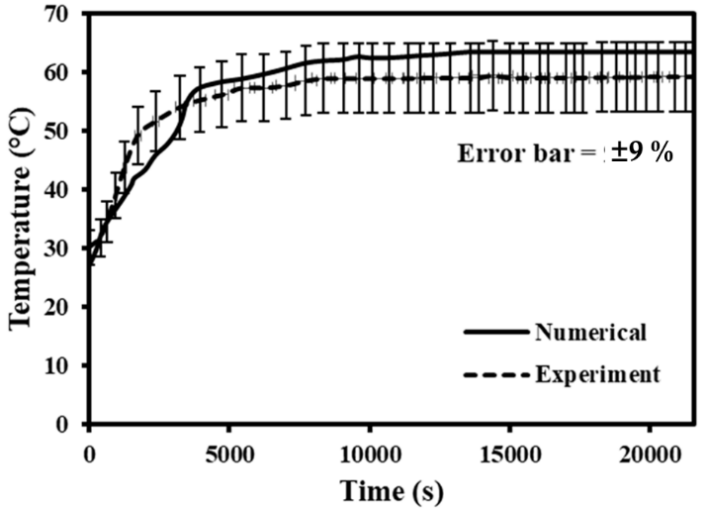

Fig. 5.4: Validation of numerical methodology with experiments for PCM temperature

5.4 Uncertainty analysis

Uncertainty analysis for the experimental parameters is important to estimate the accuracy of the performed experiments. The approach suggested by Moffat [155] has been employed to estimate the uncertainty by using the root square method. The uncertainty is calculated based on the random data taken over time. Table 5.3 shows the uncertainty associated with employed parameters. The uncertainties for energy transfer and exergy are obtained as 8.3% and 7.9%.

Table 5.3: Uncertainty of experimental parameters

Parameter	**Instrument used**	**Uncertainty**
Temperature	K-type Thermocouple	± 0.2 °C
Mass flow rate	Digital flow meter	± 0.1 L/min
Hot and cold bath temperature	Digital PID controller	±1 %

5.5 Results and discussions

The impact of inclination on the performance of LHSS when the PCM at solid state (27 °C) under simultaneous charging and discharging (SCD) is studied. The propagation of melting profile, temperature distribution, exergy efficiency and energy stored/expended with the variation of LHSS angle is analyzed. The inlet temperature of the hot and cold heat transfer fluids (HTFs) are chosen as 80°C and 27°C respectively. Whereas, 1.4 L/min mass flow rate is considered for both hot and cold HTFs.

5.5.1 Temperature distribution

Temperature distribution of PCM recorded by thermocouples shown in Fig. 5.1 located at planes 1 and 3 for various inclination angles is presented in Figs. 5.5 and 5.6. As shown in the figures thermocouples are placed near the hot HTF tube, middle of the heat exchanger, and nearer to the cold HTF tube. The figures also give an insight into the location specific duration at which the solid PCM converts to the liquid state. The region above the solidus line shown in Figs. 5.5 and 5.6 refers to the liquid state and below to solid-state of the PCM. From Fig. 5.5 it can be observed that in vertical position (90°) the thermocouple (T_1) near to the hot HTF pipe increases rapidly during the starting of the SCD process. But with the decrease of inclination i.e. from 90^o to 0^o, the magnitude of the temperature T_1 can be noted to decrease. As the position of the thermocouple T_1 moves towards the downward portion

with the decrease of inclination, the quantity of the cold denser liquid PCM near T_1 increases resulting in the decrease of temperature. It can be noted that with time the buoyancy forces drive the convection due to which the melting process of the PCM is accelerated. The hot melted PCM near the hot HTF move to the upper half of the LHSS. The liquid PCM in the upper portion comes in contact with the cold HTF becomes denser and sinks.

From Figs. 5.5 (b) and (c) the thermocouples T_2 and T_3 for 90° can be noted to be minimal during the initial stages of thermal transport. The thermocouples T_2 for 30° and T_3 for 60° can be observed to attain maximum temperature during the initial period. The behavior highlights the influence of inclination on thermal transport. From Fig. 5(c) it can be observed that to attain solidus temperature minimum time has been taken with 60° and maximum for 90°. Comparing Figs. 5.5 (b) and (c) it can be observed that T_2 reaches the solidus temperature much earlier when compared to T_3. From Fig. 5(b) it may be noted that T_2 attains solidus temperature much earlier with inclination when compared to the vertical position. This behavior infers that with orientation the gravitational force moved the natural convection effect from the axial direction to the radial direction. The variation causes less dense liquid PCM to move towards T_2 thus increasing its temperature in less time i.e. nearly 1154 s with the inclination and 4350 s for vertical position.

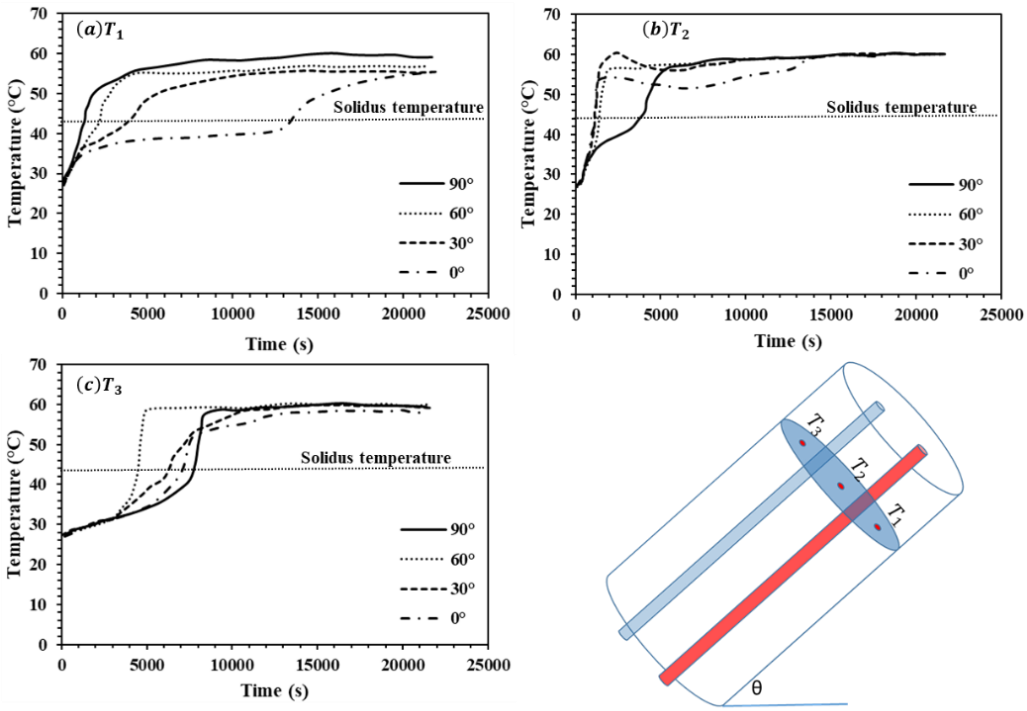

Fig. 5.5: Temperature distribution of PCM at upper section with inclination (a) T_1 (b) T_2 and (c) T_3

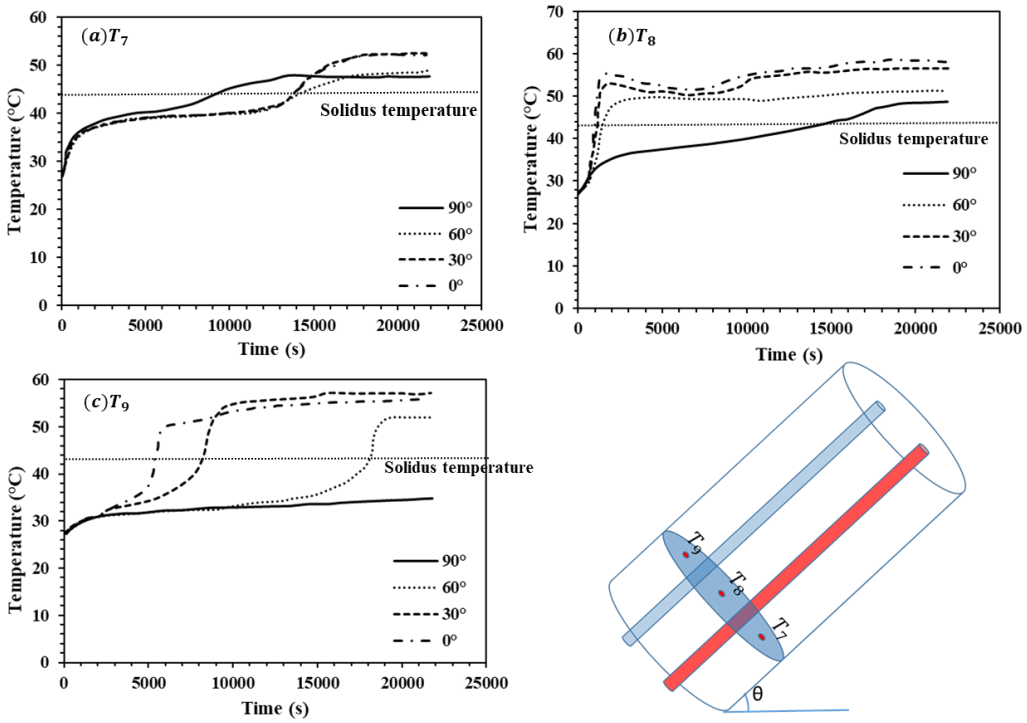

Fig. 5.6: Temperature distribution of PCM at bottom section with inclination (a) T_7 (b) T_8 and (c) T_9

Similarly, the temperature distribution of PCM at plane-3 (T_7, T_8 and T_9) in the lower half of the LHSS under SCD is presented in Fig. 5.6. A similar melting phenomenon of the PCM is observed as that of the upper half of the LHSS. But the temperature attained at the end of the SCD process is lower than the upper half. This is due to the buoyancy-driven natural convection where hot molten PCM moves upward. Therefore, the time taken to reach the solidus temperature is maximum. Overall it can be observed that the inclination of LHSS has a significant effect on temperature distribution in the case of SCD.

5.5.2 Propagation of melting profile

The melting profile evaluation versus time for different inclination angles of LHSS under the SCD process is shown in Fig. 5.7. The white and blue portion in the figure represents the unmelted PCM. In the beginning, heat transfer takes place from the hot HTF to the solid PCM and gradually a thin layer of liquid PCM is generated near the hot HTF tube. As time progress, the melted portion of the PCM in the upper half of LHSS increases. This can be inferred to the higher density of solid PCM which makes the solid PCM lump sink down due to gravity and thus pushing the liquid PCM upwards. Also, from Fig. 5.7 more liquid PCM can be noted near the hot tube (right tube for 90° and lower tube with orientation) at the end of 7200 s due to the thermal transport from hot tube to PCM, which makes the PCM

melt at the vicinity of the hot tube. Therefore the un-symmetric melting process is noted in SCD process for all the inclinations. As the accumulated heat from the PCM dissipates to the cold HTF the liquid PCM tries to solidify on the surface of the cold tube. Due to the formation of a thin layer of solid PCM on the surface of the cold tube the mode of heat transport is by conduction thus reducing the influence of natural convection at the cold tube. From Fig. 5.7 it can be noted that with the inclination more PCM got melted as compared to the vertical position (i.e. 90°). This can be inferred to more convection strength caused due to the placing of the hot HTF tube below the cold HTF tube. The positioning of the hot HTF tube below the cold HTF tube intensifies the natural convection and energy dissipates from the hot HTF tube to the liquid PCM and thus leading to effective thermal transport to the cold HTF. Placing a hot HTF tube at the bottom ensures an additional advantage when compared to the vertical position due to the exposure of cold HTF tube with the melted PCM. The melted PCM at the bottom of the heat exchange moves upward due to buoyancy and the heat absorbed by the cold HTF also increases. Moreover, with the decrease of inclination angle i.e. from 90° (vertical) to 0° (Horizontal) more melted liquid PCM can be noted in Fig. 5.7. With the progress of time, the melting of the solid PCM becomes insignificant and therefore the steady state condition can be considered to have attained. Nearly, half and one-fourth of PCM can be noticed to be unmelted for 90° and 60° angles. From Fig. 5.8 it can be understood that at the initial stage melt fraction does not differ significantly but with time due to variation of convective strength with inclination, the melt fraction also varies. At 90°, 60°, 30°, and 0° inclination angle the melt fraction of PCM are noted to be 0.71, 0.8, 0.96, and 0.98 at the end of 21600 s. With the decrease of inclination angle from 90° to 60°; there is an increase in melt fraction by 12.8 %. Further, a decrease in the orientation angle of LHSS from 60° to 0° led to an increase in melt fraction by 16.66 %.

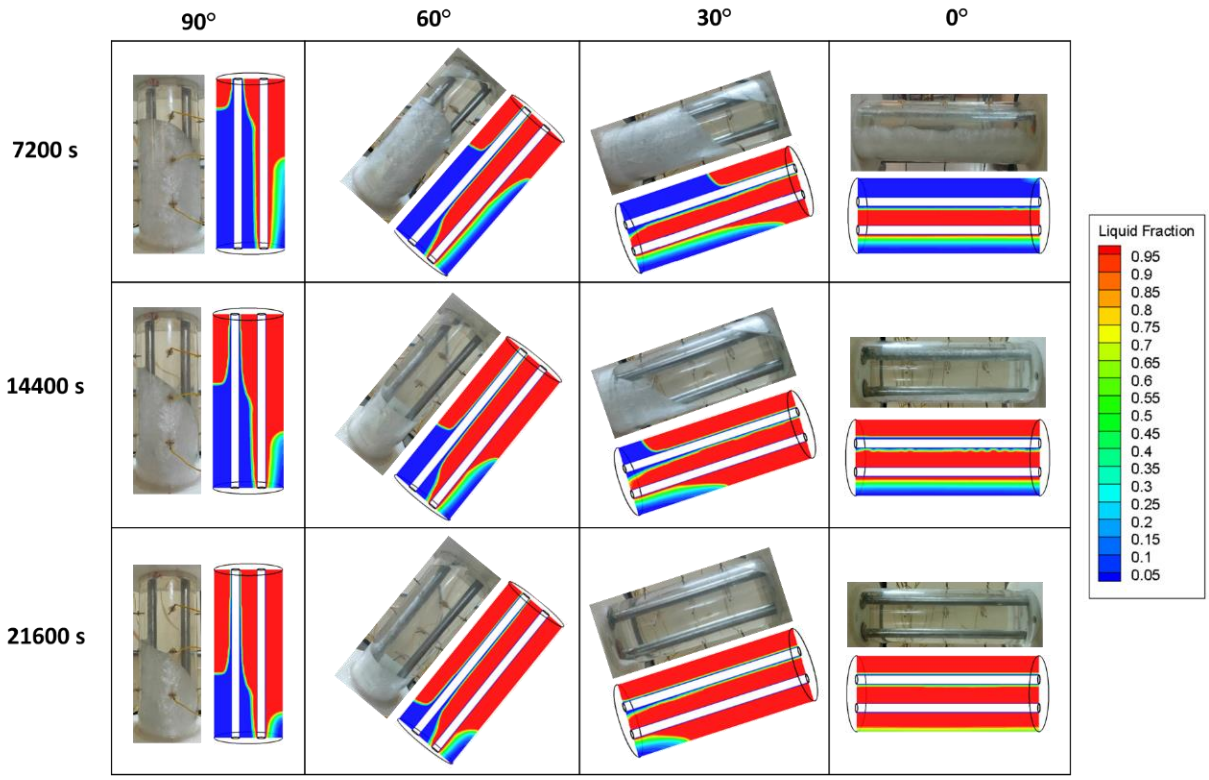

Fig. 5.7: Melting profile with time under different inclination angles

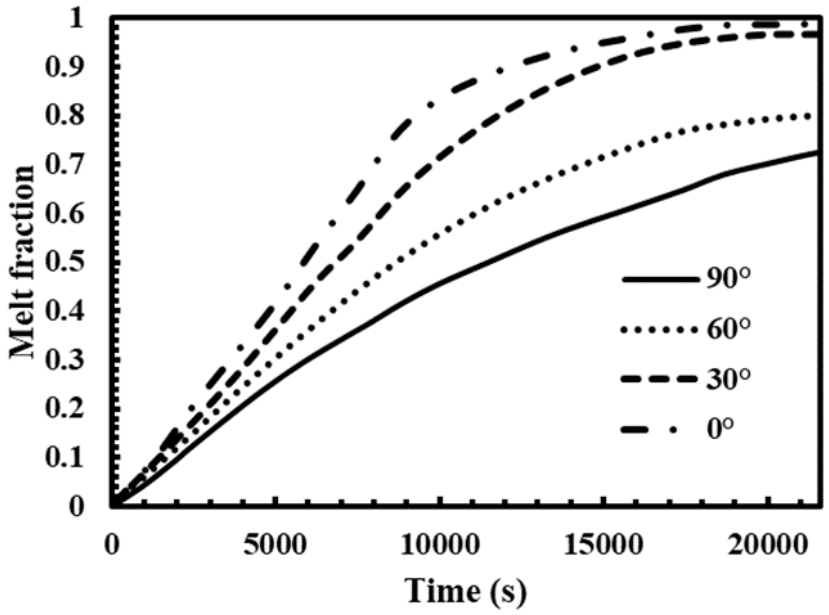

Fig. 5.8: Melt fraction of the PCM with inclination

5.5.3 PCM average temperature

Fig. 5.9 shows the average temperature during the SCD process for different inclination angles. At the initial stage, no significant variation in average temperature is observed with

inclination. The conduction mode of heat transfer can be inferred for this duration. As the melting process advances, the convection effect dominates and the average temperature of PCM got differed corresponding to the intensity of natural convection at different inclinations. In this region, the average temperature of PCM increases faster and later reached the steady-state condition. At horizontal (0°) position the melting of PCM is faster as compared to the vertical (90°). From Fig. 5.9 it can be observed that 0° and 30° inclinations took the same time for SCD to attain the steady-state condition. Here, the steady-state condition can be inferred to no further melting of PCM. After attaining steady-state condition the solid PCM no longer retains heat from the hot tube. As a result, direct thermal transport between hot and cold heat transfer fluids will occur. For SCD, LHSS is observed to attain a maximum temperature of 58°C with horizontal orientation and 50.4 °C in the vertical position.

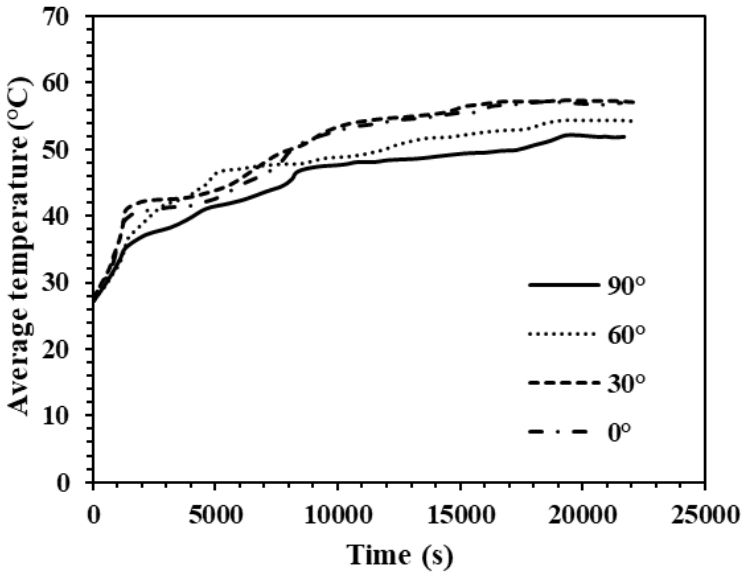

Fig. 5.9: Average temperature of PCM for different inclinations

5.5.4 Energy storage

The rate of energy stored by the PCM under the SCD process is given in Fig. 5.10 for different orientation angles of the LHSS. It can be seen that the orientation has an insignificant influence on stored energy for the initial duration i.e. up to 3600 s. As time progresses, this influence becomes noticeable. From Fig. 5.10 it is found that the lowest energy storage is 163 kJ for the vertical (90°) position. Also, it can be noticed that the energy stored increases by inclined LHSS from vertical to horizontal. The energy stored increases to 173.2, 223.9, and 231 kJ at the end of the process (i.e. 21600 s) with the 60°, 30°, and 0°

inclination angle. It is observed that the energy storage is enhanced by 41.72 % if the configuration of LHSS is changed from vertical to horizontal. The variation in energy storage is observed to differ with melt fraction. From section 5.5.2 it can be noted that the horizontal system melted to about 98% whereas, the vertical system to only 71%. Hence, the stored energy in horizontal configuration is more as compared to that of vertical position. It is observed that after 18000 s the steady-state condition is attained for 60°, 30°, and 0° (horizontal) positions. Once the steady-state is attained the thermal transport takes place directly between the cold and hot HTFs.

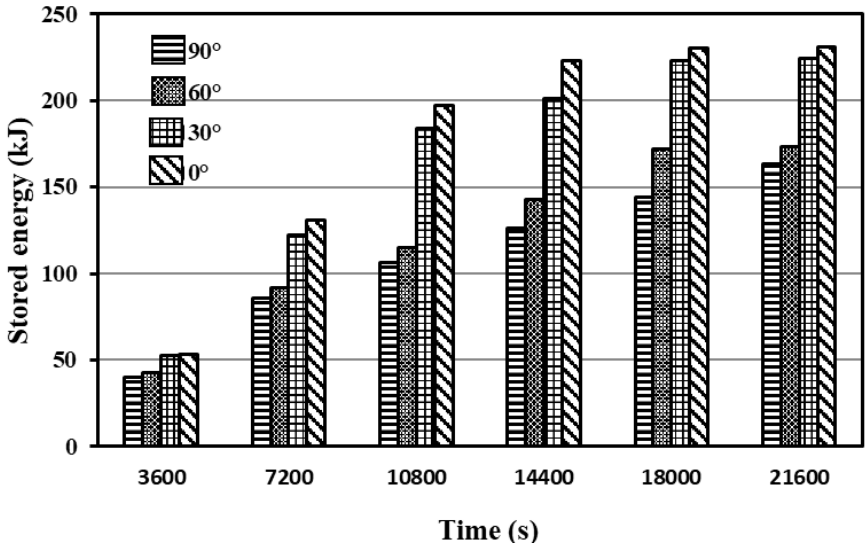

Fig. 5.10: Energy storage with time for different inclinations

5.5.5 Exergy analysis

In the performance evaluation of LHSS, exergy analysis is one of the important parameters to be considered along with the energy analysis. Therefore, it is required to evaluate the exergy efficiency of a LHSS under SCD. Fig. 5.11 shows the exergy efficiency under SCD with the orientation of LHSS. For the vertical (90°) system the maximum exergy efficiency is 6.08 % while 7.54 % is found for horizontal (0°) configuration. At the initial stage, exergy efficiency increases rapidly with time for all inclinations and follows the same value up to 1436 s. Subsequently, the exergy efficiency increases gradually and attain the steady-state condition. It can be noted that the exergy efficiency depends on the average temperature of PCM. By observing Fig. 5.9, the horizontal system shows a higher value of average temperature. This resulted in higher energy storage and hence observed to achieve higher

exergy efficiency. Also, the exergy efficiency attained the steady-state condition earlier in the case of the horizontal system.

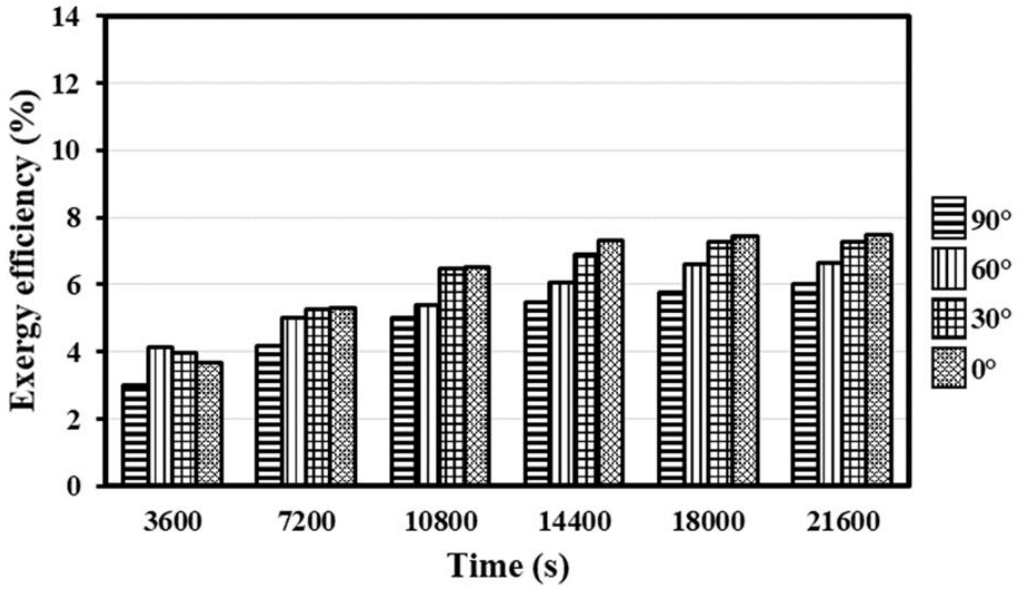

Fig. 5.11: Exergy efficiency of LHSS for different inclinations

5.5.6 Energy input and recovery

Fig. 5.12 presents the average energy input and recovery at the end of 21600 s. It can be noted from the figure that the average energy input and recovery increased as the inclination angle decreases from vertical (90°) to horizontal (0°). The variation in the quantity of the melted PCM caused the difference in thermal transport which lead to the temperature difference between inlet and outlet temperatures of the hot and cold HTFs. It can be observed from Fig. 5.7 that the melted PCM is more in horizontal (0°) and resulted to more thermal transport between the PCM and HTFs. This created more temperature difference between inlet and outlet temperatures of HTFs. Thus, the horizontal (0°) configuration has more energy input and recovery. Also, the horizontal system attained the steady-state condition earlier and further direct thermal transport between the hot and cold HTFs led to the higher energy recovery. At the end of the process, the energy input is found to be 111.23, 131.27, 177.89, and 206.54 kJ and recovery to be 48.44, 49.38, 63.75 and 65.56 kJ at 90° (vertical), 60°, 30° and 0° (horizontal) orientation respectively. However, energy transfer from LHSS to the cold HTF is limited due to the low thermal conductivity of PCM and thermal resistance offer by solid PCM around the cold HTF tube. Thus, it is suggested that more suitable heat transfer enchantment techniques should be implemented to tackle the low thermal conductivity problem.

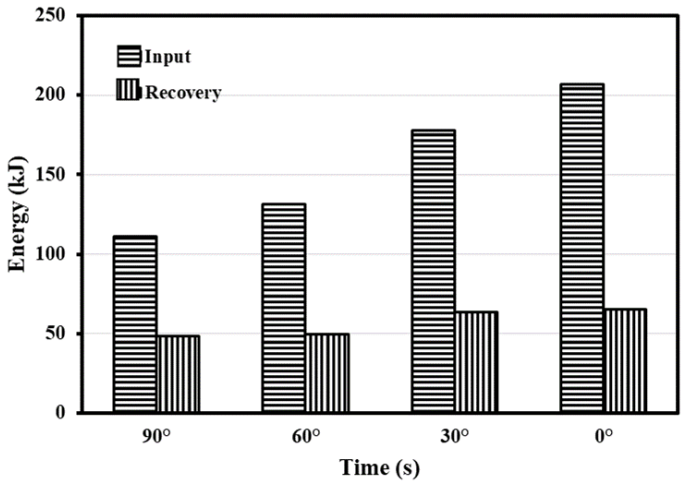

Fig. 5.12: Average energy input and recovery for different inclinations

5.5.7 Average Nusselt number

The average Nusselt number during the charging and the discharging process can be given as [154,156].

$$\overline{\mathrm{Nu}} = \frac{\mathrm{D}}{\mathrm{k}} \frac{\mathrm{q''}}{(\mathrm{T}_{w_h} - \mathrm{T_m})} \quad \text{For charging} \qquad (5.1)$$

$$\overline{\mathrm{Nu}} = \frac{\mathrm{D}}{\mathrm{k}} \frac{\mathrm{q''}}{(\mathrm{T_m} - \mathrm{T}_{w_c})} \quad \text{For discharging} \qquad (5.2)$$

Where, $\overline{\mathrm{Nu}}$ is the average Nusselt number, k is the thermal conductivity of the PCM, D is the characteristic dimension which is considered to be the diameter of pipe, $\mathrm{q''}$ is heat flux, $\mathrm{T_m}$ is the melting temperature of PCM and $\mathrm{T}_{w_h} and\ \mathrm{T}_{w_c}$ are the wall temperatures of the hot and cold tubes.

Fig. 5.13 shows the influence of inclination on the average Nusselt number under the SCD process till 21600 s. In the initial stage, the average Nusselt number rapidly decreases due to the formation of a thin layer of melted PCM near the hot HTF tube which acts as thermal resistance to heat transport. As the natural convection begins to occur the heat transfer from the hot HTF to PCM improves and hence the average Nusselt number increases with time. Later a marginal decrease is noted and finally, steady-state condition is reached. Whereas, at the same time during the discharging process, the average Nusselt number continues to increase over time until the steady-state condition is reached. This is due to the heat transport by conduction from PCM to the cold HTF at intial period. As the melting continuous, more amount of melted PCM starts to flow towards the cold HTF tube and higher heat transfer

between PCM to the cold HTF occurred. From Fig. 5.13 it can be observed that after 12000 s the average Nusselt number for discharging process exceeds that of the charging process. Therefore, it can be stated that before 12000 s the thermal transport between the hot HTF and PCM is more when compared to thermal transport between the cold HTF and PCM. After, 12000 s more heat transfer between melted PCM and cold HTF is obtained until a steady state is attained. It is also observed that the average Nusselt number for horizontal position reached the steady-state condition earlier as compared to other inclination angles. To obtain quantitative details of thermal transport for the charging and discharging processes the average Nusselt number with inclination is given in Table 5.4.

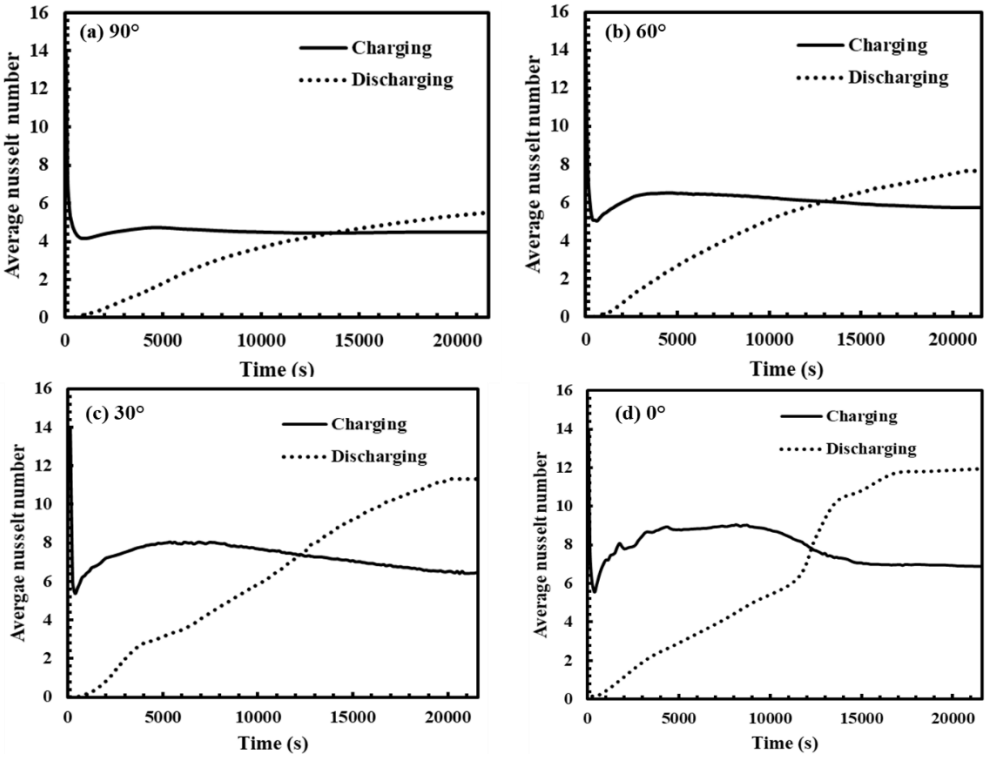

Fig. 5.13: Evolution of average Nusselt number over time for different inclinations

Table 5.4: Average Nusselt number for different inclination angles

Inclination	Average Nusselt number at the end of 21600 s	
	Charging	Discharging
90°	4.46	5.55
`60°	5.72	7.65
30°	6.34	11.77
0°	6.73	12.2

5.5.8 Flow behavior of PCM within LHSS

Fig. 5.14 illustrates the flow and convective recirculation of PCM for different inclination angles. For the sake of brevity 11600 s is considered for illustration. Based on the figure the PCM circulation can be noted nearer to the hot HTF tube which can be inferred to melted PCM. The heat from the hot HTF dissipates to the adjacent PCM and starts to melt. The melted PCM tends to move up due to buoyancy. When melted PCM reaches the upper half, the liquid PCM tends to move towards the cold HTF. When melted PCM arrive at the cold HTF, the streamlines at the cold HTF tube are nearly parallel and the liquid PCM move downwards along the cold tube. The flow behavior of the liquid PCM results in the formation of Benard cells between the two tubes. As the inclination angle decreases the size of the Benard cell becomes small and the number increases. At the horizontal (0°) configuration the size of the Benard cells are very small and larger in number. This behavior can be due to the restriction of the liquid PCM to move towards upper portions due to the presence of the cold HTF tube. This implies size and number of Benard convection cells depend on the inclination angle and position of the cold HTF tube.

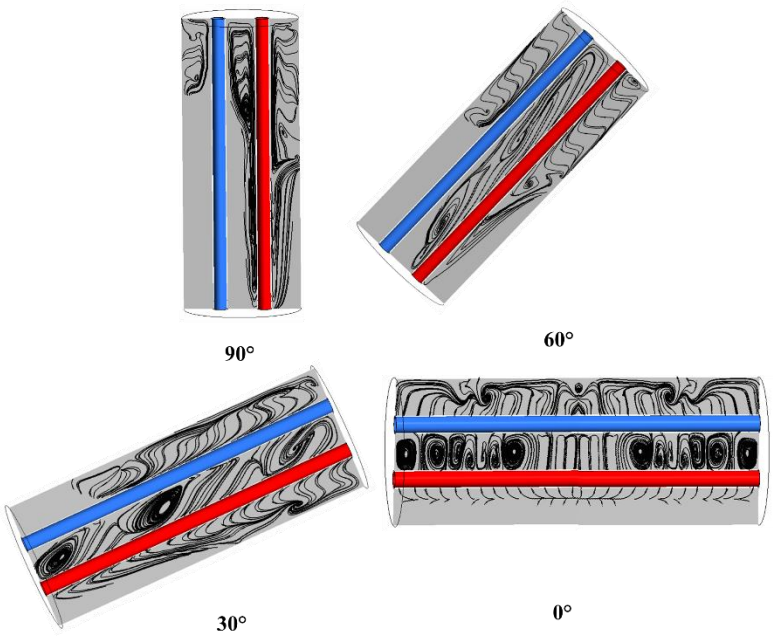

Fig. 5.14: Flow pattern of PCM for different inclination angles

5.4 Closure

The present study deals with the experimental investigation of a latent heat storage system (LHSS) with simultaneous charging and discharging (SCD) arrangement. The influence of

LHSS orientation on phase change behavior, temperature distribution, energy input/recovery and exergy efficiency are analyzed. Before commencing the experiment, the PCM is maintained at 27°C (solid state). The hot and cold heat transfer fluids are taken as water maintained at 80^{o}C and 27°C. Based on the study the following conclusions are drawn:

- The orientation significantly influences the SCD process due to the variation of thermal transport by natural convection. With orientation, the position of the cold and hot heat transfer fluid (HTF) tubes show a significant influence on the melting process.
- The steady-state condition is observed to be orientation specific. The horizontal (0°) configuration achieved steady-state condition earlier (15000 s). After attaining steady-state condition the thermal transport occurred between hot and cold HTFs.
- A maximum average temperature of 58°C, maximum exergy efficiency of 7.54% and maximum energy storage of 232 kJ is observed for horizontal (0°) position. The energy stored for the horizontal position is observed to be 41.72 % higher than the vertical (90°) position.
- The average energy input and recovery increase with the decrease of inclination angle. Energy recovery is 65.56 kJ for the horizontal position which is 35.34 % higher than the vertical position.
- Among 0^{o} (horizontal), 30^{o}, 60^{o} and 90^{o} (vertical) positions the horizontal position with the cold tube in the upper portion is observed to be promising. This arrangement of cold tube intensifies the natural convection and achieves effective thermal transport.
- The average Nusselt number for horizontal position reached the steady-state condition earlier as compared to other inclination angles. After 12000 s, the average Nusselt number in the discharging process is higher than the charging process.
- As the inclination angle decreases from vertical (90°) to horizontal (0°) the size of the Benard cell decreased and the number increased which leads to a faster melting process at the end of 11600 s.
- The low thermal conductivity of the PCM and thermal resistance over the cold HTF tube due to the formation of a solid PCM layer results in less recovery of thermal energy by the cold HTF. However, to tackle this problem suitable heat transfer improvement techniques viz. nanoparticle enhanced PCM, usage of fins, metal foam, etc. can be attempted.

Chapter 6
Experimental and numerical studies on augmentation of phase change material thermal response with circular fins

6.1 Introduction

In a previous chapter the effect of inclination on the thermal performance of PCM under SCD process was discussed. It is noted that orientation of LHSS significantly influence the SCD process. However, the performance of LHSS with SCD process depend on the thermal transport between hot and cold HTF which is hindered due to low thermal conductivity of the PCM. To overcome this issue various thermal response augmentation methods are available such as metal foam [157][158], attachment of fins [77][159] , PCM encapsulation [160][161] and dispersion of nanoparticle [162][163]. Among these, employment of fins is an easy and efficient approach to enhance the thermal performance [164]. In literature, various types of fins are taken into account viz. circular, longitudinal, tree-shaped, pin fins. Among these, circular fins showed more ability to improve the thermal transport in the conduction dominated region [165]. Hence in the current chapter thermal analysis of LHSS with fins is studied.

6.2 Experimental procedure and temperature measurement

Experimental test facility, the description of which was given in chapter 3 (Fig. 3.1) is used to carry out the investigations on SCD characteristics of PCM impregnated in a shell and tube LHSS with fin. Commercially available lauric acid is filled in the shell side and water is used as HTFs, which is made to flow through the tube by using centrifugal pump. The obtained thermophysical properties are given in Table 5.1 (Chapter 5). The shell has 101.6 mm (diameter) and 254 mm (length) with 5 mm thickness made up of polycarbonate. Two tube are used to pass the hot and cold HTFs from hot and cold baths respectively. Each tube has the inner diameter of 12.7 mm and thinness 1.4 mm. Four circular fins of diameter 88.9 mm and 0.8 mm thickness are implemented. In this study, 13 K-type thermocouples are installed. Thermocouples are arranged such that both axial and radial direction temperature measurement is possible. The position of thermocouples and dimension details of LHSS are shown in Fig. 6.1. Initially melted PCM is placed into the shell in such a way that whole

PCM fills the complete space of heat exchanger. Before, starting the experiment it is ensured that experimental setup is at atmospheric condition and there is no leakage. For SCD process, hot bath HTF is heated to a prescribed temperature and maintained the same temperature though out the experiment using PID-controller. At same time, cold bath is also maintained at the desire temperature. Then, the hot and cold HTFs are circulated through tubes simultaneously. A digital flow meter is installed to monitor the volume flow rate of HTFs. The temperature at various points are recorded by DAQ (Data acquisition system). To analyze the thermal performance of the LHSS with inclination four different inclination viz. 90°, 60°, 30°, and 0° are taken. 90° and 0° corresponds to vertical and horizontal positions respectively.

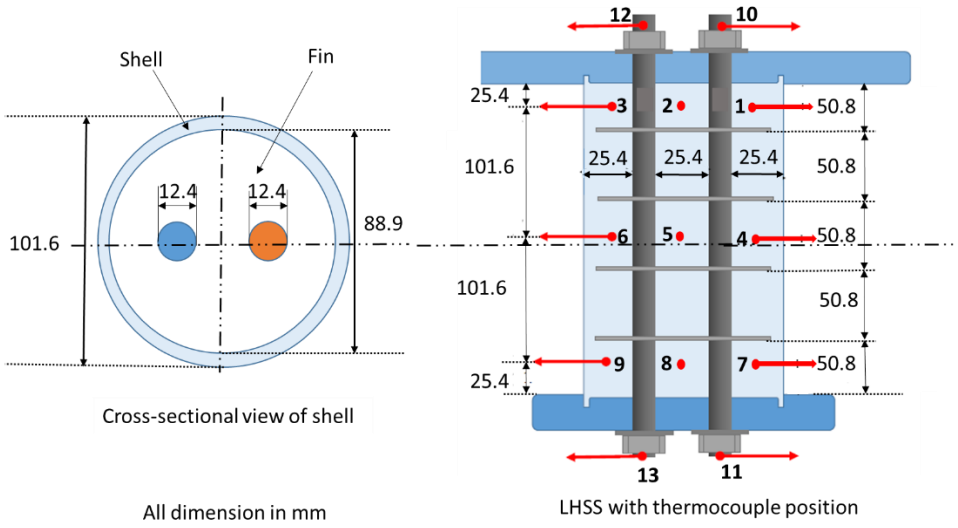

Fig. 6.1: Dimensions and thermocouple position of shell and tube heat exchanger

6.3 Grid independence and validation

The numerical procedure adopted for simulation was given in chapter 3 (Sec. 3.3). For considered LHSS, structure meshing is adopted to discretize the domain and is shown in Fig. 6.2. The mesh quality and time step have a great effect on the precision of a time-dependent problem's solution. For this, four sets of meshes elements 279424,376096,453150, and 523498 with fin as well as time steps 0.5 s, 0.4 s, 0.3, and 0.2 s are used to assess the grid and time step independency. Initial and boundary conditions are: inlet temperature of hot and cold HTFs are 80 °C and 27 °C, flow rate is 1.4 lit/min, initial temperature of the PCM is 27 °C. From Figs. 6.3 (a)-(d) show the comparison of melt fraction for the considered grid size and time step. It is observed that mesh elements of

453150 and a time step of 0.3 s for with fin is proven to be sufficient as the variation with 523498 and 0.2 s time step is less than 1%. Hence to reduce the computational effort 453150 elements with fin and a time step of 0.3 s are considered for further studies.

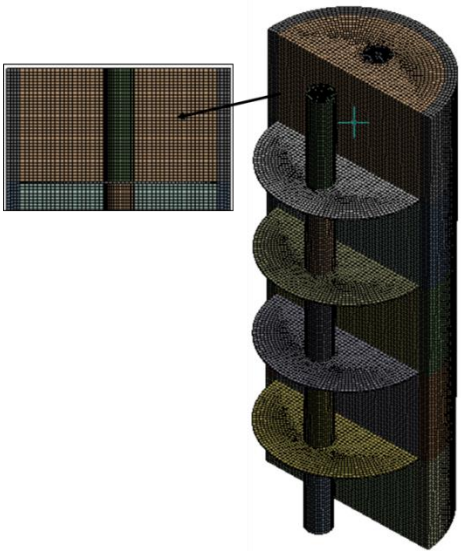

Fig. 6.2 Meshing domain

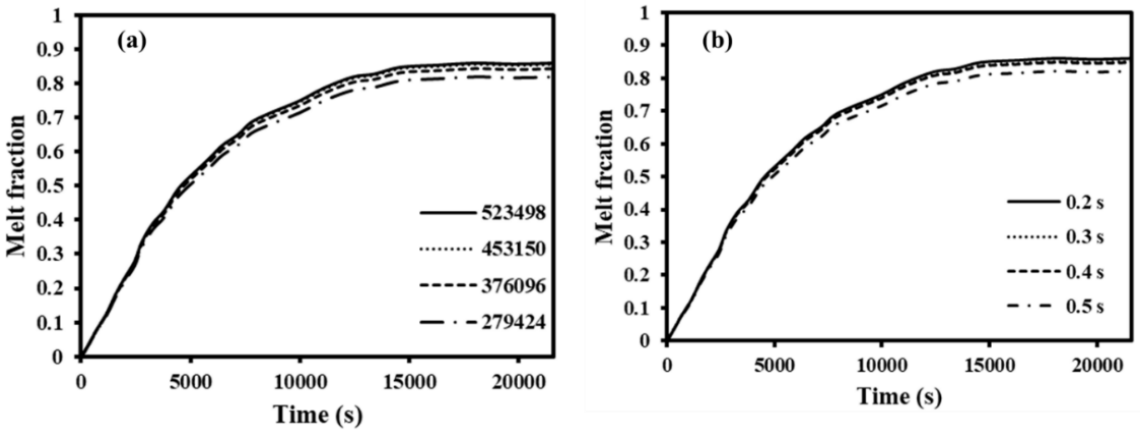

Fig. 6.3: Independence tests for (a) grid size (b) time step

To validate the current numerical methodology, the numerical result of vertically positioned LHSS is compared with experimental results of shell and tube heat exchanger. The test section of the experimental setup is shown in Fig. 6.4 (left). As discussed in section 2.4 the inlet temperature for hot and cold HTFs are circulated at 80 °C and 27 °C from constant temperature baths. Midpoint temperature of the LHSS is considered to compare the experimental and numerical data. The temperature profile from experimental is compared with the numerical result with and without fin and is shown in Fig. 6.4. The agreement between experiment and numerical results can be noted to be satisfactory with a maximum

difference of ± 8 %. Hence, detailed investigation can be performed studying the effect of inclination on thermal transport.

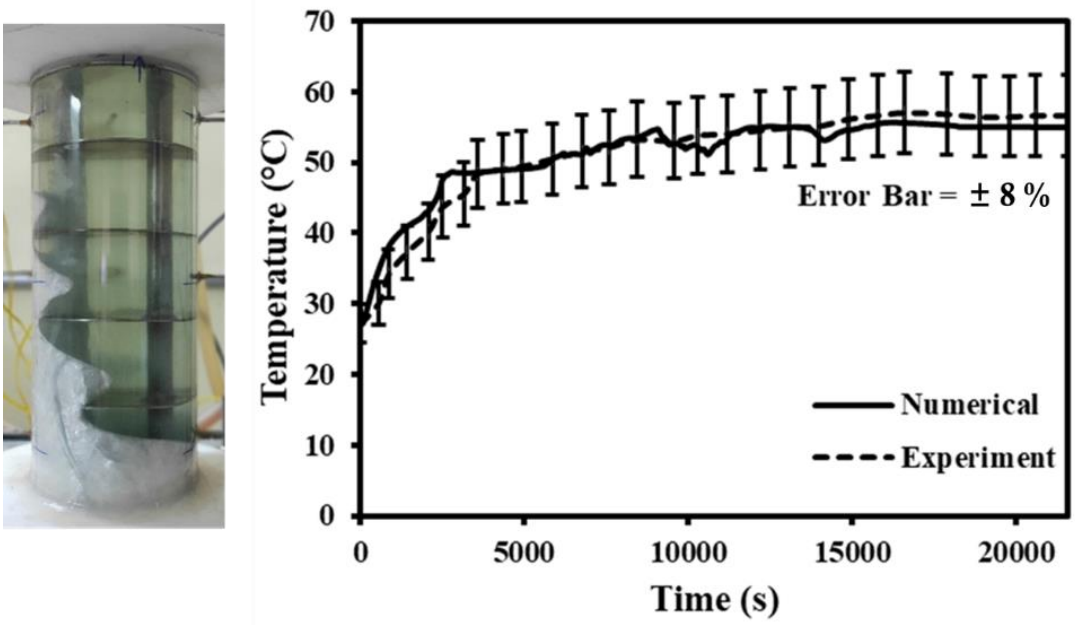

Fig.6.4: Comparison numerical data with experimental at vertical position at mid-point temperature

6.4 Uncertainty analysis

An experimental setup has various elements and each one introduce some error on the performance and calculation. These errors are used to calculate the experimental uncertainty associated within a system. In this study uncertainty analysis suggested by Robert Moffat [155] is adopted. The uncertainty of components considered in the present study is given in Table 6.1. The corresponding evaluation indicated that the amount of uncertainty subjected to energy transport is ±12.6%.

Table 6.1: Uncertainty of experimental parameters with fins

Parameter	Instrument used	Uncertainty
Temperature	K-type Thermocouple	± 0.2 °C
Mass flow rate	Digital flow meter	± 0.1 L/min
Hot and cold bath temperature	Digital PID controller	±1 %

6.5 Results and discussions

Experiments have been performed on a LHSS with simultaneous supply of hot HTF (charging) and cold HTF (discharging). Four different inclinations viz. 90°, 60°, 30°, and 0° are considered for the study. 90° and 0° corresponds to vertical and horizontal orientation of system. Results are presented in terms of temperature distribution, the average temperature of PCM, energy stored, heat input and output by HTFs, exergy and effectiveness of LHSS. Throughout the experiments the inlet temperature of hot and cold HTFs are maintained at 80 ^{o}C and 27 ^{o}C with a flow rate of 1.4 LPM.

6.5.1 Temperature distribution

Immediately after the SCD process begin, the tube absorb energy from hot water, and then the energy transfer to solid PCM takes place. Hence, the temperature near to the hot tube rises rapidly. This behavior will be same regardless of the orientation which is illustrated in Fig. 6.5. The figure highlights the temperature rise of PCM at three different locations i.e 1, 4 and 7. The locations of the thermocouples 1, 4 and 7 along the hot tube are shown in Fig.6.1. The time required to reach the solidus temperature is shown in Fig.6.5. In vertical position the time needed for thermocouple 1 to reach the solidus temperature is 1970 s. it can be noted that the time taken to attain the solidus temperature increases with the decrease in orientation. This is due to positioning of hot tube which goes below the cold HTF with the decreases in inclination. As the melting process start, due to the natural convection the melted PCM start to move towards the upper portion of LHSS. Hence, in the Fig. 6.5 it is observed that the thermocouple 7 which is at bottom portion of LHSS required more time to reach the solidus temperature as compared to upper half (1 and 4). The bottom portion thermocouple i.e 7 shows the time required to attain the solidus temperature is minimum for 90° orientation followed by 60° and 30°. For horizontal system, all thermocouples 1, 4 and 7 is exactly below to the hot tube and all the curve coincide with each other. Also, it is observed that temperature gradient between the lower and upper portions decreased with the decrease in orientation. The thermal transport in the lower half of the LHSS can be inferred to conduction due to the least increases in temperature.

Similarly, Fig. 6.6 shows the temperature distribution in axial direction towards the cold side. The location of these thermocouples (3, 6 and 9) along the cold tube are shown in Fig. 6.1. As melted PCM starts moving towards the cold side a recirculation for liquid PCM is created. This is evident in Fig. 6.6 where the time taken to reach the solidus temperature is

more towards the cold side for thermocouple 3 in vertical system. The delay in attaining solidus temperature for '3' indicates the thermal transport to the cold HTF. However, with the decrease of inclination (i.e 60°) the rise in temperature for '3' is earlier in comparison to '1'. With the decrease of inclination as the position of thermocouples 3, 6 and 9 move towards the upper section the melted PCM move up due to buoyancy. Therefore, by comparing the rise of temperature for thermocouple 6, the time taken to reach the solidus temperature is minimum for horizontal followed by 30°, 60° and 90°.

From thermal behaviour, it is noted that inclination of LHSS significantly influences the temperature distribution during SCD process due to corresponding change in natural convection. Therefore, natural convection must be taken into consideration. The temperature distribution in axial direction indicate that for vertical system (90°), the strength of natural convection is gradually increased and unsymmetrical distribution of temperature is observed. Whereas in horizontal position (0°) strength of natural convection is higher in the upper portion of LHSS and hence upper half takes lesser time to reach solidus temperature. The optimal inclination of the heat exchanger cannot be established based on the temperature distribution. To obtain a better understanding, other factors such as average temperature, energy storage should be consider which is discussed in the next section.

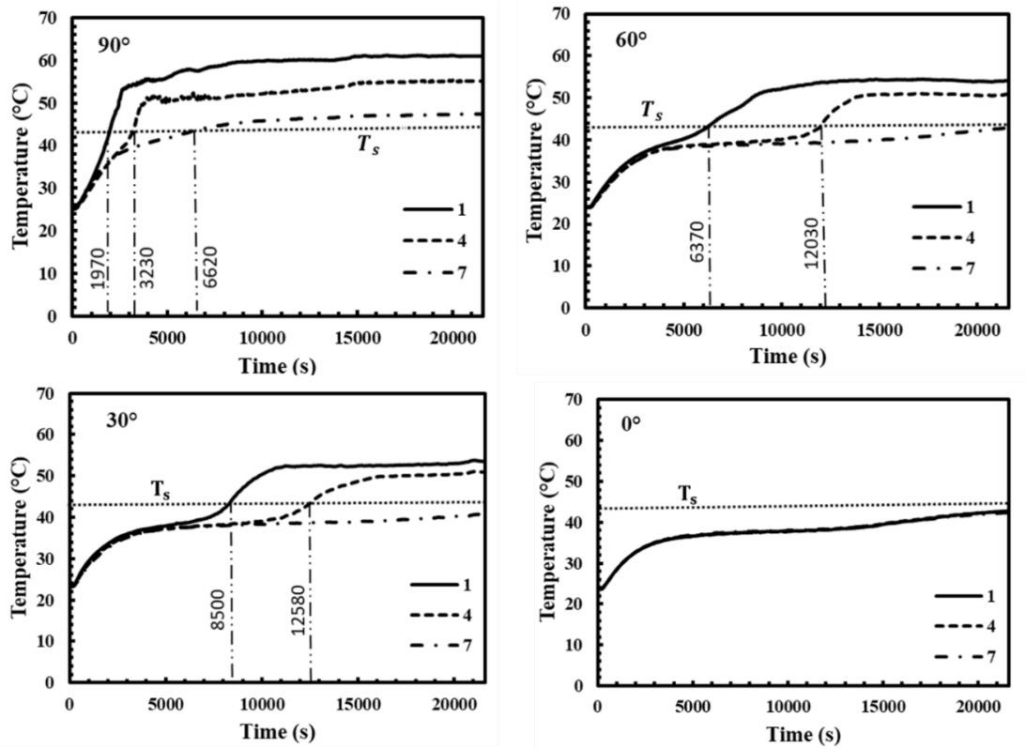

Fig. 6.5: Temperature distribution (Axial direction) towards hot side with inclination

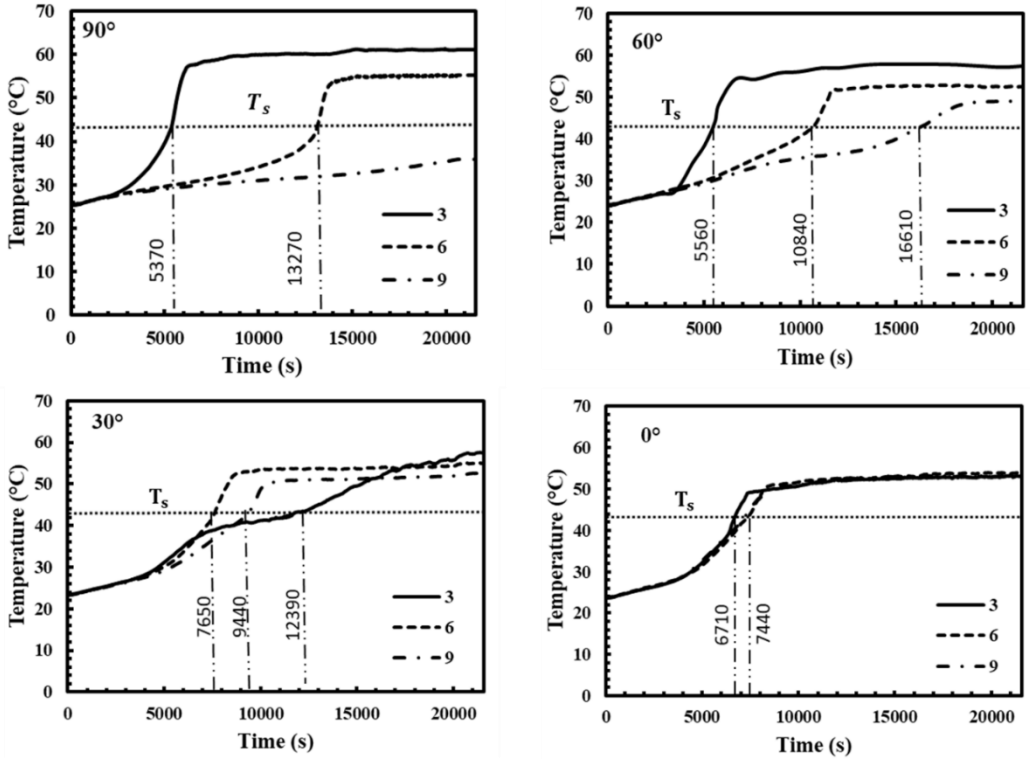

Fig. 6.6: Temperature distribution (Axial direction) towards cold side with inclination

6.5.2 Melt profile

Fig. 6.7 shows the propagation of solid-liquid interface at 7200 s, 14400 s and 21600 s of the melting process at all inclinations. At the initial stage, PCM near to the hot HTF tube melted first and due to buoyancy effect liquid PCM tends to move upwards. But because of the presence of fins the liquid PCM made to flow along the fins surface. Further, the liquid PCM start to move upwards through the gap between the fins and shell. Thus, the melted portion is observed near to the fins surface. For vertical position the melt profile is noted to form a saw tooth profile and more amount of solid PCM towards the cold HTF tube. With inclination, the melted PCM is obtained at the immediate vicinity of fins and solid PCM remained between the two successive fins. As time progress (14400 s), more amount of melted PCM is observed in horizontal position when compared to the vertical, 60° and 30° orientation. This is due to the intensification of buoyancy which escalated the natural convection and melting process. At 21600 s, more solid PCM can be observed in a vertical (90°) followed by 60°, 30° and horizontal (0°) position. This behavior can be inferred to more convection strength caused due to the positioning of the cold HTF tube above hot HTF tube. The placing of the cold HTF above the hot HTF tube strengthens the natural convection and results in effective thermal transport from the hot HTF tube to cold HTF tube.

Positioning of cold HTF tube towards the upper portion ensures an additional advantage when compared to the vertical position due to the more exposure of melted PCM. It can also be seen that thin layer of unmelted PCM is present around the cold HTF tube. This results in lowering the thermal transport from melted PCM to the cold HTF. From Fig.6.8 it can be understood that at the initial stage melt fraction is almost equal while simultaneous charging and discharging process continue with time melt fraction also varies with it. At 90°, 60°, 30°, and 0° orientation melt fraction of PCM 0.84, 0.89, 0.93 and 0.95 are noticed at the end of 21600 s. That means decreases in inclination angle from 90° to 60°; there is an increase in melt fraction of PCM by 5.61 %. Further decreases in orientation angle of LHSS from 60° to 0° the percentages of increases in melt fraction of phase change material are 6.31 %.

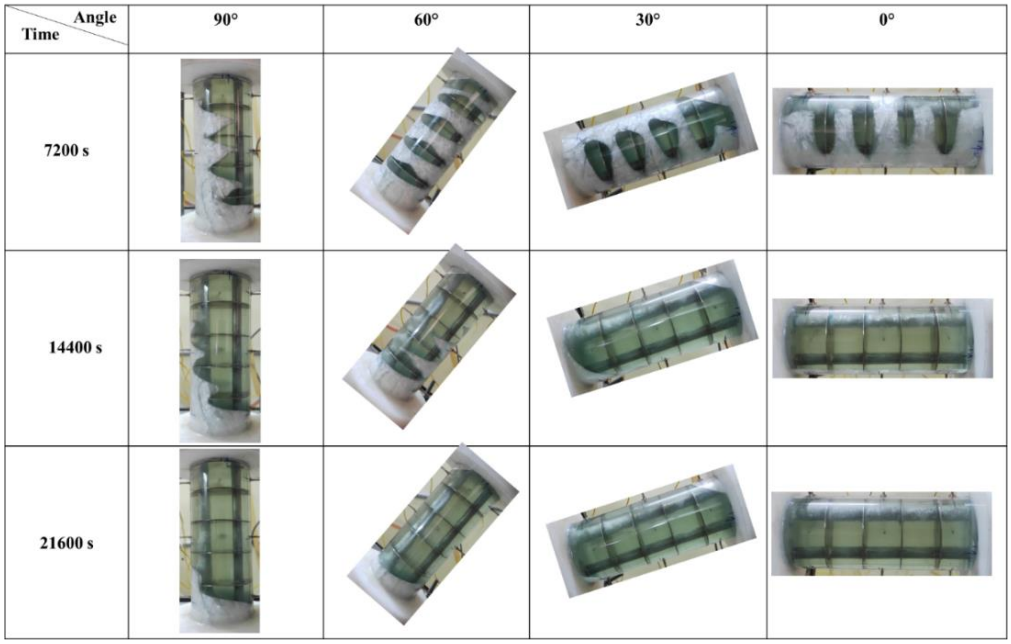

Fig. 6.7: Melt profile evolution over time with orientation

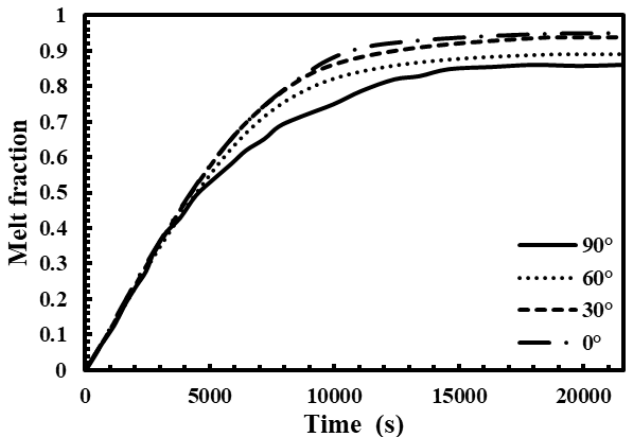

Fig. 6.8: Melt fraction over time with various orientation

6.5.3 Average temperature

Fig. 6.9 shows the average temperature of PCM with in LHSS with various inclinations. The average temperature is calculated based on method suggested by Kalapala and Devanuri [52]. From Fig. 6.9 (a) it is noted that there is no variation of average temperature with inclination at initial stage due to the conduction. After the commencement of melting process noticeable difference is observed in average temperature. This is because of natural convection which differ correspondingly with the inclination. Also, it is noted that the average temperature increases rapidly between the 1000 s and 4000 s for the 30° and horizontal configurations due to the intensification of the natural convection which drives higher amount melted PCM towards the upper half of the LHSS. However, the maximum average temperature is found in the vertical (90°) configuration followed by 60°, 30° and horizontal (0°). From Fig. 6.7 it can be noted that horizontal position has more melted PCM as compared to the other inclinations. This should result in higher average temperature for horizontal configuration. But from Fig. 6.9 the maximum average temperature is observed in the vertical position. The reason for attaining lower temperature for horizontal in comparison to vertical is due to positioning of cold HTF above the hot HTF. The melted PCM move up due to buoyancy and make good contact with cold HTF tube which leads to effective thermal transport from the PCM. From Fig. 6.9 (b) it can be observed that horizontal (0°) and 30° inclinations took the same time to attain the steady-state condition. Here, the steady-state condition can be inferred to no further melting of PCM. After attaining steady-state condition the PCM no longer retains heat from the hot tube. As a result, direct thermal transport between hot and cold heat transfer fluids will occur.

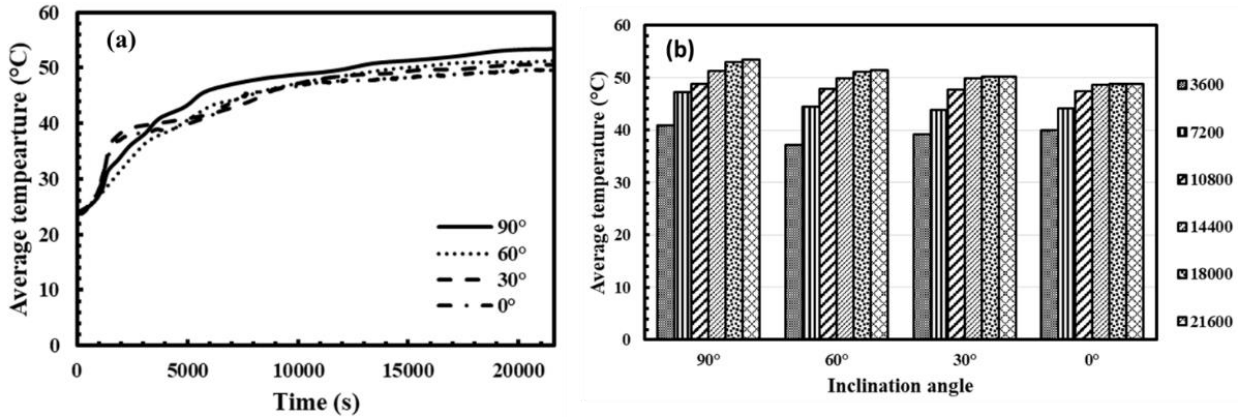

Fig. 6.9: Average temperature of PCM with inclination

6.5.4 Energy input and recovery

Fig. 6.10 presents the average energy input and recovery at the end of 21600 s. It can be noted from the figure that the average energy input and recovery increased as the inclination angle decreases from vertical (90°) to horizontal (0°). It can be observed from Fig. 6.7 that the melted PCM is more in horizontal (0°) and resulted to more thermal transport between the PCM and HTFs. This created more temperature difference between inlet and outlet temperatures of HTFs. Thus, the horizontal (0°) configuration has more energy input and recovery. At the end of the process, the maximum energy input is found to be 312 kJ and recovery to be 114 kJ at 0° (horizontal) orientation.

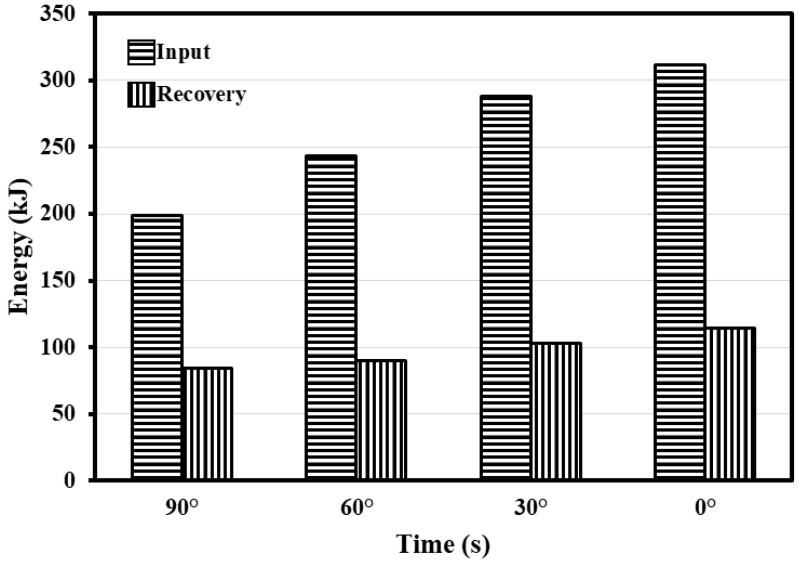

Fig. 6.10: Energy input by hot HTF and energy recovery by cold HTF

6.5.5 Energy storage

Fig. 6.11 shows the variation of energy stored by the PCM at different inclinations. The result shows that the trend of the energy storage for all inclinations is similar. It is observed that the highest value of energy stored is 224 kJ for the horizontal (0°) position and followed by the 30°, 60° and vertical (90°) system. It can be noted that the energy storage by the PCM depends on the amount of melted PCM. From Fig. 6.7 it can be observed that the unmelted PCM is less in case of horizontal configuration. Therefore, the maximum energy stored is observed in the horizontal position. From Fig. 6.11 it can be noted that with progress of time the energy storage has come to the steady state condition. As discussed in section 6.5.3 the steady state condition refers to the direct heat transfer between the hot and cold HTFs. Which indicates the energy storage by the PCM is not prevalent.

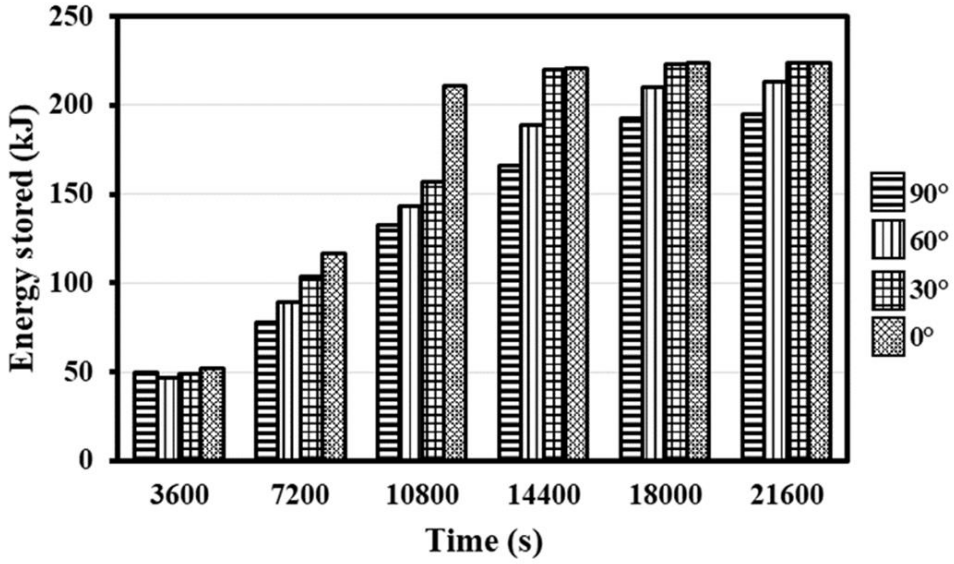

Fig. 6.11: Energy stored by the PCM at different orientation

6.5.6 Exergy efficiency

In the performance evaluation of LHSS, exergy analysis is one of the important parameters to be considered along with the energy analysis. Therefore, it is required to evaluate the exergy efficiency of a LHSS under SCD condition. Fig. 6.12 shows the exergy efficiency of LHSS at various inclinations under SCD process. The exergy efficiency can be noted to increase with the decrease in inclination from vertical to horizontal. The maximum exergy efficiency for vertical (90°) position is 9.57 % and observed to increase with the decrease of inclination. For 60°, 30° and 0° the maximum exergy efficiencies are 10.7, 11.9 and 12.9 % respectively. It can be noted that the exergy efficiency depends on the average temperature of PCM and the temperature difference between the inlet and outlet temperatures of HTFs. Owing to the maximum average temperature which is higher in vertical position the exergy efficiency is less. This can be due to the non-uniform temperature along the cold HTF tube for vertical position. The hot melted PCM move up due to buoyancy whereas the low temperature PCM settles down due to gravity. This gradient along the length of HTF tube decrease with the decrease of inclination from 90° to 0°.

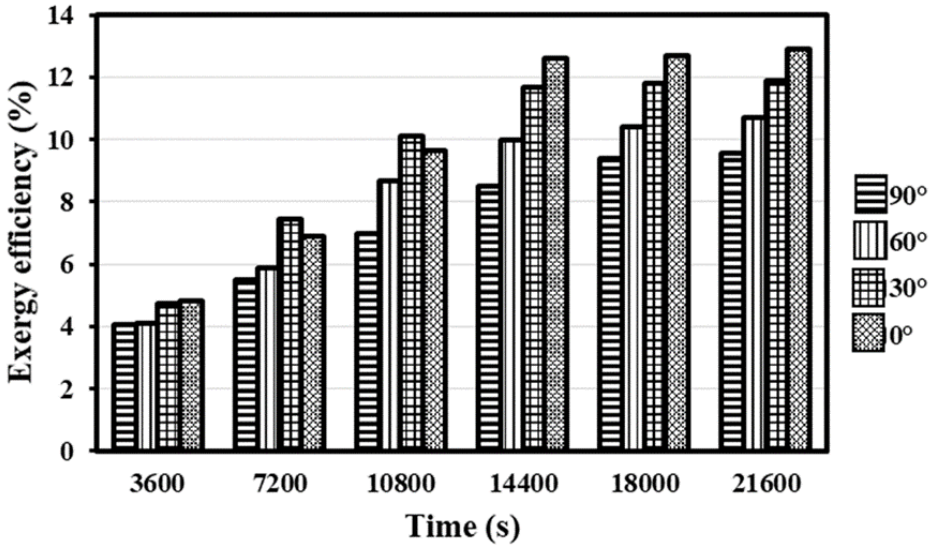

Fig. 6.12: Exergy efficiency of LHSS with inclination

6.5.7 Average Nusselt number

The variations of Nusselt number for various cases at any individual given orientation depicted in Fig.6.13. The Nusselt number diagram's trend is divided into three segments. The variations are mainly due to the consecutive change in the type of thermal transport mechanisms. To begin with, the Nusselt number drops sharply at initial state of melting. This decrease section refers to the fact that the early stages of the melting process are primarily dependent on conductive heat transfer. When the PCM surrounding to the hot tube begins to melt Nusselt number rises in its trend and continues until the significant amount of PCM melts. From Fig. 6.7 the melt front of the PCM propagates as time goes on. As a result, convective heat transfer takes over as the dominant heat transfer mode, causing the melted portions to rise. The greater the convective heat transfer, the greater the reduction of the conductive component. As a result, the Nusselt number is greatly enhanced in this section. Finally, the strength of convective heat transmission decreases as it does not have sufficient potential to melt all of the PCM within the shell. As a result, the Nusselt number begins to decline yet again. In this point of time, convective heat transfer may not contain the same high potential as it did at the start. As a result, the descending section has a relatively consistent and constant slope. Whereas, during the discharging process the average Nusselt number continues to increase over time up to the steady state condition reached. This is due to the thermal trasport between the cold HTF and solid PCM at the initial stage of phase change becomes very less and continuous to increases with respect to time during the discharging process. According to Fig. 6.13 (a)-(d), the average Nusselt

number does not varies significantly with orientation on the hot tube which indicated that energy transport from hot water to solid PCM is nearly same. However, the effect of orientation is significant on the average Nusselt number towards the cold tube. Therefore, it is noted that thermal transport from the liquid PCM to the cold HTF is differ according to orientation.

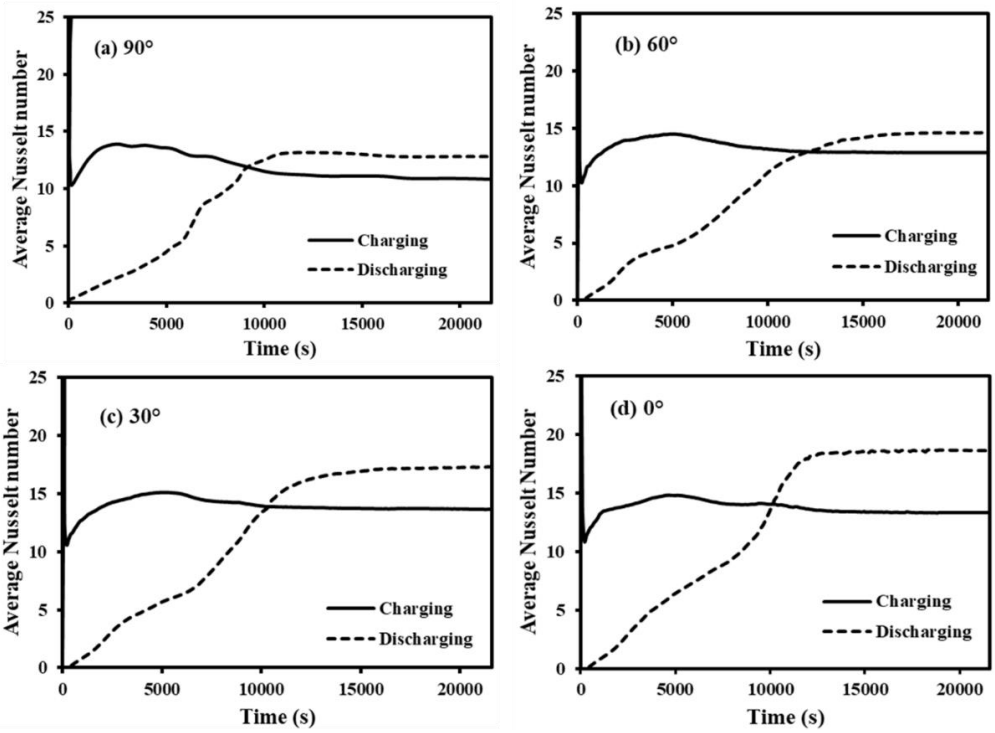

Fig. 6.13: Comparison of time averaged Nusselt number for various orientation

6.3.8 Flow behavior of PCM

Fig. 6.14 indicated the streamlines for various orientation. The Bernard cell is formed due to restricted of melted PCM flow created by the cold tube and fins. Brevity, 11400 s time consider to represent the Rayleigh-Bernard convection. At 11400 s, vertically distributed Bernard cells are observed in each successive fins. It is seen that when the orientation changed the streamline distribution in the LHSS change gradually in the direction of natural convection. Buoyancy forces induce the melted PCM to rise vertically and made to flow toward to the cold tube. The temperature of the melted PCM cools down and the flow is directed downward direction resulting in the development of a Bernard cell. The streamlines depicted in the Fig. 6.14 indicate the formation of Rayleigh–Benard convection cells between cold and hot HTFs tubes. The Bernard cells is gradually enlarged with changed in inclination from vertical to horizontal position. This demonstrates that the effects of

buoyancy force become very intense in horizontal configuration. On other hand it can be due to the flow of melted PCM directly restricted by the fins and cold HTF tube for vertical. Whereas for the horizontal position the flow of PCM restricted by the cold HTF.

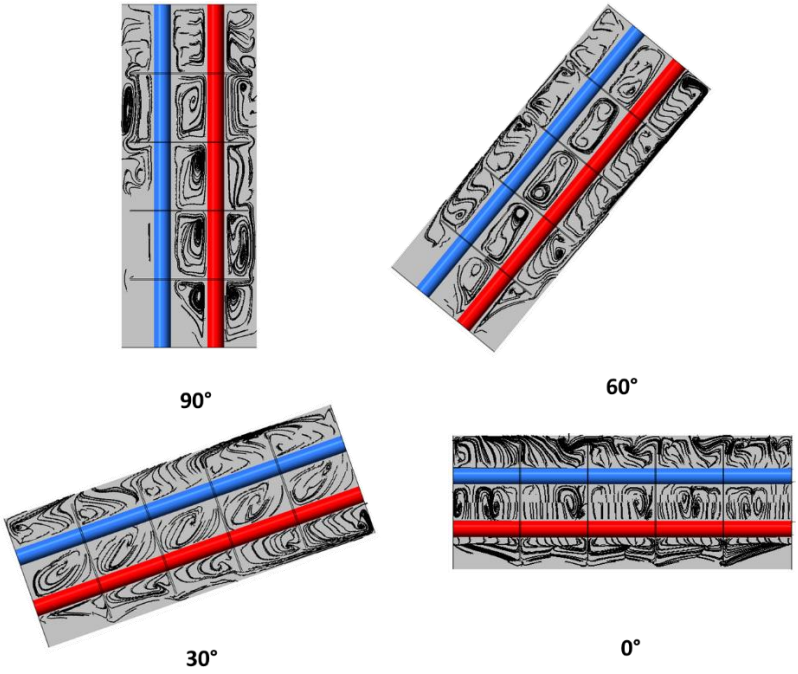

Fig.6.14: Flow behavior of PCM with fin

6.4 Closure

The thermal performance of the LHSS under SCD process is examined experimentally by employing fins. The effect of orientation on thermal transport is ascertained considering various parameters such as melt profile, average temperature, energy input and output, energy stored, effectiveness and exergy efficiency. From the thermodynamic analyses the following conclusions are drawn:

- The convective strength is observed to get intensified gradually for vertical configuration (90°). While for the horizontal position (0°) the natural convection got intensified quickly in the upper portion of the LHSS.

- The maximum average temperature is observed for the vertical position with the decrease of inclination i.e from 90° to 0° the melted PCM moved up due to buoyancy and dissipated the rest to cold HTF. This phenomenon resulted in a lower average temperature for horizontal configuration (0°).

- Energy input and recovery are significantly influenced by the orientation of the LHSS.
- It is observed that the highest value of energy stored is 224 kJ for the horizontal (0°) position and followed by the 30°, 60° and vertical (90°) system. The maximum exergy efficiency at the end of 21600 s are determined to be 12.9 % for horizontal configuration.
- The average Nusselt number shows that initially, the heat transfer is mainly due to hot HTF. As the process progressed, the heat transfer is higher from melted PCM to the cold HTF.
- By analyzing the streamline, it is observed that fins restricted the flow of melted PCM hence it can be suppressed the natural convection by adding the fins into the LHSS.

Chapter 7

Experimental investigation to assess the thermal performance of an inclined latent heat storage system with perforated fins

7.1 Introduction

From the previous chapter, it is observed that flow of the melted PCM is restricted by employing fins which leads to the suppression of natural convection. One of the possible options to overcome this problem can be perforated fins. Here the melted PCM can move through the perforation and can help to enhance natural convection. It may be noted that Kalapala and Devanuri [70] and Karmi and Kamkari [166] are the only works available pertaining to the performance analysis of shell and tube heat exchanger with perforated fins. Therefore, further investigate is required to perform the thermal performance LHSS with perforated fins. Hence, in this chapter effect of perforations on the LHSS with different inclinations under the SCD process is analyzed.

7.2 Geometry description and experiment procedure

To evaluate the effect of fins on the thermal performance, the shell and tube LHSS shown in Fig. 7.1 is considered. Lauric acid used is as a PCM due to its suitable thermal properties for low temperature application. The measured thermophysical properties for the PCM are presented in Table 5.1 (Chapter-5). The PCM is filled into a polycarbonate shell with an inner dimeter of 100 mm and a thickness 1.6 mm. Shell is filled with approximately 1.6 kg of PCM. In addition, the water used as the HTF. Water is made to flow through the two stainless steel tubes having inner diameter 12.4 mm while its thickness is 1.4 mm. The thermostats are used to maintain a constant temperature for hot and cold water baths. Ball valves are used to change the flow rate and is measured by digital flow meters. Four circular fins are attached to the HTF tubes to enhance the thermal transport from HTFs to PCM. The diameter of fins is 88 mm and thickness is 0.8 mm. For perforated fins, the hole diameter is 5.08 mm and 6 holes as shown in Fig. 7.1 are provided on each side of tubes. Fins are made of stainless steel due to its high thermal conductivity. 9 K-type of thermocouples are inserted at different location to measure the temperature of PCM. The

thermocouples are arranged in such a way that reading can be taken both in radial and axial directions. 4 thermocouples are used to obtain the inlet and outlet temperatures of hot

The experimental setup is shown in chapter 3 (Fig. 3.1). From the figure it can be noted that the experimental setup can be divided into the four parts: charging, test section, data acquisition system and discharging. Water is used as heat transfer fluids. To compensate the thermal expansion of PCM small gap is provided at the upper portion of LHSS. The charging process begins by pumping hot HTF from the constant temperature hot bath. At the same time, the discharging of PCM is enable through circulating the cold HTF from the constant temperature cold bath. The hot and cold HTFs are made to flow through tubes. The HTFs are returned to the constant temperature cold and hot baths and the process is repeated. The inlet temperatures of cold and hot HTFs are taken to be 27°C and 80°C and the flow rate of both the HTFs are 1.4 lit/min as suggested by Kalapala and Devanuri [52]. Also, based on the earlier chapter-4 it is observed that effect of flow rate and direction of HTF has insignificant influence on the melt fraction. The objective of this study to compared the thermal performance of LHSS with perforated fins. Also, the effect of orientation on the thermal transport between the hot and cold HTFs is analyzed. For these four orientation viz. 90° (vertical), 60°, 30° and 0° (horizontal) have been considered to the study.

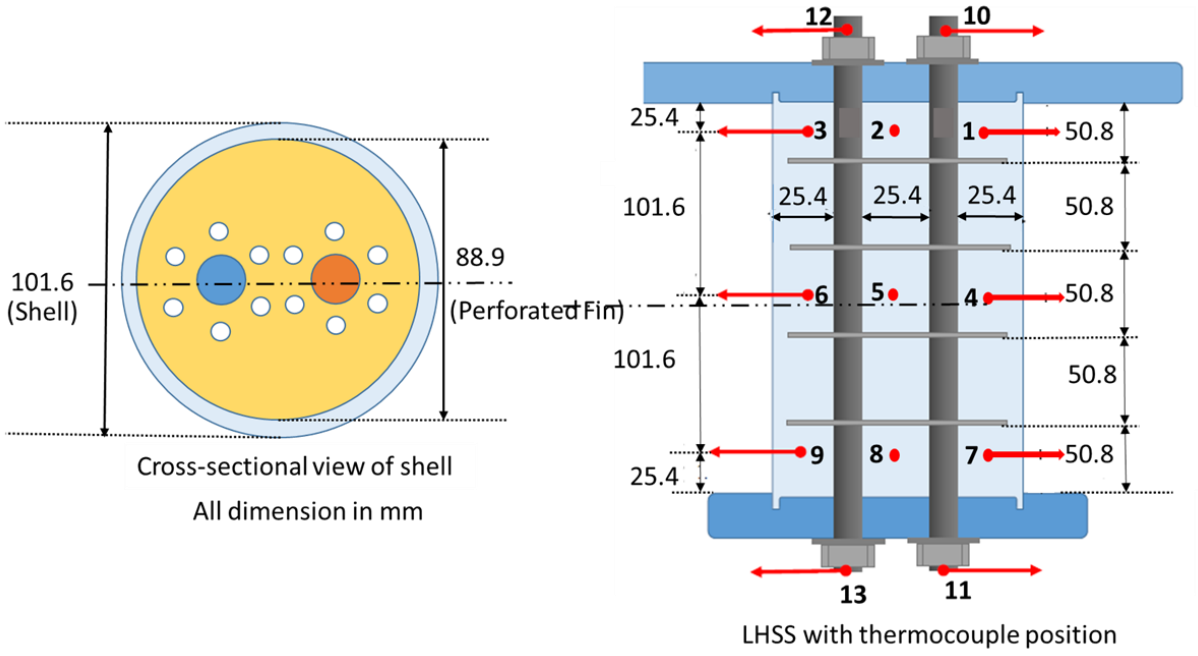

Fig. 7.1: Dimensions of shell and tube LHSS and position of thermocouples

7.3 Error analysis

To predict the error for the obtained results uncertainty of experimental parameters need to be performed. In the current analysis, the most essential parameters to be evaluated are temperature and flow rate. Uncertainty provides strength in the execution of experiments. The uncertainty of the LHSS can be calculated based on the method proposed by the Moffat [155]. Table 7.1 shows the accuracy of instruments that are used in experiments. Corresponding to present calculation the energy stored and exergy are estimated to have an uncertainty of ±11.3% and ±12.8%.

Table 7.1: Uncertainty of experimental parameters with perforated fins

Parameter	**Instrument used**	**Uncertainty**
Temperature	K-type Thermocouple	± 0.2 °C
Mass flow rate	Digital flow meter	± 0.1 L/min
Hot and cold bath temperature	Digital PID controller	±1 %

7.4 Results and discussions

In this section, the results obtained from the experiments for simultaneous charging and discharging (SCD) process are presented in detail. The results are compiled by studying the effect of orientation on the thermal performance of latent heat storage system (LHSS) with perforated fins. Also, comparison of heat transfer characteristics of LHSS without and with solid and perforated fins are analyzed. The temperature evolution, melt profile, energy stored, energy input and recovery and exergy efficiency are studied. The parameters such as inlet temperature of hot (80 °C) and cold (27 °C) HTF and mass flow rate (1.4 lit/min) are kept as constant for all the orientations.

7.4.1 Temperature distribution

Figs. 7.2-7.3 shows the timewise PCM temperature profile without and with solid and perforated fins at different inclinations. PCM temperatures are shown towards the hot and cold side at locations 1, 4, 7 and 3, 6, 9 of the LHSS. The location of the thermocouples ‘1, 4 and 7’ and ‘3, 6 and 9’ is shown in Fig. 7.1. From Figs. 7.2 and 7.3, three temperature zone can be observed. First, the temperature of PCM increases with lesser slope during this period the the solid PCM absorbs the heat from the hot tube as sensible heat. In the second

zone due to melted PCM, the natural convection comes into play. Hence, temperature profile slope sharply increases. Lastly, the zone three shows the temperature profile to be constant which shows the attained of steady state condition. Fig. 7.2 indicates the variations of the PCM temperature in the axial direction towards the hot side with different inclinations. It is observed that the thermocouple '1' near the hot HTF tube and upper portion of LHSS increase rapidly during the initial duration for all configurations except horizontal (0°). This is due to PCM nearer to the hot HTF melts first and natural convection escalates in the upper half of LHSS. The intensity of natural convection increases from the lower portion of the LHSS to the upper. With the progress of time, the liquid PCM flow towards the cold HTF. The temperature behavior (1, 4 and 7) shown in Fig. 7.2 represent that thermocouple '1' attains the melting temperature earlier than '4' followed by '7'. '1' takes 2240 s while 7 requires 13130 s to attain the same temperature for vertical LHSS. With the inclination angle, the behavior of temperature in the LHSS changes completely. This is due to the change in convective strength which is influenced by the inclination. It can be noted that with inclined LHSS from vertical (90°) to 0° (horizontal) the temperature difference between thermocouple '1' and '7' diminishes.

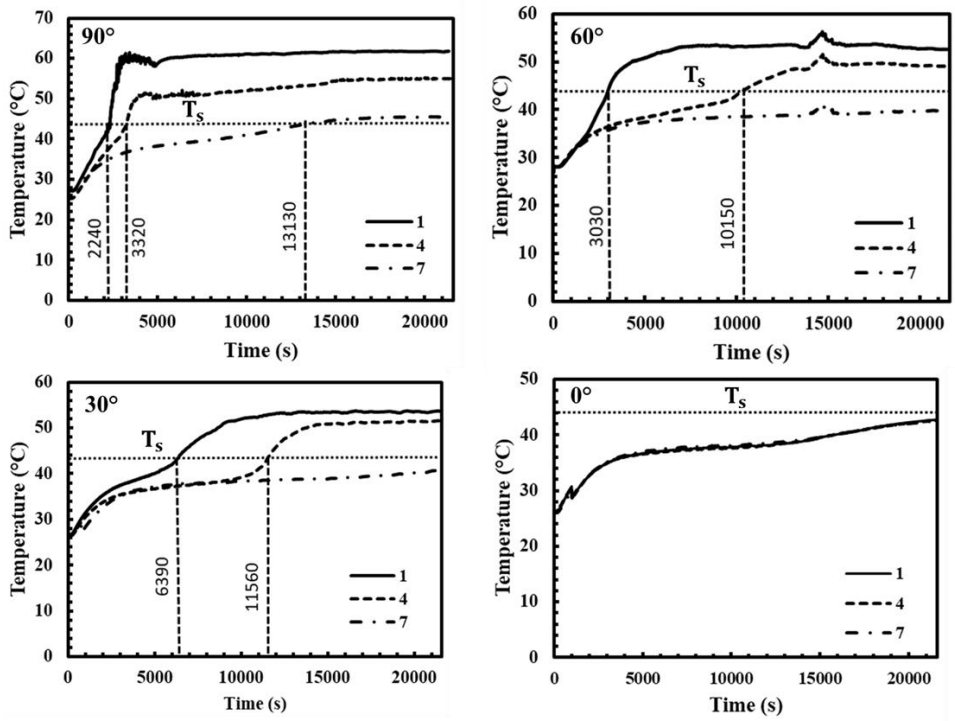

Fig. 7.2: Temperature distribution of thermocouple towards hot HTF tube

Similarly, the temperature distribution of PCM (3, 6 and 9) towards the cold side of the latent heat of storage unit under SCD with inclination is presented in Fig. 7.3. The

temperature distribution shown in Fig. 7.3 infers that thermocouple '3' reaches the melting temperature earlier than '6' and '9' for 90^{o} and 60^{o} orientation. It is observed that thermocouple '3' takes 3360 s to attain melting temperature while the bottom portion of LHSS remains unmelted for vertical (90°) position. For the orientation angle of 30°, thermocouple '3' records melting temperature by 7090 s which is higher than the vertical (90°) position. For the horizontal (0°) system, the buoyancy force acts exactly normal to the hot tube in the upward direction thus pushing the melted PCM towards the cold tube. As seen in Fig. 7.3 all the points have shown nearly equal temperature along the axial direction for horizontal (0°) configuration. Thereby, it can be concluded that the temperature difference in the axial direction becomes gradually less with decreases in the orientation.

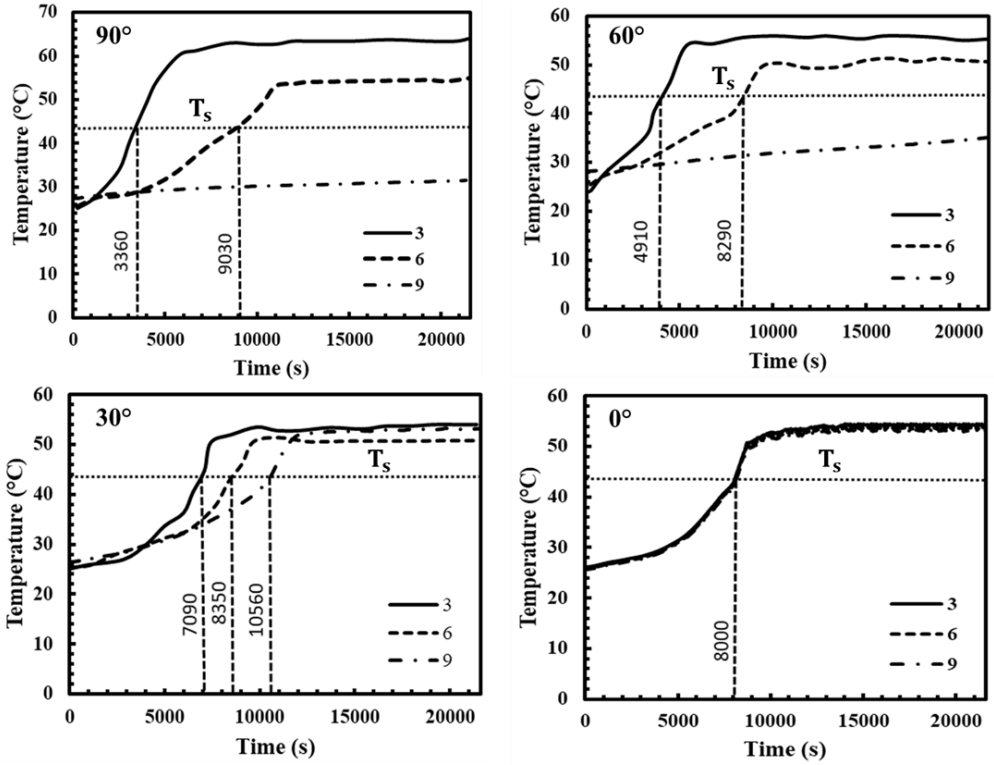

Fig. 7.3: Temperature distribution of thermocouple towards cold HTF tube

7.4.2 Average temperature

Fig. 7.4 depicts an analysis of the PCM average temperature with the variation of inclination for the LHSS with perforated fins. As the LHSS is changed from 90° to 0°, convective strength in the upper half gets intensified resulting in a faster temperature rise for the initial period. With the decrease of inclination i.e from vertical (90°) to horizontal (0°) the accumulation of melted PCM increases in the upper section of the heat exchanger.

The presence of perforated fins leads to better thermal transport to the upper section. It can also be seen that until the steady state condition is attained using perforations is more favorable in a vertical and 60° position as the average temperature is more for perforated in comparison to solid fins. The variation gets nullified with further decreases of inclination. Despite perforated fins showed a more average temperature during the beginning stages in a vertical position. The average temperature is higher for solid fins after duration of 21600 s. This is due the adding fins is equivalent to LHSS separating into a number of partitions. If solid fin is provided the melted PCM is forced to flow move in this partitions. Whereas perforation is added to the solid fin melted PCM flow through the hole towards the top. As a result weak movement in the bottom portion of LHSS and the average temperature at the bottom portion with perforated fins is slower than with solid fins.

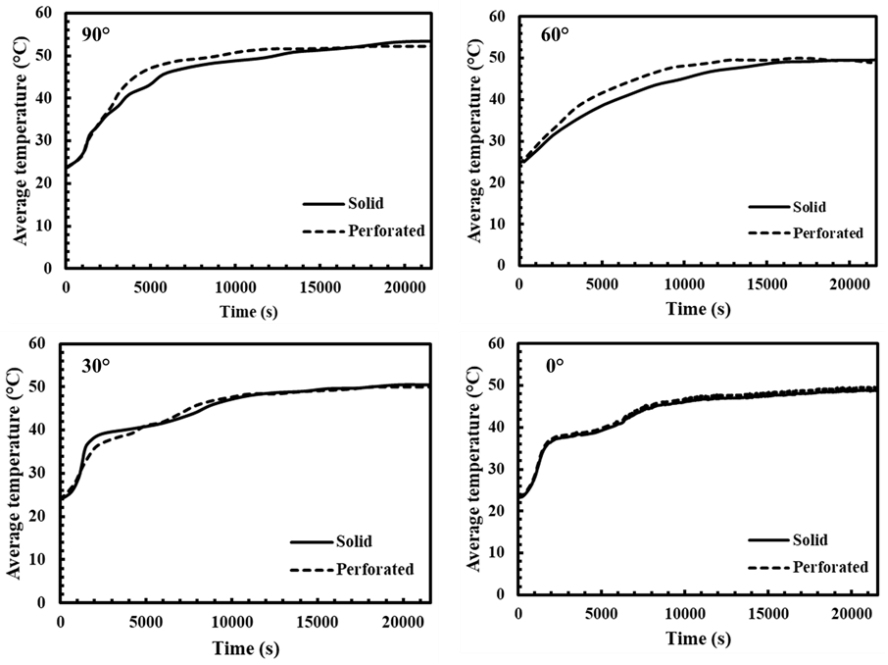

Fig. 7.4: Comparison of average temperature with orientation.

7.4.3 Melt fraction profile

The effect of orientation can be visualized from the melting behavior as shown in Fig. 7.5. At the beginning stage, the melting region occurs around the hot tube and gradually grows around the fins. As the time passes, the more melted PCM can be observed at the upper portion of LHSS due to natural convection. In the vertical position the PCM is observed to melt near the solid fins (Chapter 6, Fig. 6.7), however no such behavior is observed with perforation. Due to the non-availability of passage for solid fins the melted PCM flow along the fin surface. From the fin surface the liquid PCM tends to flow upwards via the gap

between the fin and the shell. As the perforated fins do not restrict the PCM flow the melting is more significant along the length of shell. However, perforated fins shows more unmelted PCM at the end of 21600 s. As a result, inserting perforations on the solid fins increased the SCD process in the early stages, but the charging rate reduced at the bottom of LHSS for vertical position. The perforated fins is observed to take more time to melt the PCM at the bottom of the LHSS. It is noted that effect of perforated fins on a melt profile is insignificant in horizontal position.

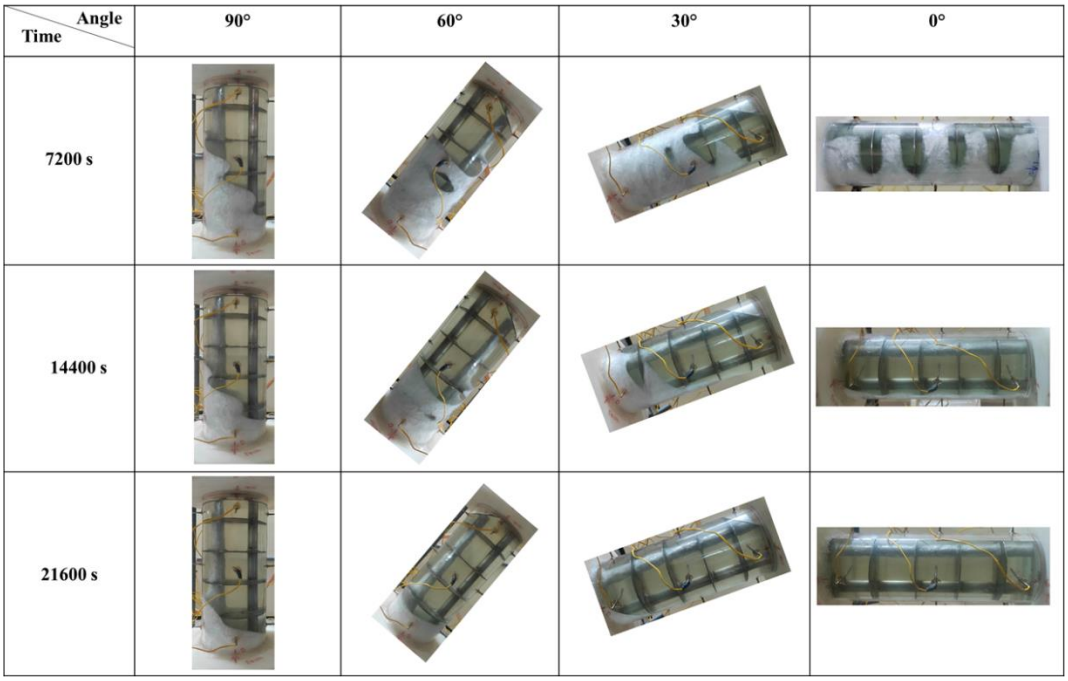

Fig. 7.5: Evolution of melted PCM with inclination

7.4.4 Energy storage

Fig. 7.6 shows the energy stored by the PCM at different time intervals with perforated fins. At initial stage (3600 s), the difference in energy stored with inclination can be observed to be negligible. Over time (7200-10800 s) the energy stored is gradually increased due to the influence of natural convection. Lastly, the energy stored by the PCM is constant and steady state condition of LHSS is attained. From Fig. 7.6 it is noted that energy storage increase as the orientation of LHSS change from vertical to horizontal. This can be inferred to the increase in the amount of melted PCM with the decrease of inclination. Comparing to the solid and perforated fins, the difference in energy storage is negligible. However, over time (7200-10800 s) the energy stored for the vertical configuration can be noted to be higher in the case of perforated fins. Based on the observation it can be understood that the strength of the natural convection more for

perforated fins LHSS for vertical position. The maximum energy storage is observed to be 227 kJ in the case of horizontal position without fins, which is only 1.34 % higher than solid fins.

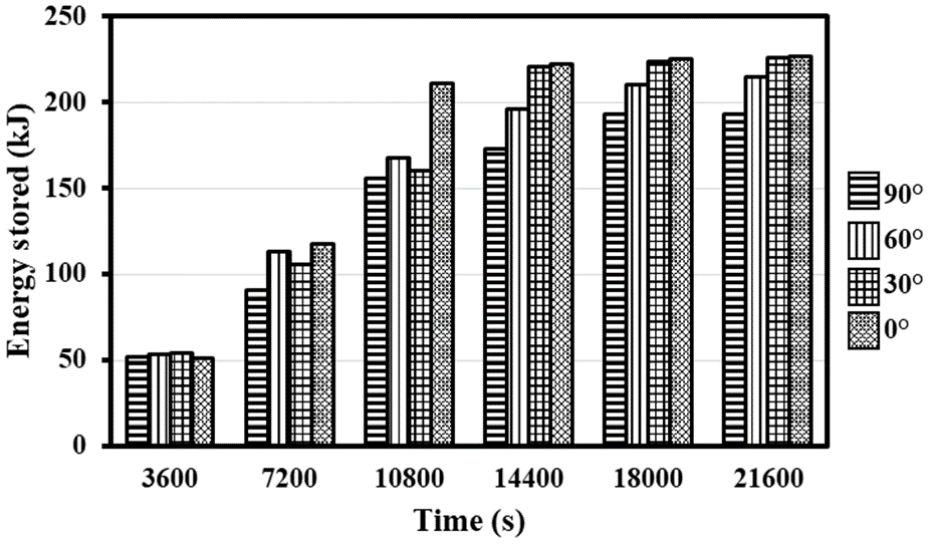

Fig. 7.6: Timewise energy stored by the PCM in LHSS with Perforated fins

7.4.5 Exergy

Fig. 7.7 illustrates the exergy efficiency of LHSS with perforated fins with the variation of inclination angle change from horizontal to vertical. As mentioned in Eqs. 3.7-3.11 (Chapter 3) the exergy efficiency depend on the inlet and outlet temperatures of HTFs and average temperature of the PCM. The exergy is observed to be more when the convection phenomenon is dominant and lastly found to be constant. However, the average temperature for horizontal configuration is lower with perforated fins but exergy efficiency is higher. This can be inferred to that increases in HTF outlet temperature and improved the thermal transport to the PCM which enhances the exergy of the LHSS. It is evident from Fig. 7.5 that for tilted LHSS from 90° to 0° the melt fraction of PCM increases. Which resulted to the higher temperature difference between the inlet and outlet temperatures of HTFs. Also, due to the presence of perforated fins the heat transfer between the hot and cold tubes improved and hence the temperature difference between the inlet and outlet HTFs increases. Moreover, the maximum exergy efficiency is 12.7 % in horizontal position.

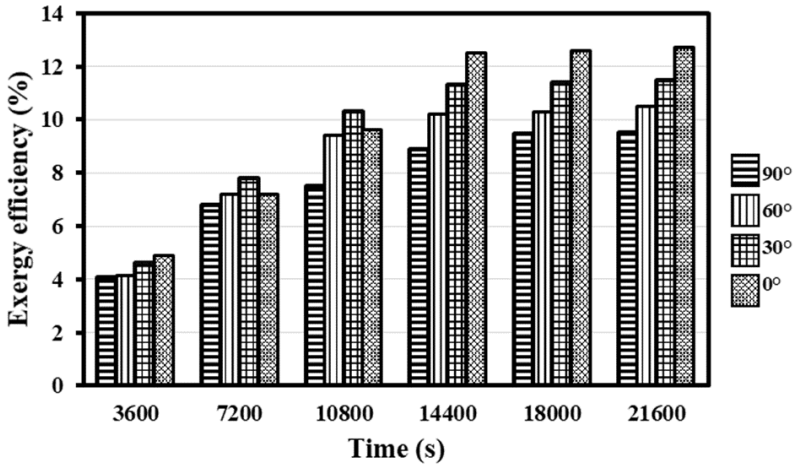

Fig. 7.7: Exergy efficiency of perforated fin with orientation

7.4.6 Heat input and Recovery

Fig. 7.8 shows the variation of energy input and output with orientation. it can be observed that average energy input and recovery increased as the orientation change from vertical to horizontal position. This is caused due to the difference in melt fraction which resulted in the variation of temperature gradient between the inlet and outlet temperatures of cold and hot HTFs. From Fig. 7.5 it can be noted that higher amount of melted PCM observed for the horizontal configuration and led to higher heat transfer between the HTFs and PCM. Therefore, higher temperature gradient can be created between the HTFs inlet and outlet temperatures. Hence, energy input and recovery can be noted to be more for the horizontal position. The maximum energy input (305 kJ) and recovery (103 kJ) is observed in horizontal position.

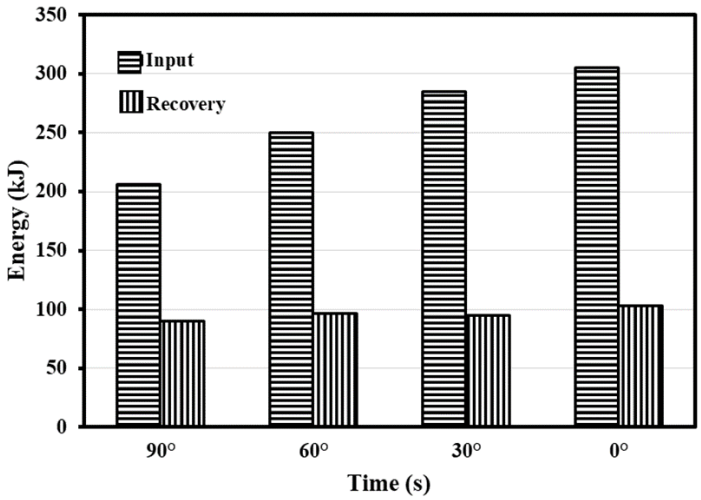

Fig. 7.8: Comparison of energy input and recovery with perforated fins

7.4.7 Comparison of unfinned, solid and perforated

Table. 7.2 Comparisons between unfinned, solid and perforated fins

	Inclinations											
	90° (Vertical)			60°			30°			0° (Horizontal)		
	Unfinned	Solid fin	Perforated fins	Unfinned	Solid fin	Perforated fins	Unfinned	Solid fin	Perforated fins	Unfinned	Solid fin	Perforated fins
Average Temp.	50.4	53.4 ↑ (5.9%)	52.2 ↑ (3.5%)	52.1	49.7 ↓ (4.6%)	49 ↓ (4.6%)	56.2	50.5 ↓ (10.1%)	50 ↓ (11.03%)	58	49.6 ↓ (14.48%)↓ (1.56%)	49.52 ↓ (14.62%)
Energy storage	163	195 ↑ (19.6%)	193 ↑ (18.4%)	173.2	213 ↑ (22.9%)	215 ↑ (24.13%)	223.9	224 ↓ (0.04%)	226 ↓ (0.94%)	231	224 ↓ (3.03%) ↑ (37.42%)	227 ↓ (1.73%)
Exergy efficiency (%)	6.08	9.57 ↑ (57.7%)	9.52 ↑ (56.6%)	6.66	10.7 ↑ (60.6%)	10.3 ↑ (54.4%)	7.28	11.9 ↑ (63.4%)	11.5 ↑ (57.97%)	7.54	12.9 ↑ (71.09%)↑ (112.3%)	12.7 ↑ (68.44%)
Energy Input	111.23	199 ↑ (78.9%)	206 ↑ (85.2%)	131.2	243.1 ↑ (85.2%)	250 ↑ (90.5%)	177.8	288 ↑ (61.8%)	285 ↑ (60.29%)	206.5	312 ↑ (51.09%)↑ (180.3%)	305 ↑ (47.7%)
Energy Recovery	48.44	84.6 ↑ (74.6%)	89.58 ↑ (84.9%)	49.38	90 ↑ (82.2%)	96.3 ↑ (95.02%)	63.75	103 ↑ (61.5%)	98 ↑ (43.75%)	65.56	114 ↑ (73.89%)↑ (135.3%)	103 ↑ (57.11%)

Table. 7.2 shows the comparisons of various parameters with unfinned, with solid and perforated fins. It is noted that the average temperature without fins is higher for 60°, 30° and horizontal (0°) except vertical position. With the decrease of inclination i.e from vertical (90°) to horizontal (0°) the accumulation of melted PCM increases in the upper section of the heat exchanger. The presence of fins leads to better thermal transport from the cold HTF to the upper section due to which low temperature can be observed for finned LHSS in comparison to unfinned LHSS with the decrease of inclination. Compared with and without fins energy stored is improved with fins for vertical and 60° configurations. The maximum energy stored for vertical configuration with solid fins is 195 kJ which is 19.63 % higher than without fins. However, there is a negligible difference in energy storage for horizontal configuration. The maximum energy storage is observed to be 231 kJ in the case of horizontal position without fins, which is only 3.03 % higher than solid fins. By comparing the obtained exergy efficiencies the LHSS with solid fins gave 71.09 % higher exergy efficiency than without fins for horizontal configuration. The maximum energy stored and energy recovery for vertical configuration with solid fins is 19.6 % and 85.2 % higher than without fins. By comparing the obtained exergy efficiencies and energy recovery with solid fins gave 71.09 % and 73.89 % higher than without fins for horizontal configuration. In a practical application, energy stored by the PCM as well as retrieved heat from the system is important. From Table 7.2 it is observed that maximum energy stored is observed in case of without fins in the horizontal position. However, compared to important aspect such as exergy efficiency and heat recovery LHSS with solid fins shows improved thermal performance. From Table 7.2 it is noted that perforations on solid fins gave higher thermal performance on vertical and 60° positions. Moreover, overall solid fins with horizontal positions LHSS shows better thermodynamics behavior in SCD process.

7.5 Closure

In this study, an experimental investigation of the shell and tube latent heat storage system (LHSS) filled with PCM is carried out. The temperature evolution and thermodynamic characteristics under the simultaneous charging and discharging process (SCD) are studied. The effect orientation on the thermal performance is investigated. Also, the experimental results for perforated fins have been compared with solid fins and without fins. According to the obtained results, the following conclusions are drawn.

- It is observed that perforated fins improved the thermal performance in the vertical configuration during the initial stages of melting.
- Employing perforated fins gave a better thermal performance of the LHSS at 60° position.
- However, the effect of perforations is nullified at the end stage of the melting process.
- In the vertical position, the melting behavior in the upper half of the LHSS is more with perforated fins
- Over time (7200-10800 s) the thermal performances for the vertical and 60° configuration can be noted to be higher in the case of perforated fins.
- Irrespective of usage or non-usage of perforated or solid fins when the orientation of the LHSS changed from vertical to horizontal the convective strength increased. Also, the position of the hot HTF tube placed at the bottom of LHSS with inclination provides a more natural convection-dominated zone resulted a higher melting rate.
- The maximum energy stored and energy recovery for vertical configuration with solid fins is 19.63 % and 74.6 % higher than without fins.
- The obtained exergy efficiencies and energy recovery with solid fins gave 71.09 % and 73.89 % higher than without fins for horizontal configuration.

Chapter 8
Conclusions and scope for future work

The present research work is aimed at analyzing the influence of different parameters on the thermal performance of a latent heat storage unit (LHSS) under simultaneous charging and discharging process (SCD). Lauric acid is chosen as the phase change material (PCM) which is filled in the annular space of shell and tubes. Two types of circular fins: solid fins and perforated fins are considered for heat transfer augmentation. Experiments were performed to compare the performance of these two kinds of fins and to realize the effect of LHSS orientation on its thermal performance. Numerical simulations based on the enthalpy porosity approach are also carried out for the proper understanding of the melting behavior of PCM. The heat transfer fluid parameters viz. direction, mass flow rate, temperature gradient between inlet temperature of hot and cold are analyzed. Finally, the effect of orientation with solid and perforated fins and without fins are compared based on energy storage, exergy efficiency, energy input and recovery. From the present experimental and numerical investigations, the following conclusions are drawn.

- In a shell and tube LHSS phase change process is un-symmetric in nature and the melting of PCM is largely assisted by natural convection.
- Melting time is mostly influenced by the inlet temperature of the HTF. 47% reduction in melting time is noted by increasing the inlet temperature gradient by 20 ° C in the vertical system.
- Flow direction and flow rate of HTF have a negligible effect on total melting time.
- The effect of temperature gradient by varying cold HTF inlet temperature shows a negligible effect on the melting process in the horizontal position.
- Changing the orientation from vertical to horizontal resulted in a higher rate of melting process.
- The orientation significantly influences the SCD process due to the variation of thermal transport by natural convection.
- With orientation, the position of the cold and hot heat transfer fluid (HTF) tubes show a significant influence on the melting process.

- With the decrease in inclination angle from 90° to 0°; there is an increase in the melt fraction of PCM by 39.44 % without fins.
- The steady-state condition is observed to be orientation specific. After attaining steady-state condition the thermal transport occurred between hot and cold HTFs.
- In the LHSS without fins the low thermal conductivity of the PCM and thermal resistance over the cold HTF tube due to the formation of a solid PCM layer results in less recovery of thermal energy by the cold HTF.
- Employing fins improved the thermal performance of the LHSS.
- The maximum energy stored and energy recovery for vertical configuration with solid fins are 19.63 % and 70.46 % higher than without fins.
- By comparing the obtained exergy efficiencies and energy recovery the solid fins gave 71.09 % and 73.89 % higher than without fins for horizontal configuration.
- The average Nusselt number shows that initially the heat transfer is mainly due to hot HTF. As the process progressed, the heat transfer is higher from melted PCM to the cold HTF.
- Due to the restriction for the flow of the melted PCM by the fins the natural convection is observed to be suppressed.
- Perforated fins gave a better thermal performance in vertical and 60° configurations.
- However, the effect of perforation nullifies at the end stage of the melting process hence melting is unaffected by the type of fins.
- The maximum energy stored is observed in the case of horizontal position without fins.
- However, comparing to important aspects such as exergy efficiency and heat recovery, the LHSS with solid fins shows improved thermal performance.
- Overall the LHSS with solid fins in the horizontal position gave a better thermal performance.

Scope for future work

- The SCD process is at the early stage of development and most of the literature focused on the thermal performance of PCMs. Thus, more effort should be focused on designing the SCD process.
- Hybrid heat transfer augmentation techniques such as fins + nano particle dispersion, fins + cascading of PCMs, fins + metal foam can be implemented
- Perforated fins showed promising results during the initial stages of melting, hence optimization of perforations in terms of size and shape could further improve the thermal performance of the LHSS
- Optimizing the geometric parameters to augment the convective heat transfer can be explored with the SCD process.

REFERENCES

[1] IEA, Technology Roadmap: Energy Storage - 2014 edition, (2014) 64.

[2] S. Wu, C. Zhou, E. Doroodchi, R. Nellore, B. Moghtaderi, A review on high-temperature thermochemical energy storage based on metal oxides redox cycle, Energy Convers. Manag. 168 (2018) 421–453. https://doi.org/10.1016/j.enconman.2018.05.017.

[3] G.L. Kyriakopoulos, G. Arabatzis, Electrical energy storage systems in electricity generation: Energy policies, innovative technologies, and regulatory regimes, Renew. Sustain. Energy Rev. 56 (2016) 1044–1067. https://doi.org/10.1016/j.rser.2015.12.046.

[4] A.D. Monde, A. Shrivastava, P.R. Chakraborty, Solar Thermal Energy Storage, Energy, Environ. Sustain. (2018) 131–162. https://doi.org/10.1007/978-981-10-7206-2_8.

[5] M. Beaudin, H. Zareipour, A. Schellenberglabe, W. Rosehart, Energy storage for mitigating the variability of renewable electricity sources: An updated review, Energy Sustain. Dev. 14 (2010) 302–314. https://doi.org/10.1016/j.esd.2010.09.007.

[6] P.K.S. Rathore, S.K. Shukla, Enhanced thermophysical properties of organic PCM through shape stabilization for thermal energy storage in buildings: A state of the art review, E(2021) 110799. https://doi.org/10.1016/j.enbuild.2021.110799.

[7] Y. Zhao, X. Zhang, W. Hua, Review of preparation technologies of organic composite phase change materials in energy storage, J. Mol. Liq. 336 (2021) 115923. https://doi.org/10.1016/j.molliq.2021.115923.

[8] M.F. Junaid, Z. ur Rehman, M. Čekon, J. Čurpek, R. Farooq, H. Cui, I. Khan, Inorganic phase change materials in thermal energy storage: A review on perspectives and technological advances in building applications, Energy Build. 252 (2021). https://doi.org/10.1016/j.enbuild.2021.111443.

[9] Y. Lin, G. Alva, G. Fang, Review on thermal performances and applications of thermal energy storage systems with inorganic phase change materials, Energy. 165 (2018) 685–708. https://doi.org/10.1016/j.energy.2018.09.128.

[10] P. Singh, R.K. Sharma, A.K. Ansu, R. Goyal, A. Sarı, V. V. Tyagi, A comprehensive review on development of eutectic organic phase change materials and their composites for low and medium range thermal energy storage applications, Sol. Energy Mater. Sol.

Cells. 223 (2021) 110955. https://doi.org/10.1016/j.solmat.2020.110955.

[11] F.S. Javadi, H.S.C. Metselaar, P. Ganesan, Performance improvement of solar thermal systems integrated with phase change materials (PCM), a review, Sol. Energy. 206 (2020) 330–352. https://doi.org/10.1016/j.solener.2020.05.106.

[12] E. Douvi, C. Pagkalos, G. Dogkas, M.K. Koukou, V.N. Stathopoulos, Y. Caouris, M.G. Vrachopoulos, Phase change materials in solar domestic hot water systems: A review, Int. J. Thermofluids. 10 (2021) 100075. https://doi.org/10.1016/j.ijft.2021.100075.

[13] P.B. Salunkhe, D. Jaya Krishna, Investigations on latent heat storage materials for solar water and space heating applications, J. Energy Storage. 12 (2017) 243–260. https://doi.org/10.1016/j.est.2017.05.008.

[14] J. Luo, D. Zou, Y. Wang, S. Wang, L. Huang, Battery thermal management systems (BTMs) based on phase change material (PCM): a comprehensive review, Chem. Eng. J. 430 (2021) 132741. https://doi.org/10.1016/j.cej.2021.132741.

[15] Z.G. Shen, S. Chen, X. Liu, B. Chen, A review on thermal management performance enhancement of phase change materials for vehicle lithium-ion batteries, Renew. Sustain. Energy Rev. 148 (2021) 111301. https://doi.org/10.1016/j.rser.2021.111301.

[16] S. Landini, J. Leworthy, T.S. O'Donovan, A Review of Phase Change Materials for the Thermal Management and Isothermalisation of Lithium-Ion Cells, J. Energy Storage. 25 (2019) 100887. https://doi.org/10.1016/j.est.2019.100887.

[17] J. Jaguemont, N. Omar, P. Van den Bossche, J. Mierlo, Phase-change materials (PCM) for automotive applications: A review, Appl. Therm. Eng. 132 (2018) 308–320. https://doi.org/10.1016/j.applthermaleng.2017.12.097.

[18] V.P. Katekar, S.S. Deshmukh, A review of the use of phase change materials on performance of solar stills, J. Energy Storage. 30 (2020) 101398. https://doi.org/10.1016/j.est.2020.101398.

[19] V. V. Tyagi, K. Chopra, B. Kalidasan, A. Chauhan, U. Stritih, S. Anand, A.K. Pandey, A. Sarı, R. Kothari, Phase change material based advance solar thermal energy storage systems for building heating and cooling applications: A prospective research approach, Sustain. Energy Technol. Assessments. 47 (2021) 101318. https://doi.org/10.1016/j.seta.2021.101318.

[20] K. Faraj, M. Khaled, J. Faraj, F. Hachem, C. Castelain, A review on phase change materials for thermal energy storage in buildings: Heating and hybrid applications, J. Energy Storage. 33 (2021) 101913. https://doi.org/10.1016/j.est.2020.101913.

[21] S.M. Shalaby, M.A. Bek, A.A. El-Sebaii, Solar dryers with PCM as energy storage medium: A review, Renew. Sustain. Energy Rev. 33 (2014) 110–116. https://doi.org/10.1016/j.rser.2014.01.073.

[22] H. Selvnes, Y. Allouche, R.I. Manescu, A. Hafner, Review on cold thermal energy storage applied to refrigeration systems using phase change materials, Therm. Sci. Eng. Prog. 22 (2021) 100807. https://doi.org/10.1016/j.tsep.2020.100807.

[23] A.A.M. Omara, H.A. Mohammed, I.J. Al Rikabi, M.A. Abuelnour, A.A.A. Abuelnuor, Performance improvement of solar chimneys using phase change materials: A review, Sol. Energy. 228 (2021) 68–88. https://doi.org/10.1016/j.solener.2021.09.037.

[24] S.H. Zaferani, M.W. Sams, R. Ghomashchi, Z.-G. Chen, Thermoelectric Coolers as Thermal Management Systems for Medical Applications: Design, Optimization, and Advancement, Nano Energy. 90 (2021) 106572. https://doi.org/10.1016/j.nanoen.2021.106572.

[25] A.S. Farooq, P. Zhang, Fundamentals, materials and strategies for personal thermal management by next-generation textiles, Compos. Part A Appl. Sci. Manuf. 142 (2021) 106249. https://doi.org/10.1016/j.compositesa.2020.106249.

[26] S.D. Sharma, K. Sagara, Latent Heat Storage Materials and Systems : A Review, 5075 (2007). https://doi.org/10.1081/GE-200051299.

[27] H. Akeiber, P. Nejat, M.Z.A. Majid, M.A. Wahid, F. Jomehzadeh, I. Zeynali Famileh, J.K. Calautit, B.R. Hughes, S.A. Zaki, A review on phase change material (PCM) for sustainable passive cooling in building envelopes, Renew. Sustain. Energy Rev. 60 (2016) 1470–1497. https://doi.org/10.1016/j.rser.2016.03.036.

[28] A. Sharma, V. V. Tyagi, C.R. Chen, D. Buddhi, Review on thermal energy storage with phase change materials and applications, Renew. Sustain. Energy Rev. 13 (2009) 318–345. https://doi.org/10.1016/j.rser.2007.10.005.

[29] P.B. Salunkhe, D. Jaya Krishna, Investigations on latent heat storage materials for solar water and space heating applications, J. Energy Storage. 12 (2017) 243–260.

https://doi.org/10.1016/j.est.2017.05.008.

[30] F. Agyenim, N. Hewitt, P. Eames, M. Smyth, A review of materials, heat transfer and phase change problem formulation for latent heat thermal energy storage systems (LHTESS), Renew. Sustain. Energy Rev. 14 (2010) 615–628. https://doi.org/10.1016/j.rser.2009.10.015.

[31] Y. Cao, A. Faghri, Performance characteristics of a thermal energy storage module: a transient PCM/forced convection conjugate analysis, Int. J. Heat Mass Transf. 34 (1991) 93–101. https://doi.org/10.1016/0017-9310(91)90177-G.

[32] A. Agarwal, R.M. Sarviya, An experimental investigation of shell and tube latent heat storage for solar dryer using paraffin wax as heat storage material, Eng. Sci. Technol. an Int. J. 19 (2016) 619–631. https://doi.org/10.1016/j.jestch.2015.09.014.

[33] S. Seddegh, M.M. Joybari, X. Wang, F. Haghighat, Experimental and numerical characterization of natural convection in a vertical shell-and-tube latent thermal energy storage system, Sustain. Cities Soc. 35 (2017) 13–24. https://doi.org/10.1016/j.scs.2017.07.024.

[34] M.A. Kibria, M.R. Anisur, M.H. Mahfuz, R. Saidur, I.H.S.C. Metselaar, Numerical and experimental investigation of heat transfer in a shell and tube thermal energy storage system, Int. Commun. Heat Mass Transf. 53 (2014) 71–78. https://doi.org/10.1016/j.icheatmasstransfer.2014.02.023.

[35] M. Esen, A. Durmus, A. Durmus, Geometric design of soler-aided latent heat store depending on various parameters and phase change materials, Sol. Energy. 62 (1998) 19–28.

[36] W.W. Wang, K. Zhang, L.B. Wang, Y.L. He, Numerical study of the heat charging and discharging characteristics of a shell-and-tube phase change heat storage unit, Appl. Therm. Eng. 58 (2013) 542–553. https://doi.org/10.1016/j.applthermaleng.2013.04.063.

[37] Y. Wang, L. Wang, N. Xie, X. Lin, H. Chen, Experimental study on the melting and solidification behavior of erythritol in a vertical shell-and-tube latent heat thermal storage unit, Int. J. Heat Mass Transf. 99 (2016) 770–781. https://doi.org/10.1016/j.ijheatmasstransfer.2016.03.125.

[38] M. Akgün, O. Aydin, K. Kaygusuz, Experimental study on melting/solidification

characteristics of a paraffin as PCM, Energy Convers. Manag. 48 (2007) 669–678. https://doi.org/10.1016/j.enconman.2006.05.014.

[39] A. Sari, K. Kaygusuz, Thermal performance of a eutectic mixture of lauric and stearic acids as PCM encapsulated in the annulus of two concentric pipes, Sol. Energy. 72 (2002) 493–504. https://doi.org/10.1016/S0038-092X(02)00026-9.

[40] S. Seddegh, X. Wang, A.D. Henderson, A comparative study of thermal behaviour of a horizontal and vertical shell-and-tube energy storage using phase change materials, Appl. Therm. Eng. 93 (2016) 348–358. https://doi.org/10.1016/j.applthermaleng.2015.09.107.

[41] H.E.S. Fath, Heat exchanger performance for latent heat thermal energy storage system, Energy Convers. Manag. 31 (1991) 149–155. https://doi.org/10.1016/0196-8904(91)90067-S.

[42] M. Lacroix, Numerical simulation of a shell-and-tube latent heat thermal energy storage unit, Sol. Energy. 50 (1993) 357–367. https://doi.org/10.1016/0038-092X(93)90029-N.

[43] M.A. Kibria, M.R. Anisur, M.H. Mahfuz, R. Saidur, I.H.S.C. Metselaar, Numerical and experimental investigation of heat transfer in a shell and tube thermal energy storage system, Int. Commun. Heat Mass Transf. 53 (2014) 71–78. https://doi.org/10.1016/j.icheatmasstransfer.2014.02.023.

[44] M. Avci, M.Y. Yazici, Experimental study of thermal energy storage characteristics of a paraffin in a horizontal tube-in-shell storage unit, Energy Convers. Manag. 73 (2013) 271–277. https://doi.org/10.1016/j.enconman.2013.04.030.

[45] S. Seddegh, X. Wang, M.M. Joybari, F. Haghighat, Investigation of the effect of geometric and operating parameters on thermal behavior of vertical shell-and-tube latent heat energy storage systems, Energy. 137 (2017) 69–82. https://doi.org/10.1016/j.energy.2017.07.014.

[46] L. Kalapala, J.K. Devanuri, Influence of operational and design parameters on the performance of a PCM based heat exchanger for thermal energy storage – A review, J. Energy Storage. 20 (2018) 497–519. https://doi.org/10.1016/j.est.2018.10.024.

[47] H.A. Adine, H. El Qarnia, Numerical analysis of the thermal behaviour of a shell-and-tube heat storage unit using phase change materials, Appl. Math. Model. 33 (2009) 2132–2144. https://doi.org/10.1016/j.apm.2008.05.016.

[48] M.J. Hosseini, M. Rahimi, R. Bahrampoury, Experimental and computational evolution of a shell and tube heat exchanger as a PCM thermal storage system, Int. Commun. Heat Mass Transf. 50 (2014) 128–136. https://doi.org/10.1016/j.icheatmasstransfer.2013.11.008.

[49] A. Trp, K. Lenic, B. Frankovic, Analysis of the influence of operating conditions and geometric parameters on heat transfer in water-paraffin shell-and-tube latent thermal energy storage unit, Appl. Therm. Eng. 26 (2006) 1830–1839. https://doi.org/10.1016/j.applthermaleng.2006.02.004.

[50] N. Kousha, M.J. Hosseini, M.R. Aligoodarz, R. Pakrouh, R. Bahrampoury, Effect of inclination angle on the performance of a shell and tube heat storage unit – An experimental study, Appl. Therm. Eng. 112 (2017) 1497–1509. https://doi.org/10.1016/j.applthermaleng.2016.10.203.

[51] I. Al Siyabi, S. Khanna, T. Mallick, S. Sundaram, An experimental and numerical study on the effect of inclination angle of phase change materials thermal energy storage system, J. Energy Storage. 23 (2019) 57–68. https://doi.org/10.1016/j.est.2019.03.010.

[52] L. Kalapala, J.K. Devanuri, Energy and exergy analyses of latent heat storage unit positioned at different orientations – An experimental study, Energy. 194 (2020) 116924. https://doi.org/10.1016/j.energy.2020.116924.

[53] T. Bouzennada, F. Mechighel, T. Ismail, L. Kolsi, K. Ghachem, Heat transfer and fluid flow in a PCM-filled enclosure: Effect of inclination angle and mid-separation fin, Int. Commun. Heat Mass Transf. 124 (2021) 105280. https://doi.org/10.1016/j.icheatmasstransfer.2021.105280.

[54] M.S. Mahdi, A.F. Hasan, H.B. Mahood, A.N. Campbell, A.A. Khadom, A.M. em A. Karim, A.O. Sharif, Numerical study and experimental validation of the effects of orientation and configuration on melting in a latent heat thermal storage unit, J. Energy Storage. 23 (2019) 456–468. https://doi.org/10.1016/j.est.2019.04.013.

[55] R. Karami, B. Kamkari, Investigation of the effect of inclination angle on the melting enhancement of phase change material in finned latent heat thermal storage units, Appl. Therm. Eng. 146 (2019) 45–60. https://doi.org/10.1016/j.applthermaleng.2018.09.105.

[56] L. Kalapala, J.K. Devanuri, Effect of orientation on thermal performance of a latent heat storage system equipped with annular fins – An experimental and numerical investigation,

Appl. Therm. Eng. 183 (2021). https://doi.org/10.1016/j.applthermaleng.2020.116244.

[57] S. Seddegh, X. Wang, A.D. Henderson, A comparative study of thermal behaviour of a horizontal and vertical shell-and-tube energy storage using phase change materials, Appl. Therm. Eng. 93 (2016) 348–358. https://doi.org/10.1016/j.applthermaleng.2015.09.107.

[58] X. Yang, Z. Lu, Q. Bai, Q. Zhang, L. Jin, J. Yan, Thermal performance of a shell-and-tube latent heat thermal energy storage unit: Role of annular fins, Appl. Energy. 202 (2017) 558–570. https://doi.org/10.1016/j.apenergy.2017.05.007.

[59] L. Pu, S. Zhang, L. Xu, Y. Li, Thermal performance optimization and evaluation of a radial finned shell-and-tube latent heat thermal energy storage unit, Appl. Therm. Eng. 166 (2020) 114753. https://doi.org/10.1016/j.applthermaleng.2019.114753.

[60] H. Cheng, T. Luo, J. Yu, X. Yang, Y. Liu, Z. Gu, L. Jin, Experimental study of a shell-and-tube phase change heat exchanger unit with/without circular fins, Energy Procedia. 152 (2018) 990–996. https://doi.org/10.1016/j.egypro.2018.09.105.

[61] R. V. Seeniraj, R. Velraj, N.L. Narasimhan, Thermal analysis of a finned-tube LHTS module for a solar dynamic power system, Heat Mass Transf. Und Stoffuebertragung. 38 (2002) 409–417. https://doi.org/10.1007/s002310100268.

[62] D. Zhao, G. Tan, Numerical analysis of a shell-and-tube latent heat storage unit with fins for air-conditioning application, Appl. Energy. 138 (2015) 381–392. https://doi.org/10.1016/j.apenergy.2014.10.051.

[63] W. Ogoh, D. Groulx, Effects of the number and distribution of fins on the storage characteristics of a cylindrical latent heat energy storage system: A numerical study, Heat Mass Transf. Und Stoffuebertragung. 48 (2012) 1825–1833. https://doi.org/10.1007/s00231-012-1029-3.

[64] I. Jmal, M. Baccar, Numerical study of PCM solidification in a finned tube thermal storage including natural convection, Appl. Therm. Eng. 84 (2015) 320–330. https://doi.org/10.1016/j.applthermaleng.2015.03.065.

[65] V. Thirunavukkarasu, G. Balaji, M. Sornanathan, Experimental analysis of shell and tube thermal energy storage system with finned tube, J. Chem. Pharm. Sci. 9 (2016) 3138–3141.

[66] A. Shahsavar, A. Goodarzi, H.I. Mohammed, A. Shirneshan, P. Talebizadehsardari,

Thermal performance evaluation of non-uniform fin array in a finned double-pipe latent heat storage system, Energy. 193 (2020) 116800. https://doi.org/10.1016/j.energy.2019.116800.

[67] M.J. Hosseini, M. Rahimi, R. Bahrampoury, Thermal analysis of PCM containing heat exchanger enhanced with normal annular fines, Mech. Sci. 6 (2015) 221–234. https://doi.org/10.5194/ms-6-221-2015.

[68] Z. Elmaazouzi, M. El Alami, H. Agalit, E.G. Bennouna, Performance evaluation of latent heat TES system-case study: Dimensions improvements of annular fins exchanger, Energy Reports. 6 (2020) 294–301. https://doi.org/10.1016/j.egyr.2019.08.059.

[69] F.S. dos Santos, K.A.R. Ismail, F.A.M. Lino, A. Arabkoohsar, T.G.S. Lago, Parametric investigation of the enhancing effects of finned tubes on the solidification of PCM, Int. J. Heat Mass Transf. 152 (2020) 119485. https://doi.org/10.1016/j.ijheatmasstransfer.2020.119485.

[70] L. Kalapala, J. Krishna Devanuri, Comparative analysis of solid and perforated fins for thermal enhancement of a latent heat storage unit positioned at various inclinations, Energy Sources, Part A Recover. Util. Environ. Eff. 00 (2021) 1–20. https://doi.org/10.1080/15567036.2021.1886202.

[71] Z. Khan, Z.A. Khan, Experimental investigations of charging/melting cycles of paraffin in a novel shell and tube with longitudinal fins based heat storage design solution for domestic and industrial applications, Appl. Energy. 206 (2017) 1158–1168. https://doi.org/10.1016/j.apenergy.2017.10.043.

[72] A. Raul, S.K. Saha, M. Jain, Transient performance analysis of concentrating solar thermal power plant with finned latent heat thermal energy storage, Renew. Energy. 145 (2020) 1957–1971. https://doi.org/10.1016/j.renene.2019.07.117.

[73] M.K. Rathod, J. Banerjee, Thermal performance enhancement of shell and tube Latent Heat Storage Unit using longitudinal fins, Appl. Therm. Eng. 75 (2015) 1084–1092. https://doi.org/10.1016/j.applthermaleng.2014.10.074.

[74] C. Zhang, Q. Sun, Y. Chen, Solidification behaviors and parametric optimization of finned shell-tube ice storage units, Int. J. Heat Mass Transf. 146 (2020) 118836. https://doi.org/10.1016/j.ijheatmasstransfer.2019.118836.

[75] C.R.E.S. Nóbrega, K.A.R. Ismail, F.A.M. Lino, Enhancement of ice formation around vertical finned tubes for cold storage applications, Int. J. Refrig. 99 (2019) 251–263. https://doi.org/10.1016/j.ijrefrig.2018.12.018.

[76] M. Shademan, A. Hossein Nezhad, Numerical investigation of a vertical finned-tube and shell energy storage system using coupled boundary condition, J. Energy Storage. 41 (2021) 102831. https://doi.org/10.1016/j.est.2021.102831.

[77] H. Li, C. Hu, Y. He, D. Tang, K. Wang, Influence of fin parameters on the melting behavior in a horizontal shell-and-tube latent heat storage unit with longitudinal fins, J. Energy Storage. 34 (2021) 102230. https://doi.org/10.1016/j.est.2020.102230.

[78] F. ul Hasnain, M. Irfan, M.M. Khan, L.A. Khan, H.F. Ahmed, Melting performance enhancement of a phase change material using branched fins and nanoparticles for energy storage applications, J. Energy Storage. 38 (2021). https://doi.org/10.1016/j.est.2021.102513.

[79] T. Wang, Y. Zhao, Y. Diao, C. Ma, Y. Zhang, X. Lu, Experimental investigation of a novel thermal storage solar air heater (TSSAH) based on flat micro-heat pipe arrays, Renew. Energy. 173 (2021) 639–651. https://doi.org/10.1016/j.renene.2021.04.027.

[80] N. Sharifi, S. Wang, T.L. Bergman, A. Faghri, Heat pipe-assisted melting of a phase change material, Int. J. Heat Mass Transf. 55 (2012) 3458–3469. https://doi.org/10.1016/j.ijheatmasstransfer.2012.03.023.

[81] H. Shabgard, T.L. Bergman, N. Sharifi, A. Faghri, High temperature latent heat thermal energy storage using heat pipes, Int. J. Heat Mass Transf. 53 (2010) 2979–2988. https://doi.org/10.1016/j.ijheatmasstransfer.2010.03.035.

[82] K. Nithyanandam, R. Pitchumani, Analysis and optimization of a latent thermal energy storage system with embedded heat pipes, Int. J. Heat Mass Transf. 54 (2011) 4596–4610. https://doi.org/10.1016/j.ijheatmasstransfer.2011.06.018.

[83] S. Motahar, R. Khodabandeh, Experimental study on the melting and solidification of a phase change material enhanced by heat pipe, Int. Commun. Heat Mass Transf. 73 (2016) 1–6. https://doi.org/10.1016/j.icheatmasstransfer.2016.02.012.

[84] A. Ebrahimi, M.J. Hosseini, A.A. Ranjbar, M. Rahimi, R. Bahrampoury, Melting process investigation of phase change materials in a shell and tube heat exchanger

enhanced with heat pipe, Renew. Energy. 138 (2019) 378–394. https://doi.org/10.1016/j.renene.2019.01.110.

[85] K. Chopra, V. V. Tyagi, A.K. Pathak, A.K. Pandey, A. Sari, Experimental performance evaluation of a novel designed phase change material integrated manifold heat pipe evacuated tube solar collector system, Energy Convers. Manag. 198 (2019) 111896. https://doi.org/10.1016/j.enconman.2019.111896.

[86] H. jie Song, W. Zhang, Y. qi Li, Z. wei Yang, A. bo Ming, Exergy analysis and parameter optimization of heat pipe receiver with integrated latent heat thermal energy storage for space station in charging process, Appl. Therm. Eng. 119 (2017) 304–311. https://doi.org/10.1016/j.applthermaleng.2017.03.080.

[87] Z. Khan, Z.A. Khan, P. Sewell, Heat transfer evaluation of metal oxides based nano-PCMs for latent heat storage system application, Int. J. Heat Mass Transf. 144 (2019) 118619. https://doi.org/10.1016/j.ijheatmasstransfer.2019.118619.

[88] K. Kant, A. Shukla, A. Sharma, P. Henry Biwole, Heat transfer study of phase change materials with graphene nano particle for thermal energy storage, Sol. Energy. 146 (2017) 453–463. https://doi.org/10.1016/j.solener.2017.03.013.

[89] R. Du, W. Li, T. Xiong, X. Yang, Y. Wang, K.W. Shah, Numerical investigation on the melting of nanoparticle-enhanced PCM in latent heat energy storage unit with spiral coil heat exchanger, Build. Simul. 12 (2019) 869–879. https://doi.org/10.1007/s12273-019-0527-3.

[90] R. Daneshazarian, S. Antoun, S.B. Dworkin, Performance Assessment of Nano-enhanced Phase Change Material for Thermal Storage, Int. J. Heat Mass Transf. 173 (2021) 121256. https://doi.org/10.1016/j.ijheatmasstransfer.2021.121256.

[91] B. Akhmetov, M.E. Navarro, A. Seitov, A. Kaltayev, Z. Bakenov, Y. Ding, Numerical study of integrated latent heat thermal energy storage devices using nanoparticle-enhanced phase change materials, Sol. Energy. 194 (2019) 724–741. https://doi.org/10.1016/j.solener.2019.10.015.

[92] S. Salyan, S. Suresh, Study of thermo-physical properties and cycling stability of D-Mannitol-copper oxide nanocomposites as phase change materials, J. Energy Storage. 15 (2018) 245–255. https://doi.org/10.1016/j.est.2017.10.013.

[93] X. Li, D. Zhu, X. Wang, Evaluation on dispersion behavior of the aqueous copper nano-suspensions, J. Colloid Interface Sci. 310 (2007) 456–463. https://doi.org/10.1016/j.jcis.2007.02.067.

[94] T. Xiong, L. Zheng, K.W. Shah, Nano-enhanced phase change materials (NePCMs): A review of numerical simulations, Appl. Therm. Eng. 178 (2020) 115492. https://doi.org/10.1016/j.applthermaleng.2020.115492.

[95] S. Sami, N. Etesami, Improving thermal characteristics and stability of phase change material containing TiO2 nanoparticles after thermal cycles for energy storage, Appl. Therm. Eng. 124 (2017) 346–352. https://doi.org/10.1016/j.applthermaleng.2017.06.023.

[96] C.J. Ho, J.Y. Gao, An experimental study on melting heat transfer of paraffin dispersed with Al2O3 nanoparticles in a vertical enclosure, Int. J. Heat Mass Transf. 62 (2013) 2–8. https://doi.org/10.1016/j.ijheatmasstransfer.2013.02.065.

[97] L. Liu, J. Li, J. Niu, J.Y. Wu, Evaluation of the energy storage performance of PCM nano-emulsion in a small tubular heat exchanger, Case Stud. Therm. Eng. 26 (2021) 101156. https://doi.org/10.1016/j.csite.2021.101156.

[98] M. Ghalambaz, S.A.M. Mehryan, A. Veismoradi, M. Mahdavi, I. Zahmatkesh, Z. Kazemi, O. Younis, M. Ghalambaz, A.J. Chamkha, Melting process of the nano-enhanced phase change material (NePCM) in an optimized design of shell and tube thermal energy storage (TES): Taguchi optimization approach, Appl. Therm. Eng. 193 (2021). https://doi.org/10.1016/j.applthermaleng.2021.116945.

[99] Y. Zhang, M. Wang, J. Li, H. Wang, Y. Zhao, Improving thermal energy storage and transfer performance in solar energy storage: Nanocomposite synthesized by dispersing nano boron nitride in solar salt, Sol. Energy Mater. Sol. Cells. 232 (2021) 111378. https://doi.org/10.1016/j.solmat.2021.111378.

[100] N. Pradeep, K. Paramasivam, T. Rajesh, V. Subash Purusothamanan, S. Iyahraja, Silver nanoparticles for enhanced thermal energy storage of phase change materials, Mater. Today Proc. 45 (2021) 607–611. https://doi.org/10.1016/j.matpr.2020.02.671.

[101] J. Li, X. Hu, C. Zhang, W. Luo, X. Jiang, Enhanced thermal performance of phase-change materials supported by mesoporous silica modified with polydopamine/nano-metal particles for thermal energy storage, Renew. Energy. 178 (2021) 118–127.

https://doi.org/10.1016/j.renene.2021.06.021.

[102] C. Yang, Y. Xu, X. Cai, Z.-J. Zheng, Effect of the circumferential and radial graded metal foam on horizontal shell-and-tube latent heat thermal energy storage unit, Sol. Energy. 226 (2021) 225–235. https://doi.org/10.1016/j.solener.2021.08.027.

[103] A. Chibani, S. Merouani, F. Benmoussa, Computational analysis of the melting process of Phase change material-metal foam-based latent thermal energy storage unit: The heat exchanger configuration, J. Energy Storage. 42 (2021) 103071. https://doi.org/10.1016/j.est.2021.103071.

[104] P.T. Sardari, H.I. Mohammed, D. Giddings, G.S. walker, M. Gillott, D. Grant, Numerical study of a multiple-segment metal foam-PCM latent heat storage unit: Effect of porosity, pore density and location of heat source, Energy. 189 (2019) 116108. https://doi.org/10.1016/j.energy.2019.116108.

[105] J. Lei, Y. Tian, D. Zhou, W. Ye, Y. Huang, Y. Zhang, Heat transfer enhancement in latent heat thermal energy storage using copper foams with varying porosity, Sol. Energy. 221 (2021) 75–86. https://doi.org/10.1016/j.solener.2021.04.013.

[106] Z. Wang, J. Wu, D. Lei, H. Liu, J. Li, Z. Wu, Experimental study on latent thermal energy storage system with gradient porosity copper foam for mid-temperature solar energy application, Appl. Energy. 261 (2020) 114472. https://doi.org/10.1016/j.apenergy.2019.114472.

[107] X. Chen, X. Li, X. Xia, C. Sun, R. Liu, Thermal storage analysis of a foam-filled PCM heat exchanger subjected to fluctuating flow conditions, Energy. 216 (2021) 119259. https://doi.org/10.1016/j.energy.2020.119259.

[108] W. Tian, S. Dang, G. Liu, Z. Guo, X. Yang, Thermal transport in phase change materials embedded in metal foam: evaluation on inclination configuration, J. Energy Storage. 33 (2021) 102166. https://doi.org/10.1016/j.est.2020.102166.

[109] J. Duan, F. Li, Transient heat transfer analysis of phase change material melting in metal foam by experimental study and artificial neural network, J. Energy Storage. 33 (2021) 102160. https://doi.org/10.1016/j.est.2020.102160.

[110] H. Li, C. Hu, Y. He, D. Tang, K. Wang, X. Hu, Visualized-experimental investigation on the energy storage performance of PCM infiltrated in the metal foam with varying pore

densities, Energy. 237 (2021) 121540. https://doi.org/10.1016/j.energy.2021.121540.

[111] B. Buonomo, H. Celik, D. Ercole, O. Manca, M. Mobedi, Numerical study on latent thermal energy storage systems with aluminum foam in local thermal equilibrium, Appl. Therm. Eng. 159 (2019) 113980. https://doi.org/10.1016/j.applthermaleng.2019.113980.

[112] X. Xiao, P. Zhang, M. Li, Effective thermal conductivity of open-cell metal foams impregnated with pure paraffin for latent heat storage, Int. J. Therm. Sci. 81 (2014) 94–105. https://doi.org/10.1016/j.ijthermalsci.2014.03.006.

[113] N. Prasanth, M. Sharma, R.N. Yadav, P. Jain, Designing of latent heat thermal energy storage systems using metal porous structures for storing solar energy, J. Energy Storage. 32 (2020) 101990. https://doi.org/10.1016/j.est.2020.101990.

[114] A. Parida, A. Bhattacharya, P. Rath, Effect of convection on melting characteristics of phase change material-metal foam composite thermal energy storage system, J. Energy Storage. 32 (2020) 101804. https://doi.org/10.1016/j.est.2020.101804.

[115] A. Kumar, S.K. Saha, Latent heat thermal storage with variable porosity metal matrix: A numerical study, Renew. Energy. 125 (2018) 962–973. https://doi.org/10.1016/j.renene.2018.03.030.

[116] J. Yu, Y. Yang, X. Yang, Q. Kong, Y. Liu, J. Yan, Effect of porous media on the heat transfer enhancement for a thermal energy storage unit, Energy Procedia. 152 (2018) 984–989. https://doi.org/10.1016/j.egypro.2018.09.104.

[117] P. Zhang, Z.N. Meng, H. Zhu, Y.L. Wang, S.P. Peng, Melting heat transfer characteristics of a composite phase change material fabricated by paraffin and metal foam, Appl. Energy. 185 (2017) 1971–1983. https://doi.org/10.1016/j.apenergy.2015.10.075.

[118] K. Venkateshwar, S.H. Tasnim, H. Simha, S. Mahmud, Empirical correlations to quantify the effect of metal foam on solidification process in constant thermal capacity and constant volume systems, J. Energy Storage. 30 (2020) 101482. https://doi.org/10.1016/j.est.2020.101482.

[119] A. Alhusseny, N. Al-Zurfi, A. Nasser, A. Al-Fatlawi, M. Aljanabi, Impact of using a PCM-metal foam composite on charging/discharging process of bundled-tube LHTES units, Int. J. Heat Mass Transf. 150 (2020) 119320. https://doi.org/10.1016/j.ijheatmasstransfer.2020.119320.

[120] P.T. Sardari, D. Giddings, D. Grant, M. Gillott, G.S. Walker, Discharge of a composite metal foam/phase change material to air heat exchanger for a domestic thermal storage unit, Renew. Energy. 148 (2020) 987–1001. https://doi.org/10.1016/j.renene.2019.10.084.

[121] G. Liu, T. Xiao, J. Guo, P. Wei, X. Yang, K. Hooman, Melting and solidification of phase change materials in metal foam filled thermal energy storage tank : Evaluation on gradient in pore structure, Appl. Therm. Eng. 212 (2022) 118564. https://doi.org/10.1016/j.applthermaleng.2022.118564.

[122] T. Xu, J.N. Chiu, B. Palm, S. Sawalha, Experimental investigation on cylindrically macro-encapsulated latent heat storage for space heating applications, Energy Convers. Manag. 182 (2019) 166–177. https://doi.org/10.1016/j.enconman.2018.12.056.

[123] S. Aziz, N.A.M. Amin, M.S. Abdul Majid, M. Belusko, F. Bruno, CFD simulation of a TES tank comprising a PCM encapsulated in sphere with heat transfer enhancement, Appl. Therm. Eng. 143 (2018) 1085–1092. https://doi.org/10.1016/j.applthermaleng.2018.08.013.

[124] Z. He, X. Wang, X. Du, M. Amjad, L. Yang, C. Xu, Experiments on comparative performance of water thermocline storage tank with and without encapsulated paraffin wax packed bed, Appl. Therm. Eng. 147 (2019) 188–197. https://doi.org/10.1016/j.applthermaleng.2018.10.051.

[125] Y. Fang, Z.G. Qu, Y.D. Fu, Experimental study of the thermal characteristics of microencapsulated phase change composite cylinders, Appl. Therm. Eng. 114 (2017) 1256–1264. https://doi.org/10.1016/j.applthermaleng.2016.11.111.

[126] N.A.M. Amin, F. Bruno, M. Belusko, Effectiveness-NTU correlation for low temperature PCM encapsulated in spheres, Appl. Energy. 93 (2012) 549–555. https://doi.org/10.1016/j.apenergy.2011.12.006.

[127] Y.T. Lee, S.W. Hong, J.D. Chung, Effects of capsule conduction and capsule outside convection on the thermal storage performance of encapsulated thermal storage tanks, Sol. Energy. 110 (2014) 56–63. https://doi.org/10.1016/j.solener.2014.08.034.

[128] Z. Liu, Z. Wang, C. Ma, An experimental study on the heat transfer characteristics of a heat pipe heat exchanger with latent heat storage. Part II: Simultaneous charging/discharging modes, Energy Convers. Manag. 47 (2006) 967–991. https://doi.org/10.1016/j.enconman.2005.06.007.

[129] Z. Wang, Y. Diao, Y. Zhao, C. Chen, L. Liang, T. Wang, Thermal performance investigation of an integrated collector–storage solar air heater on the basis of lap joint-type flat micro-heat pipe arrays: Simultaneous charging and discharging mode, Energy. 181 (2019) 882–896. https://doi.org/10.1016/j.energy.2019.05.197.

[130] L. Liang, Y.H. Diao, Y.H. Zhao, Z.Y. Wang, C.Q. Chen, Experimental and numerical investigations of latent thermal energy storage using combined flat micro-heat pipe array–metal foam configuration: Simultaneous charging and discharging, Renew. Energy. 171 (2021) 416–430. https://doi.org/10.1016/j.renene.2021.02.022.

[131] N. Sharifi, A. Faghri, T.L. Bergman, C.E. Andraka, Simulation of heat pipe-assisted latent heat thermal energy storage with simultaneous charging and discharging, Int. J. Heat Mass Transf. 80 (2015) 170–179. https://doi.org/10.1016/j.ijheatmasstransfer.2014.09.013.

[132] R.E. Murray, D. Groulx, Experimental study of the phase change and energy characteristics inside a cylindrical latent heat energy storage system: Part 2 simultaneous charging and discharging, Renew. Energy. 63 (2014) 724–734. https://doi.org/10.1016/j.renene.2013.10.004.

[133] Y. Fang, Z.G. Qu, J.F. Zhang, H.T. Xu, G.L. Qi, Simultaneous charging and discharging performance for a latent thermal energy storage system with a microencapsulated phase change material, Appl. Energy. 275 (2020). https://doi.org/10.1016/j.apenergy.2020.115353.

[134] A.P. Omojaro, C. Breitkopf, Study on solid liquid interface heat transfer of PCM under simultaneous charging and discharging (SCD) in horizontal cylinder annulus, Heat Mass Transf. Und Stoffuebertragung. 53 (2017) 2223–2240. https://doi.org/10.1007/s00231-017-1971-1.

[135] P. Omojaro, C. Breitkopf, Investigating and modeling of simultaneous charging and discharging of a PCM heat exchanger, Energy Procedia. 48 (2014) 413–422. https://doi.org/10.1016/j.egypro.2014.02.048.

[136] A.R. Mazhar, A. Shukla, S. Liu, Numerical analysis of rectangular fins in a PCM for low-grade heat harnessing, Int. J. Therm. Sci. 152 (2020) 106306. https://doi.org/10.1016/j.ijthermalsci.2020.106306.

[137] Els.S. ELSihy, X. Wang, C. Xu, X. Du, Numerical investigation on simultaneous

charging and discharging process of molten-salt packed-bed thermocline storage tank employing in CSP plants, Renew. Energy. 172 (2021) 1417–1432. https://doi.org/10.1016/j.renene.2020.11.139.

[138] A. Mahdavi, M.A. Erfani Moghaddam, A. Mahmoudi, Simultaneous charging and discharging of multi-tube heat storage systems using copper fins and Cu nanoparticles, Case Stud. Therm. Eng. 27 (2021) 101343. https://doi.org/10.1016/j.csite.2021.101343.

[139] J.M. Mahdi, S. Lohrasbi, D.D. Ganji, E.C. Nsofor, Simultaneous energy storage and recovery in the triplex-tube heat exchanger with PCM, copper fins and Al2O3 nanoparticles, Energy Convers. Manag. 180 (2019) 949–961. https://doi.org/10.1016/j.enconman.2018.11.038.

[140] M.M. Joybari, F. Haghighat, S. Seddegh, Numerical investigation of a triplex tube heat exchanger with phase change material- Simultaneous charging and discharging, Energy Build. (2017) 426–438. https://doi.org/http://dx.doi.org/10.1016/j.enbuild.2017.01.034.

[141] M.M. Joybari, F. Haghighat, S. Seddegh, A.A. Al-Abidi, Heat transfer enhancement of phase change materials by fins under simultaneous charging and discharging, Energy Convers. Manag. 152 (2017) 136–156. https://doi.org/10.1016/j.enconman.2017.09.018.

[142] J.C.Y. Wang, S. Lin, C.C.K. Kwok, (s)Δ C where, T, 106 (2009) 1982–1984.

[143] M. Arıcı, E. Tütüncü, M. Kan, H. Karabay, Melting of nanoparticle-enhanced paraffin wax in a rectangular enclosure with partially active walls, Int. J. Heat Mass Transf. 104 (2017) 7–17. https://doi.org/10.1016/j.ijheatmasstransfer.2016.08.017.

[144] C. Nie, S. Deng, H. Guo, J. Liu, Effects of partially thermally active walls on simultaneous charging and discharging of paraffin wax in a square cavity, Energy Convers. Manag. 202 (2019). https://doi.org/10.1016/j.enconman.2019.112201.

[145] Y. Hong, W.B. Ye, J. Du, S.M. Huang, Solid-liquid phase-change thermal storage and release behaviors in a rectangular cavity under the impacts of mushy region and low gravity, Int. J. Heat Mass Transf. 130 (2019) 1120–1132. https://doi.org/10.1016/j.ijheatmasstransfer.2018.11.024.

[146] Y. Hong, W.B. Ye, S.M. Huang, M. Yang, J. Du, Thermal storage characteristics for rectangular cavity with partially active walls, Int. J. Heat Mass Transf. 126 (2018) 683–702. https://doi.org/10.1016/j.ijheatmasstransfer.2018.05.005.

[147] D. Jaya Krishna, S. Kochar, The Metallographic Study of Corrosion of Metals with Latent Heat Storage Materials Suitable for Solar Hot Water System, Trans. Indian Ceram. Soc. 76 (2017) 133–141. https://doi.org/10.1080/0371750X.2016.1268072.

[148] Voller, Prakash, A Fixed grid numerical modelling methodology for convection diffusion mushy region phase change problems, Int. Jounal Heat Mass Transf. 30 (1978) 1709–1719. https://doi.org/0017-9310/87.

[149] M. Kumar, D.J. Krishna, Influence of Mushy Zone Constant on Thermohydraulics of a PCM, Energy Procedia. 109 (2017) 314–321. https://doi.org/10.1016/j.egypro.2017.03.074.

[150] R. Kandasamy, X.Q. Wang, A.S. Mujumdar, Transient cooling of electronics using phase change material (PCM)-based heat sinks, Appl. Therm. Eng. 28 (2008) 1047–1057. https://doi.org/10.1016/j.applthermaleng.2007.06.010.

[151] U.M. Gaddala, J.K. Devanuri, A Hybrid Decision-Making Method for the selection of a PCM for Thermal Energy Storage, J. Therm. Sci. Eng. Appl. (2019). https://doi.org/10.1115/1.4046056.

[152] J.K. Devanuri, U.M. Gaddala, V. Kumar, Investigation on compatibility and thermal reliability of phase change materials for low-temperature thermal energy storage, Mater. Renew. Sustain. Energy. 9 (2020) 1–16. https://doi.org/10.1007/s40243-020-00184-4.

[153] M. Longeon, A. Soupart, J.F. Fourmigué, A. Bruch, P. Marty, Experimental and numerical study of annular PCM storage in the presence of natural convection, Appl. Energy. 112 (2013) 175–184. https://doi.org/10.1016/j.apenergy.2013.06.007.

[154] L. Kalapala, J.K. Devanuri, Optimization of Fin Parameters to Reduce Entropy Generation and Melting Time of a Latent Heat Storage Unit, J. Sol. Energy Eng. 142 (2020) 1–12. https://doi.org/10.1115/1.4046878.

[155] R.J. Moffat, Describing the uncertainties in experimental results, Exp. Therm. Fluid Sci. 1 (1988) 3–17. https://doi.org/10.1016/0894-1777(88)90043-X.

[156] X.H. Yang, S.C. Tan, J. Liu, Numerical investigation of the phase change process of low melting point metal, Int. J. Heat Mass Transf. 100 (2016) 899–907. https://doi.org/10.1016/j.ijheatmasstransfer.2016.04.109.

[157] B. Buonomo, D. Ercole, O. Manca, S. Nardini, Numerical Analysis on a Latent Thermal Energy Storage System with Phase Change Materials and Aluminum Foam, Heat

Transf. Eng. 41 (2020) 1075–1084. https://doi.org/10.1080/01457632.2019.1600875.

[158] B. Buonomo, H. Celik, D. Ercole, O. Manca, M. Mobedi, Numerical study on latent thermal energy storage systems with aluminum foam in local thermal equilibrium, Appl. Therm. Eng. 159 (2019) 113980. https://doi.org/10.1016/j.applthermaleng.2019.113980.

[159] A.K. Hassan, J. Abdulateef, M.S. Mahdi, A.F. Hasan, Experimental evaluation of thermal performance of two different finned latent heat storage systems, Case Stud. Therm. Eng. 21 (2020) 100675. https://doi.org/10.1016/j.csite.2020.100675.

[160] N. Mallya, S. Haussener, Buoyancy-driven melting and solidification heat transfer analysis in encapsulated phase change materials, Int. J. Heat Mass Transf. 164 (2021) 120525. https://doi.org/10.1016/j.ijheatmasstransfer.2020.120525.

[161] Y. Zhong, B. Zhao, J. Lin, F. Zhang, H. Wang, Z. Zhu, Z. Dai, Encapsulation of high-temperature inorganic phase change materials using graphite as heat transfer enhancer, Renew. Energy. 133 (2019) 240–247. https://doi.org/10.1016/j.renene.2018.09.107.

[162] Y. Song, N. Zhang, Y. Jing, X. Cao, Y. Yuan, F. Haghighat, Experimental and numerical investigation on dodecane/expanded graphite shape-stabilized phase change material for cold energy storage, Energy. 189 (2019) 116175. https://doi.org/10.1016/j.energy.2019.116175.

[163] Q. Yu, C. Zhang, Y. Lu, Q. Kong, H. Wei, Y. Yang, Q. Gao, Y. Wu, A. Sciacovelli, Comprehensive performance of composite phase change materials based on eutectic chloride with SiO2 nanoparticles and expanded graphite for thermal energy storage system, Renew. Energy. 172 (2021) 1120–1132. https://doi.org/10.1016/j.renene.2021.03.061.

[164] A.M. Abdulateef, S. Mat, J. Abdulateef, K. Sopian, A.A. Al-Abidi, Geometric and design parameters of fins employed for enhancing thermal energy storage systems: a review, Renew. Sustain. Energy Rev. 82 (2018) 1620–1635. https://doi.org/10.1016/j.rser.2017.07.009.

[165] Z. Ma, W.W. Yang, F. Yuan, B. Jin, Y.L. He, Investigation on the thermal performance of a high-temperature latent heat storage system, Appl. Therm. Eng. 122 (2017) 579–592. https://doi.org/10.1016/j.applthermaleng.2017.04.085.

[166] R. Karami, B. Kamkari, Experimental investigation of the effect of perforated fins

on thermal performance enhancement of vertical shell and tube latent heat energy storage systems, Energy Convers. Manag. 210 (2020) 112679. https://doi.org/10.1016/j.enconman.2020.112679.

ARTICLES PUBLISHED BASED ON THE PRESENT WORK

1. **S. Khobragade**, Devanuri JK. Energy and exergy analyses of simultaneous charging and discharging latent heat storage system at different inclination angles — An Experimental Study 2021: **ASME, Journal of Energy Resources and Technology**; 143:1–9. https://doi.org/10.1115/1.4051049. **(IF = 2.903)**

2. **S. Khobragade**, J.K. Devanuri, Impact of inclination on the thermal performance of shell and tube latent heat storage system under simultaneous charging and discharging : Numerical investigation, **Elsevier, Applied Thermal Engineering;** 214 (2022) 118811. https://doi.org/10.1016/j.applthermaleng.2022.118811. **(IF = 6.465)**

3. **S. Khobragade**, J.K. Devanuri, Thermal analysis of latent heat storage system in vertical and horizontal configurations under simultaneous charging and discharging processes, **Elsevier, Thermal Science and Engineering Progress (Revision submitted)**

4. **S. Khobragade**, J.K. Devanuri, Augmentation of phase change materials thermal response with circular fins under simultaneous charging and discharging (SCD) processes, **Elsevier, Journal of Thermofluids (Under review)**

5. **S. Khobragade**, J.K. Devanuri, Experimental investigation to assess the influence of inclination on thermal performance of latent heat storage system with solid and perforated fins under simultaneous charging and discharging process, **Elsevier, Thermal Science and Engineering Progress (Under review)**

6. **S. Khobragade**, J.K. Devanuri, Numerical study on thermal enhancement of latent heat storage system with and without fins during simultaneous charging and discharging process, **SAGE, Proceeding of the Institute of Mechanical Engineers Part-E (Under review)**

Conference

1. **S. Khobragade**, J.K. Devanuri, Impact of flow direction and mass flow rate on the melting process for simultaneous charging and discharging based latent heat storage system. *26thNational and 4th International ISHMT-ASTFE Heat and Mass Transfer Conference (IHMTC-2021), IIT Madras, India.*